Summary of Activities

2021

CANADA-NUNAVUT
GEOSCIENCE OFFICE

ᑲᓇᑕᐅᑉ-ᓄᓇᕘᑦᑐ
ᐅᔭᖅᑲᓂᒃ ᖃᐅᔨᓴᖅᑎᖏᑦ

BUREAU GÉOSCIENTIFIQUE
CANADA-NUNAVUT

KANATAMI-NUNAVUMI
GEOSCIENCE TITIGAKVIIT

CANADA-NUNAVUT GEOSCIENCE OFFICE

ᑲᓇᑕᐅᑉ-ᓄᓇᕗᒡᒧ ᐅᔪᖅᑲᓂᒃ ᖃᐅᔨᓴᖅᑎᖏᑦ

BUREAU GÉOSCIENTIFIQUE CANADA-NUNAVUT

KANATAMI-NUNAVUMI GEOSCIENCE TITIGAKVIIT

SUMMARY OF ACTIVITIES 2021

This publication is available, free of charge, as colour digital files in Adobe Acrobat® PDF format from the Canada-Nunavut Geoscience Office website: https://cngo.ca/. Le présent volume est aussi disponible en français sur https://cngo.ca/fr/.

All papers in this volume, except Gagnier et al., were submitted in English and each was translated to French for inclusion in that volume. Gagnier et al. was submitted in French and was translated to English for inclusion in this volume.

Every reasonable effort is made to ensure the accuracy of the information contained in this report, but the Canada-Nunavut Geoscience Office does not assume any liability for errors that may occur. Source references are included in the report and users should verify critical information.

When using information from this publication in other publications or presentations, due acknowledgment should be given to Canada-Nunavut Geoscience Office. The recommended reference is included on the title page of each paper. The complete volume should be referenced as follows:

Canada-Nunavut Geoscience Office (2022): Summary of Activities 2021; Canada-Nunavut Geoscience Office, 68 p.

ISSN 2291-1243 Canada-Nunavut Geoscience Office Summary of Activities (Online)

Front cover photo: Normal fault plane related to the Frobisher Bay half-graben, exposed on a recently excavated wall, Iqaluit, Nunavut. Photo by Tommy Tremblay, Canada-Nunavut Geoscience Office.

Back cover photo: Photograph from an unmanned aerial vehicle of the RV *Nuliajuk* mapping the seafloor in Pangnirtung Fiord, Nunavut. Photo by Angus Robertson and Geneviève Philibert, Geological Survey of Canada.

Foreword

It is my great pleasure to introduce you to the Canada-Nunavut Geoscience Office's annual *Summary of Activities* for 2021. For the second year, the publication is being published in both English and French, as two completely separate volumes.

The Canada-Nunavut Geoscience Office (CNGO) was established in 1999. It is a partnership between the territorial government—the Department of Economic Development and Transportation of the Government of Nunavut (GN-EDT)—and the federal government, specifically Natural Resources Canada (NRCan) and Crown-Indigenous Relations and Northern Affairs Canada (CIRNAC). Nunavut Tunngavik Incorporated (NTI) is an ex-officio member of the CNGO Management Board that provides operational oversight for the office.

The governments of Nunavut and Canada signed an Agreement-in-Principle (AIP) in mid-August 2019; under this AIP, Crown lands and oil, gas and mineral resources will be devolved from the Government of Canada to the Government of Nunavut. The final devolution agreement will be in place in the near future and will be followed by drafting of the legislation needed to bring devolution into effect—likely by 2025. At that time, professionals from the CNGO, CIRNAC and the GN will amalgamate and form the Nunavut Geological Survey, a new entity within the GN.

The CNGO has expertise in Precambrian, Paleozoic and Quaternary geology, GIS and cartography, and online data dissemination. The mandate of the office is to provide Nunavut with accessible geoscience information and expertise to support responsible resource exploration and development, responsible infrastructure development, and geoscience education, training and awareness.

The CNGO and its office partners co-manage and disseminate data through two websites (https://cngo.ca/ and https://NunavutGeoscience.ca/). Updating and revamping these websites is a priority for the office. The *Summary of Activities* volumes and the accompanying Geoscience Data Series and Open File Map Series disseminate the results of geological mapping (bedrock and surficial) and analyses of samples (rock, till, soil, lake sediment and stream sediment).

The world has been struggling since 2020 with the appearance of COVID-19 and offices across Canada shifted to working remotely. Some offices (e.g., the labs of NRCan) have partially reopened since the first wave of COVID; others, such as the CNGO, remain closed, with professionals working from home. In addition, CNGO projects requiring fieldwork were postponed in 2020 and 2021. Without this fieldwork, professionals in the CNGO have focused their efforts on writing up research results and planning for the coming summer (2022), which will hopefully include a fieldwork component.

The first paper in this volume is a summary by a CNGO researcher of the work she carried out, both independently and in collaboration with colleagues from NRCan's Geological Survey of Canada (GSC), on phases 1 and 2 of the Geo-mapping for Energy and Minerals (GEM) program from 2008 to 2020. She discusses her use of conodonts (microfossils) to unravel the stratigraphy of the Paleozoic, and some Mesozoic, rocks of Nunavut that cover more than 30% of the territory, mainly in the Hudson Bay Basin area and the High Arctic islands.

The second paper is from two CNGO professionals who are working on a database of analyses of surficial materials compiled from various publications on Nunavut. The database, which is currently in its initial stage, includes the geographic co-ordinates of the sample stations. Next steps for this database are to include, and link to the sample co-ordinates, the surficial geochemical, mineralogical and sedimentological data.

The third paper discusses the work of a graduate student who is being assisted by the CNGO with her Master's thesis under a bursary from NRCan's Research Associate Program (RAP). Her thesis involves mapping and dating (by K-Ar) of brittle faulting in the Frobisher Bay graben, in the vicinity of Iqaluit on southern Baffin Island. The paper presents the initial results of fieldwork undertaken in 2020 and 2021 to refine understanding of the brittle fault activity of Iqaluit. The results of this work may have implications for local resource potential (petroleum, diamonds), as well as geohazards related to fault activity.

The next two papers deal with a common theme of submarine landslides of eastern Baffin Island. The GSC has worked for many years on a Public Safety Geoscience Program to identify potential offshore marine hazards; since 2009, this work has focused on Baffin Bay. The first paper reports on factors related to understanding the distribution, timing and potential triggers of submarine landslides in Pangnirtung Fiord. The community of Pangnirtung is situated at the water's edge on the coast of Pangnirtung Fiord, and the topography of this area is comparable to that of fiords in Greenland and Alaska where recent work has investigated the damage caused by landslide-generated tsunamis. The second paper reports on the geotechnical characteristics of the sediments in a submarine landslide in Southwind Fiord, southeast of Pangnirtung.

The final paper in the volume outlines a collaboration between two Government of Nunavut departments—Community and Government Services (CGS) and Environment (DoE)—and the CNGO. The CGS regularly (one to four times a year) collects water-quality data from drinking-water sources in 25 communities across Nunavut, and work is being done with the DoE and CNGO to consolidate the data. There are currently stressors involved in the management of Arctic drinking-water systems, including water availability, staffing challenges within the organizations responsible for water management, and other logistical issues.

These papers report on work carried out by professionals of the CNGO, their partners and collaborators from other organizations, and other researchers working in Nunavut. I am proud of the work done by the CNGO and our colleagues, particularly during the past two years of a pandemic that has necessitated imaginative and resourceful ways to conduct and report on field-based studies when fieldwork was not permitted. I sincerely thank Celine Gilbert, CNGO's GIS Specialist, who oversees this publication from start to finish; Celine's hard work keeps us all focused and on track to meet the necessary publication deadlines. I am confident that everyone (our partners, collaborators and supporters) involved in, and with, the CNGO shares in this pride of the high-quality research presented in this volume.

Acknowledgments

The CNGO staff thank all authors of papers in this *Summary of Activities*. Their dedication is greatly appreciated and, as always, is critical in helping the CNGO deliver such a quality product. RnD Technical is also thanked for their technical editing, translating and assembling of the two volumes. In addition, special thanks are extended to the reviewers of papers:

Christopher Barnes	University of Victoria (emeritus)
Pierre-Marc Godbout	Geological Survey of Canada
Melissa Lafrenière	Queen's University
Michel Lamothe	Université du Québec à Montréal
Danika Ouellette	Geological Survey of Canada–Atlantic
Tommy Tremblay	Canada-Nunavut Geoscience Office

Linda Ham
Chief Geologist
Canada-Nunavut Geoscience Office
https://cngo.ca/

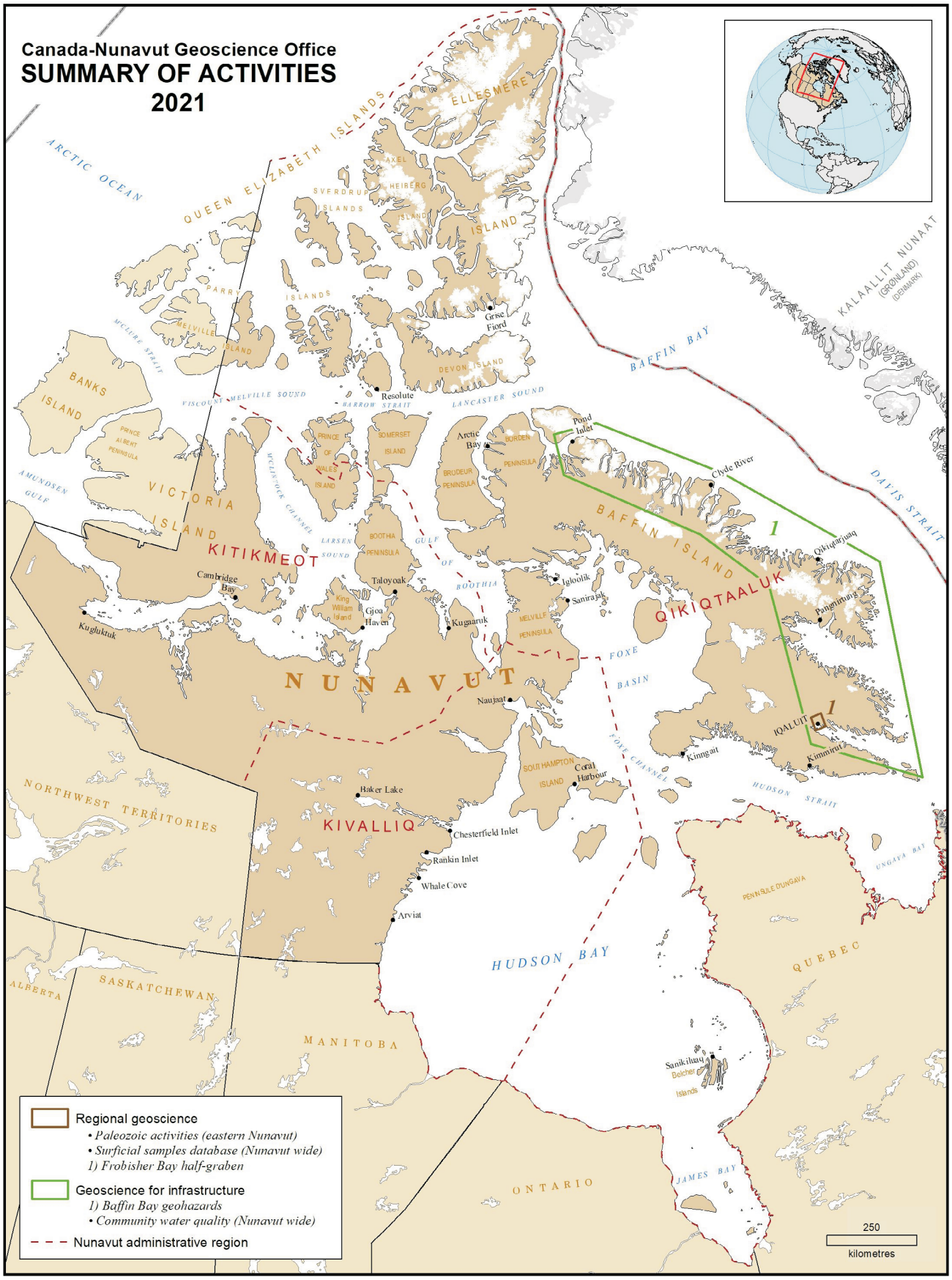
Canada-Nunavut Geoscience Office
SUMMARY OF ACTIVITIES
2021
ARCTIC OCEAN
QUEEN ELIZABETH ISLANDS
ELLESMERE ISLAND
AXEL HEIBERG ISLAND
SVERDRUP ISLANDS
PARRY ISLANDS
MELVILLE ISLAND
DEVON ISLAND
Grise Fiord
Resolute
BANKS ISLAND
PRINCE ALBERT PENINSULA
VICTORIA ISLAND
KITIKMEOT
AMUNDSEN GULF
PRINCE OF WALES ISLAND
SOMERSET ISLAND
BOOTHIA PENINSULA
Cambridge Bay
Kugluktuk
King William Island
Gjoa Haven
Taloyoak
Kugaaruk
GULF OF BOOTHIA
LARSEN SOUND
M'CLINTOCK CHANNEL
VISCOUNT MELVILLE SOUND
M'CLURE STRAIT
BARROW STRAIT
LANCASTER SOUND
BAFFIN BAY
DAVIS STRAIT
KALAALLIT NUNAAT (GRØNLAND) (DENMARK)
Arctic Bay
Pond Inlet
BURDEN PENINSULA
BRODEUR PENINSULA
Clyde River
BAFFIN ISLAND
QIKIQTAALUK
Iglulik
Sanirajak
MELVILLE PENINSULA
Qikiqtarjuaq
Pangnirtung
FOXE BASIN
NUNAVUT
Naujaat
IQALUIT
Kinngait
Kimmirut
SOUTHAMPTON ISLAND
Coral Harbour
FOXE CHANNEL
HUDSON STRAIT
NORTHWEST TERRITORIES
KIVALLIQ
Baker Lake
Chesterfield Inlet
Rankin Inlet
Whale Cove
Arviat
UNGAVA BAY
PENINSULE D'UNGAVA
QUEBEC
HUDSON BAY
ALBERTA
SASKATCHEWAN
MANITOBA
Sanikiluaq
Belcher Islands
ONTARIO
JAMES BAY
Regional geoscience
• Paleozoic activities (eastern Nunavut)
• Surficial samples database (Nunavut wide)
1) Frobisher Bay half-graben
Geoscience for infrastructure
1) Baffin Bay geohazards
• Community water quality (Nunavut wide)
Nunavut administrative region
250
kilometres

Contents

Regional geoscience

Summary of contributions from the Canada-Nunavut Geoscience Office to the projects related to energy and Paleozoic stratigraphy under phases 1 and 2 of the Geo-mapping for Energy and Minerals program
S. Zhang 1

Database of the locations of surficial material sample stations in Nunavut
T. Tremblay and S. Basso 15

Studies of the Frobisher Bay half-graben: X-ray diffraction analysis of fault gouges exposed in the Iqaluit area, Baffin Island, Nunavut
F. Gagnier, B.M. Saumur, T. Tremblay, L. Lebeau, C. Sasseville and M. Preda 21

Geoscience for infrastructure

Submarine landslides in Pangnirtung Fiord, Baffin Island, Nunavut
P. Sedore, A. Normandeau and V. Maselli 31

Geotechnical characterization of a submarine landslide in Southwind Fiord, Baffin Island, Nunavut
M. Macquarrie, K. MacKillop and A. Normandeau 47

Community water quality data across Nunavut: an introduction to available data for community water supplies
J. Elliott, M.G. Clayden, K. Clouter, S. Collins, T. Tremblay and M. LeBlanc-Havard 57

Summary of contributions from the Canada-Nunavut Geoscience Office to the projects related to energy and Paleozoic stratigraphy under phases 1 and 2 of the Geo-mapping for Energy and Minerals program

Shunxin Zhang[1]

[1]*Canada-Nunavut Geoscience Office, Iqaluit, Nunavut, shunxin.zhang@nrcan-rncan.gc.ca*

This work, which is part of the Geo-mapping for Energy and Minerals program (GEM-1 and GEM-2; 2008–2020), is related mainly to energy and stratigraphy and is led by the Canada-Nunavut Geoscience Office (CNGO) in collaboration with the Geological Survey of Canada (GSC). The study areas include the Paleozoic Hudson Bay, Hudson Strait and Foxe basins, and the Mesozoic Baffin Bay basins, as well as Boothia Peninsula. The objective of this work was to evaluate the hydrocarbon potential and better understand the Paleozoic stratigraphy in these areas.

Zhang, S. 2022: Summary of contributions from the Canada-Nunavut Geoscience Office to the projects related to energy and Paleozoic stratigraphy under phases 1 and 2 of the Geo-mapping for Energy and Minerals program; *in* Summary of Activities 2021, Canada-Nunavut Geoscience Office, p. 1–14.

Abstract

The Canada-Nunavut Geoscience Office (CNGO) participated in several projects related to energy potential and Paleozoic stratigraphy under phases 1 and 2 of the Geo-mapping for Energy and Minerals (GEM) program during the years 2008–2020, including the Hudson Bay and Foxe Basins, Hudson-Ungava, Baffin Bay Basins, Baffin Geological Synthesis, Baffin Island, and Boothia Peninsula–Somerset Island projects. The aim of the projects was to evaluate the hydrocarbon potential in the Paleozoic Hudson Bay, Hudson Strait and Foxe basins and the Mesozoic Baffin Bay basins, and to better understand the Paleozoic stratigraphy in the Hudson Platform area and on the islands of the Canadian Arctic Archipelago. This paper summarizes the major research activities carried out under these projects and the contributions made to them by the CNGO.

Introduction

Natural Resources Canada (NRCan) launched the Geo-mapping for Energy and Minerals (GEM) program in 2008, under the leadership of the Geological Survey of Canada (GSC). After the completion of phase 1 (GEM-1, 2008–2013), the program was renewed and a new round of research activities was defined as phase 2 (GEM-2, 2014–2020). During the two phases, the CNGO made important and significant contributions to several projects related to the energy potential in the Paleozoic Hudson Bay, Hudson Strait and Foxe basins and the Mesozoic Baffin Bay basins, and the Paleozoic stratigraphy across the Hudson Platform and on the islands of the Canadian Arctic Archipelago. These contributions include the Hudson Bay and Foxe Basins project and the Baffin Bay Basins project of GEM-1, and the Hudson-Ungava project, Baffin Island project, Boothia Peninsula–Somerset Island project and Baffin Geological Synthesis project of GEM-2 (Figure 1).

Except for the Boothia Peninsula–Somerset Island project, the overall research goals of the above-mentioned projects were to propose a new understanding of the geological framework of the Paleozoic Hudson Bay, Hudson Strait and Foxe basins, as well as the Mesozoic Baffin Bay basins, and to provide improved knowledge of hydrocarbon systems in the basins. To achieve these goals, the most important approach was to conduct research to understand the stratigraphy, particularly that of the hydrocarbon source rocks. Prior to and during the GEM program, the CNGO undertook this essential work mainly on the Paleozoic stratigraphy and especially that of the hydrocarbon source rocks in Nunavut. The outputs of these projects have been separately published as journal papers, GSC open file reports and Canada-Nunavut Geoscience Office *Summary of Activities* papers (see references). Results of these works have been successively presented at a number of national and international scientific conferences (see references). The aim of this paper is to summarize the research activities carried out, and the achievements made, by the CNGO for these projects, organized by basin and area.

Hudson Bay Basin

The Hudson Bay Basin (Figure 1) is one of the largest Paleozoic sedimentary basins in North America. Industry stakeholders initially explored the basin for hydrocarbon re-

This publication is available, free of charge, as colour digital files in Adobe Acrobat® PDF format from the Canada-Nunavut Geoscience Office website: https://cngo.ca/. Il est aussi disponible en français sur https://cngo.ca/fr/.

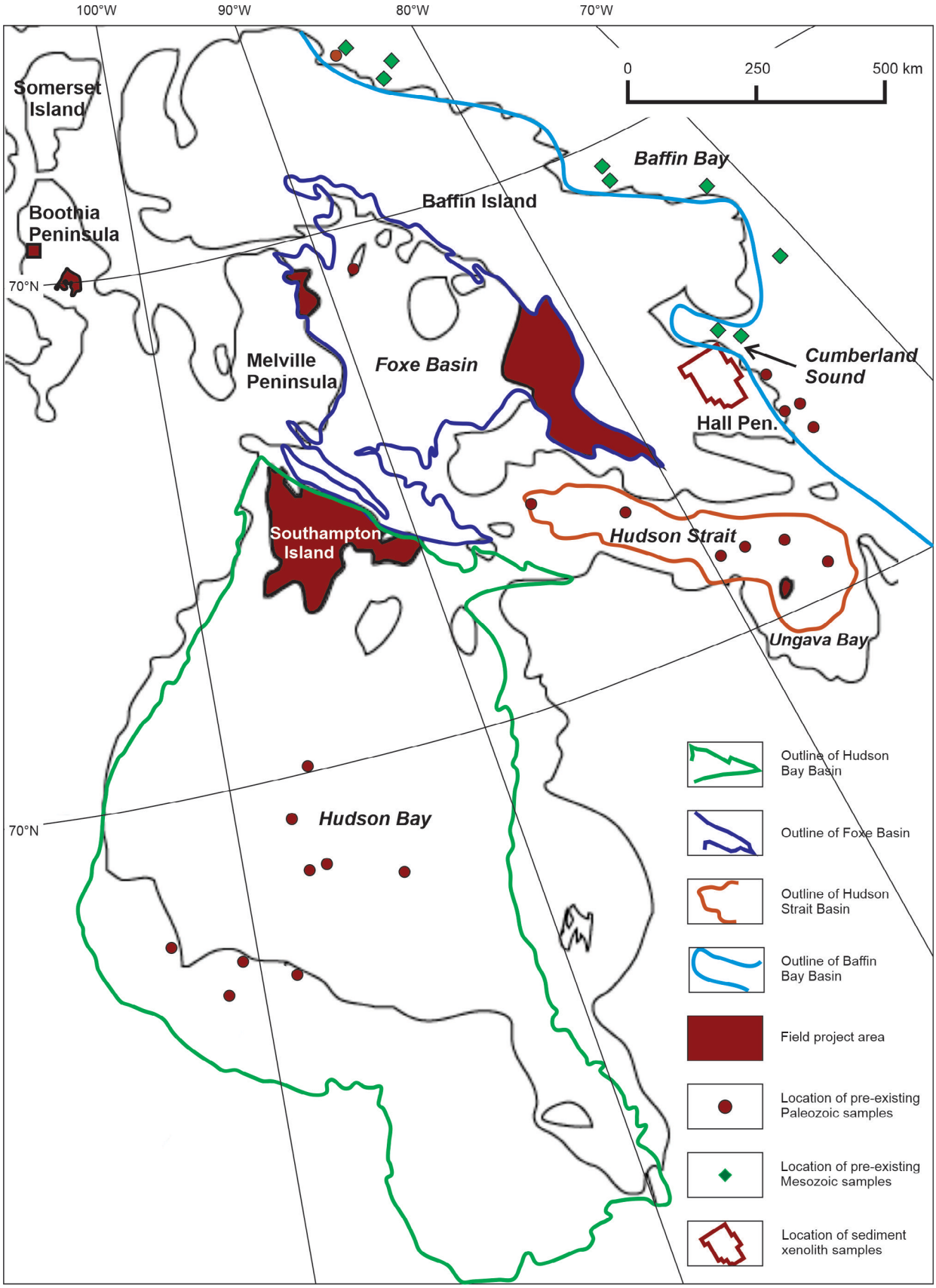

Figure 1: Eastern Nunavut, showing energy-related and Paleozoic-stratigraphy project areas of the Canada-Nunavut Geoscience Office contributing to phases 1 and 2 of the Geo-mapping for Energy and Minerals program (GEM-1 and GEM-2), with outlines of sedimentary basins. Abbreviation: Pen., Peninsula

sources, at a reconnaissance scale, nearly 50 years ago. The Paleozoic succession of the basin comprises approximately 2000 m of Upper Ordovician (Bad Cache Rapids and Churchill River groups, and Red Head Rapids Formation), lower Silurian (Severn River, Ekwan River and Attawapiskat formations) and Devonian (Kenogami River, Kwataboahegan, Stooping River, Moose River, Murray Island, Williams Island and Long Rapids formations) strata. These formations comprise mainly carbonate rocks consisting of alternating fossiliferous limestone, evaporitic and reefal dolostone, and minor clastic rocks.

Prior to the Hudson Bay and Foxe Basins project

Hudson Bay Lowlands and offshore area

Upper Ordovician and lower Silurian conodont biostratigraphy

Not long before the GEM-1 Hudson Bay and Foxe Basins project was launched in 2008, the CNGO had carried out a study of Upper Ordovician and lower Silurian conodont biostratigraphy in the Hudson Bay Basin. For this research, Zhang and Barnes (2007a, b) recovered about 4500 conodonts (microfossils) from 390 conodont-bearing samples from continuous cores and well cuttings from six exploration wells in the Hudson Bay Lowlands and offshore area. The research resulted in identifying 50 species representing 28 genera, and has significantly improved the understanding of the Late Ordovician and early Silurian geology. The main outputs are as follows:

- The conodont zones and their stratigraphic ranges are clearly defined. Seven zones were established for the Upper Ordovician–lower Silurian interval: the *Belodina confluens, Amorphognathus ordovicicus, Rhipidognathus symmetricus, Ozarkodina elibata, Kockelella*? *trifurcata* and *Distomodus staurognathoides* interval zones, and the *Pterospathodus celloni–P. eopennatus* Assemblage Zone.
- The biostratigraphic control for the different formations is precisely identified. Upper Ordovician and lower Silurian formations are dated as Edenian–Richmondian and early Rhuddanian–middle Telychian, respectively.
- The position of the Ordovician–Silurian boundary is recognized, typically associated with the global hiatus created by the terminal Ordovician glaciation in Gondwana.
- Most of the conodonts from the six wells studied have a Colour Alteration Index (CAI) value of 1, indicating little alteration of organic matter and that the strata have not reached burial temperatures greater than 80ºC. However, slightly higher CAI values are recorded from the deepest part of the wells in the offshore area of the basin, indicating burial temperatures just within the oil window.

Efforts in identifying petroleum source rocks

In order to understand the petroleum potential in the Hudson Bay Basin, particularly the occurrence and extent of petroleum source rocks in the Hudson Bay offshore area, the author collected 216 samples of well-cuttings and core from three exploration wells for Rock-Eval 6 analysis (Zhang et al., 2007; Zhang and Dewing, 2008); two of these exploration wells were in the Hudson Bay offshore area and one was on the Hudson Bay Lowlands. Unfortunately, most samples contain less than 0.3% total organic carbon (TOC) and have Tmax values below 435°C. These data indicated that the petroleum source rock does not occur in the areas near the three selected wells and that the burial temperature is not high enough for petroleum generation, even if the source rocks were present. However, this study provided essential data for further study in the Hudson Bay and Foxe Basins project.

Southampton Island

Southampton Island (Figure 1), where the Paleozoic strata are well exposed, was located on the northern margin of the Hudson Bay Basin during the Paleozoic; hence, the island plays a key role in understanding the Paleozoic geology of the basin. In 2007, the CNGO and GSC-Ottawa, with participation from universities, launched the Southampton Island Integrated Geoscience project that included three components: Precambrian mapping, Paleozoic stratigraphy and surficial mapping.

Ordovician petroleum source-rock stratigraphy

The Paleozoic stratigraphy subproject on Southampton Island, led and carried out by the author, focused on the Ordovician conodont biostratigraphy, petroleum source-rock stratigraphy and petroleum potential. During the field season, 14 stratigraphic sections were measured, and 300 and 40 samples were collected for biostratigraphic and geochemical studies, respectively.

The Upper Ordovician Bad Cache Rapids and Churchill River groups and Red Head Rapids Formation on Southampton Island are dominated by carbonate rocks but contain thin organic-rich shale units that were discovered on the island during the 1970s and informally named ‘Boas River shale’ and ‘Sixteen Mile Brook shale’, and then collectively formally named the Boas River Formation. However, the stratigraphy and hydrocarbon potential of these shale units have been poorly understood since then. There has been considerable debate surrounding these organic-rich shale units, which focused on such fundamental issues as

- are there one, two or three oil-shale intervals within the Ordovician sequence?
- what are their precise stratigraphic positions and their extent within the Hudson Bay offshore area?
- what is their hydrocarbon potential?

The most important contribution from the field studies of Upper Ordovician and lowest Silurian strata on Southampton Island to the geological study of the Hudson Bay Basin was the discovery of the three oil-shale intervals in a continuous section in the Cape Donovan area (Zhang, 2007, 2008a, b; Zhang and Lavoie, 2013; Figure 2), which unequivocally demonstrated that

- the three oil-shale intervals in the Cape Donovan area are within the lower Red Head Rapids Formation rather than between the Bad Cache Rapids and Churchill River groups, as previously interpreted; and
- the Cape Donovan lower oil-shale interval can be correlated with the 'Boas River shale', and the Cape Donovan middle or upper oil-shale interval can be correlated with the 'Sixteen Mile Brook shale'.

Petroleum potential

A total of 40 samples was collected from the three oil-shale intervals in the Cape Donovan sections for Rock-Eval 6 analysis, which led to the recognition of Type I–Type II kerogen and unusually high yield and TOC, as summarized in Table 1. Rocks of Late Ordovician age with such high yield and TOC had not been previously recognized in Canada and have been reported from only a few locations globally, such as the kukursite in the Baltic Oil Shale Basin in Estonia and northwestern Russia.

New data from Southampton Island supporting the presence of organic intervals in Hudson Bay offshore

The discovery of three oil-shale intervals in the Red Head Rapids Formation on Southampton Island encouraged the author to re-study the materials from the Hudson Bay offshore area (Zhang and Dewing, 2008). This resulted in recognition of the three organic-rich intervals in the same formation in several offshore wells. The presence of three organic-rich intervals in the Hudson Bay offshore area is supported by three lines of evidence obtained from the lower Red Head Rapids Formation in the exploration wells (Zhang, 2008a, b):

- Three prominent positive gamma-ray kicks were observed.
- Organic-rich fragments were found under the microscope by carefully hand-picking well-cutting samples that were initially studied by Zhang and Dewing (2008).
- Some reasonably high TOC values (2.29–5.73%) were obtained from several samples within the interval covering the three positive gamma-ray kicks, by using preferentially picked organic-rich fragments from the well cuttings.

During the Hudson Bay and Foxe Basins project

Because of the above-mentioned research, the CNGO played an important role when the Hudson Bay and Foxe Basins project of GEM-1 was launched in 2008.

Ordovician conodont biostratigraphy on Southampton Island

During the initial stages of GEM-1, the CNGO continued working on the materials previously collected on Southampton Island. The main outcomes from this pioneer work are the Upper Ordovician biostratigraphy and petroleum source-rock biostratigraphy (Zhang, 2011c; Figure 2), both of which were achieved for the first time on the island:

- Approximately 15 000 conodont specimens were recovered from 269 conodont-bearing samples from 14 localities, based on which four interval zones throughout the Upper Ordovician were established for the first time on the island. These zones are the *Belodina confluens* and *Pseudobelodina v. vulgaris* zones in the Bad Cache Rapids Group, correlative with the upper Edenian–lowest Richmondian Stage; the *Amorphognathus ordovicicus* Zone from the uppermost Bad Cache Rapids Group to the top of Churchill River Group, correlative with the lower Richmondian Stage; and the *Rhipidognathus symmetricus* Zone in the Red Head Rapids Formation, correlative with the upper Richmondian Stage.
- Most importantly, the biostratigraphic position of the organic-rich intervals on Southampton Island was correctly located during this study (Zhang, 2011c). The organic-rich intervals in the lower Red Head Rapids Formation, exposed at Cape Donovan, Sixteen Mile Brook and Boas River, are correlated with the lower *R. symmetricus* Zone of the upper Richmondian Stage, not the older Maysvillian Stage as previously interpreted (Figure 2).

Biomarker and vitrinite-reflectance study on the Ordovician organic-rich samples from Southampton Island

In addition to the previous Rock-Eval 6 study (Zhang, 2008a), six and nine samples of oil shales from Southampton Island were analyzed by two different labs, respectively, for biomarker and vitrinite reflection (Zhang and Hefter, 2009; Zhang, 2011b; Hefter et al., 2017), in order to better understand the petroleum potential of the three organic-rich intervals in the Red Head Rapids Formation in the Hudson Bay Basin. The data from these analyses include

- vitrinite reflectance and visual kerogen;
- kerogen carbon isotope, whole-extract carbon isotope and carbon isotope of saturates and aromatics fractions;
- Soxhlet extraction;
- medium-pressure liquid chromatography (MPLC);
- whole-extract bulk composition by Iatroscan® analysis;
- thermal-extract gas chromatography; and
- high-resolution gas chromatography.

These data are useful in determining the primary contributors to the organic matter in the oil shales and their thermal maturity, and in helping to characterize the hydrocarbon

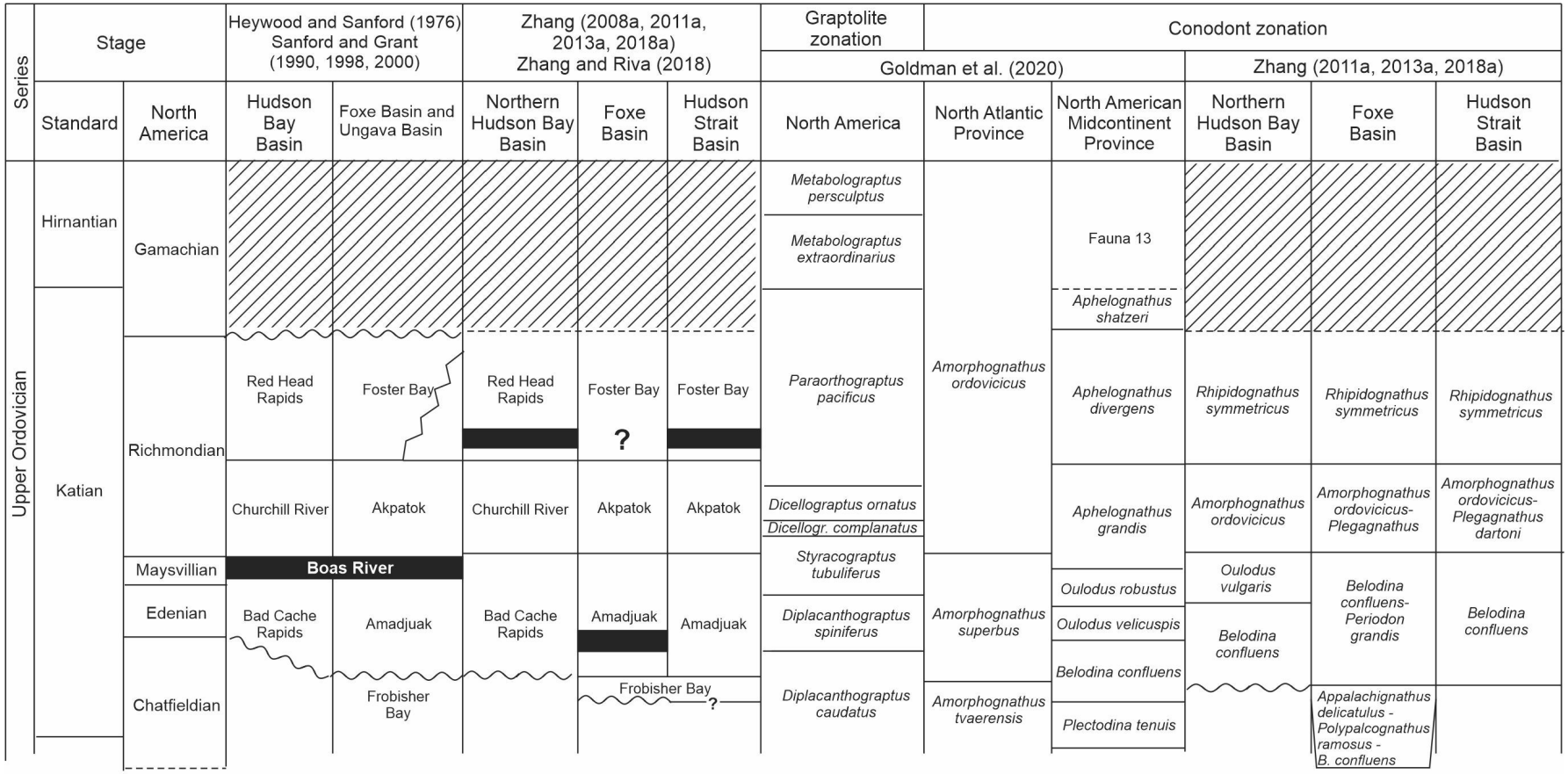

Goldman, D., Sadler, P.M. and Leslie, S.A. 2020: The Ordovician Period; Chapter 20 *in* The Geological Time Scale 2020, F.M. Gradstein, J.G. Ogg, M. Schmitz, and G. Ogg (ed.), Elsevier B.V., p. 631–694.
Heywood, W.W. and Sanford, B.V. 1976: Geology of Southampton, Coats and Mansel Islands, District of Keewatin, Northwest Territories; Geological Survey of Canada, Memoir 382, 35 p.
Sanford, B.V. and Grant, A.C. 1990: New findings relating to stratigraphy and structure of the Hudson Platform; *in* Current Research, Part D, Geological Survey of Canada, Paper 90-1D, p. 17–30.
Sanford, B.V. and Grant, A.C. 1998: Paleozoic and Mesozoic Geology of the Hudson and Southeast Arctic platforms; Geological Survey of Canada, Open File 3595, 2 sheets, URL <https://doi.org/10.4095/210108> [January 2022].
Sanford, B.V. and Grant, A.C. 2000: Geological framework of Ordovician System in the Southeast Arctic Platform, Nunavut; Geological Survey of Canada, Bulletin 557, p. 13–38.
See reference list for others.

Figure 2: Stratigraphy of Hudson Bay, Foxe and Hudson Strait basins, the Upper Ordovician organic-rich intervals in the basins, and their correlation with the Ordovician chronostratigraphic and biostratigraphic framework. The black stripes represent the stratigraphic position of the Upper Ordovician organic-rich intervals (unscaled).

Table 1: Summary of petroleum potential of the three organic-rich black shale intervals, lower Red Head Rapids Formation, Southampton Island, Nunavut (for detailed data, see Zhang, 2008a).

Interval	Thickness (m)	Lithology	No. of samples	Yield (kg/tonne)		Total organic carbon (TOC, %)		Hydrocarbon Index (HI)
				Average	Maximum	Average	Maximum	
Upper	0.35–0.5	Black shale with minor laminated argillaceous limestone	11	128.7	230.3	18.3	31	550–800
Middle	0.3–0.4	Black shale with minor laminated argillaceous limestone	8	145.9	261.1	22.4	34.1	550–800
Lower	1–1.25	Dark brown laminated argillaceous limestone with black shale	21	58.5	112.5	9.8	13.7	500–700

source potential of these organic-rich rocks and to analyze the relationship between source rocks and sea-level events (Zhang and Hefter, 2009; Zhang, 2011b; Hefter et al., 2017).

Recognition of Devonian hydrocarbon source rocks

In addition to the Upper Ordovician petroleum source rocks, the Devonian succession (Stooping River, Kwataboahegan, Moose River, Murray Island and William Island formations) in the Hudson Bay Basin also contains organic-rich intervals, but their hydrocarbon potential remains less understood than that of the Upper Ordovician.

While carrying out the work reported in Zhang and Dewing (2008), the author also collected a total of 50 well-cutting samples from depths of 875–630 m in the Devonian succession in the Hudson Bay offshore Beluga O-23 well. The author examined these samples under the microscope and hand-picked dark, organic-rich fragments from 28 samples; these fragments were later analyzed using the Rock-Eval 6 pyrolysis technique.

The Rock-Eval 6 data show that the Devonian succession in the Beluga O-23 well contains immature high-yield hydrocarbon source rocks with TOC ranging from 1.6% to 17.64% (average 9.07%) and with a Type II kerogen signature (Zhang and Hu, 2013). A well-log study was subsequently carried out to better understand the stratigraphic position of these Devonian source rocks. This well-log interpretation showed that these hydrocarbon potential source rocks are mainly concentrated in five narrow zones within the selected interval from the upper part of the Stooping River Formation to the lower part of the Williams Island Formation (Zhang and Hu, 2013).

Field trip on Southampton Island

During GEM-1, geologists recognized the key role of Southampton Island in understanding the geology of the Hudson Bay Basin and the important contributions by the CNGO to the new understanding of Ordovician stratigraphy, biostratigraphy and petroleum potential in the Hudson Bay Basin (Zhang, 2007, 2008a, b; Zhang and Barnes, 2007a, b). In the summer of 2010, the leader of the Hudson Bay and Foxe Basins project invited the CNGO to lead a field trip to examine the Upper Ordovician stratigraphy and oil shales on Southampton Island (Zhang, 2010), which was funded by the project.

The field trip, which ran from July 25 to 29, 2010, was led by a field trip guide (Zhang, 2010) from the CNGO and attended by eight geologists from GSC-Quebec, the Ontario Geological Survey, the Manitoba Geological Survey and Shell Oil Company in the United States and the United Kingdom. The field trip covered all 14 sections measured and sampled by the author during the 2007 field season (Zhang, 2007, 2008a, b, 2010). This excursion provided a rare and productive opportunity for geologists involved in the Hudson Bay and Foxe Basins project, and interested in the petroleum potential of the Hudson Bay Basin, to advance their understanding of the geology and source-rock potential of the basin.

Foxe Basin

The Foxe Basin, which is the second largest Paleozoic sedimentary basin in the Hudson Platform (Figure 1), includes the present-day Foxe Basin, southern Baffin Island and northeastern Melville Peninsula. It was explored for hydrocarbon resources in the 1970s at a reconnaissance scale. The Paleozoic sedimentation in the Foxe Basin is composed of four cycles: 1) sandstone and dolostone of the middle(?) Cambrian Gallery Formation and Lower Ordovician Turner Cliffs Formation; 2) dolostone and sandstone of the Lower to Middle(?) Ordovician Ship Point Formation; 3) variably dolomitic limestone of the Upper Ordovician Frobisher Bay, Amadjuak, Akpatok and Foster Bay formations; and 4) limestone of the lower Silurian Severn River Formation. The Rowley M-04 well, drilled in the 1970s, intersected 511.4 m of this entire Paleozoic sequence in the present-day Foxe Basin; however, the first cycle was not deposited on northeastern Melville Peninsula, and the first and second cycles were not deposited on southern Baffin Island.

Prior to the Hudson Bay and Foxe Basins project

In order to understand the petroleum potential in Foxe Basin, the author (in Zhang and Dewing, 2008) collected a total of 30 samples, covering the interval from the upper part of the Lower to Middle(?) Ordovician Ship Point Formation to lower Silurian Severn River Formation, from the

cores of the Rowley M-04 well for Rock-Eval 6 analysis. Unfortunately, most of the samples have TOC between 0.3% and 2% and Tmax below 435°C, which means there is no petroleum potential in the area of the Foxe Basin near the well.

During the Hudson Bay and Foxe Basins project

Northeastern Melville Peninsula

Northeastern Melville Peninsula preserves the stratigraphic record of the northwestern margin of the Foxe Basin. The Ordovician sequence on the peninsula includes the Lower and Middle(?) Ordovician Ship Point Formation and Upper Ordovician Frobisher Bay, Amadjuak, Akpatok and Foster Bay formations. Their biostratigraphic ages and correlations were poorly understood prior to GEM-1; in particular, it was unclear whether any Ordovician organic-rich intervals exist on the peninsula.

In 2009, the CNGO joined the GEM-1 Melville Peninsula Integrated Geoscience project, which included three subprojects: Precambrian mapping, Paleozoic stratigraphy and surficial mapping. The author led and carried out the Paleozoic stratigraphy subproject.

During the field season, more than 100 samples were collected for the biostratigraphic study at 24 outcrops and 38 frost-shattered rubble localities in three areas on northeastern Melville Peninsula. These samples stratigraphically cover the uppermost Lower to Middle(?) Ordovician Ship Point Formation and the Upper Ordovician Frobisher Bay, Amadjuak, Akpatok and Foster Bay formations (Zhang, 2011a, 2013a).

After the field season, more than 5000 conodont specimens were recovered from the samples and 56 conodont species representing 38 genera were identified. Based on the stratigraphic distribution of these conodonts, five conodont assemblages were recognized for the first time within the Ordovician sequence on northeastern Melville Peninsula (Zhang, 2011a, 2013a):

- *Oepikodus communis–Jumudontus gananda* Assemblage in units 2–4 of the Ship Point Formation, correlated with the *Reutterodus andinus* Zone in the uppermost Lower Ordovician;
- *Appalachignathus delicatulus–Polyplacognathus ramosus–Belodina confluens* Assemblage in the Frobisher Bay Formation, correlated with the upper Chatfieldian Stage of the lower Upper Ordovician;
- *Belodina confluens–Periodon grandis* Assemblage in the Amadjuak Formation, correlated with the Edenian, Maysvillian and lowest Richmondian stages of the Upper Ordovician;
- *Amorphognathus ordovicicus–Plegagnathus* Assemblage in the Akpatok Formation, correlated with the lower Richmondian Stage of the Upper Ordovician;
- *Rhipidognathus symmetricus–Aphelognathus* cf. *A. divergens* Assemblage in the Foster Bay Formation, correlated with the upper Richmondian Stage of the Upper Ordovician.

Field observations, paleontological data and stratigraphic analysis of northeastern Melville Peninsula were combined with GIS and Google Earth™ technologies to calculate the thickness of different lithostratigraphic units, to recognize faults and calculate fault throw, and to modify the regional geological map. The results of this work reduced the likelihood of Ordovician organic-rich intervals being present on Melville Peninsula to a minimum (Zhang, 2011a, 2013a).

Southern Baffin Island

Southern Baffin Island preserves the stratigraphic record of the southeastern part of the Foxe Basin. The Ordovician sequence on southern Baffin Island includes the Upper Ordovician Frobisher Bay, Amadjuak and Akpatok formations. Their biostratigraphic ages and correlations were better understood than those on Melville Peninsula prior to GEM-1, but there still were some errors and uncertainty. In particular, it was unclear

- what the exact thickness of the organic-rich interval is within the Ordovician succession on southern Baffin Island;
- whether this organic-rich interval is widely distributed;
- whether the stratigraphic position of the Ordovician organic-rich interval is the same as that on Southampton Island; and
- whether the youngest preserved Ordovician strata belong, in fact, to the Foster Bay Formation, as previously interpreted.

In 2011, with funding from the Hudson Bay and Foxe Basins project, the CNGO undertook a Paleozoic stratigraphy project on southern Baffin Island, led by the author. Field studies in 2011 were designed to address the questions listed above. A total of 39 localities was visited throughout the Paleozoic strata on southern Baffin Island and samples were collected from 15 of these localities. A total of 130 carbonate and 46 shale samples was collected for conodont biostratigraphic study and Rock-Eval 6 analysis, respectively. This project (Zhang, 2011d, 2012a, b)

- confirmed that the Upper Ordovician organic-rich interval is about 2 m in thickness in outcrop on southern Baffin Island;
- established that the stratigraphic position of the organic-rich black shale interval is in the lower part of the Upper Ordovician Amadjuak Formation, rather than between the Amadjuak and Akpatok formations as previously interpreted (Figure 2);
- found the organic-rich black shale to have TOC values ranging from 1.68% to 14.9% and averaging about 11%;

- determined that the organic matter is thermally immature and consists of Type I kerogen;
- demonstrated that the organic-rich black shale interval of the lower Amadjuak Formation changes laterally (northwesterly) into inorganic shale, meaning that it does not have a wide geographic distribution on southern Baffin Island;
- recognized, in characteristic rubble, another low-yield shale interval with TOC values ranging from 2.82% to 5.13% and averaging 4.21%, at a higher stratigraphic level (Foster Bay Formation); in fact, this formation has been eroded from the study area; and
- demonstrated that the previously interpreted Foster Bay Formation overlying the Akpatok Formation does not outcrop; the unit has likely been eroded from southern Baffin Island, so modifications were made to the existing geological map of southern Baffin Island.

Hudson Strait Basin

Studying Paleozoic stratigraphy and petroleum potential in the Hudson Strait Basin was part of the GEM-2 Hudson-Ungava project. The Hudson Strait Basin includes present-day Hudson Strait and northern Ungava Bay. In comparison to the Hudson Bay and Foxe basins, it is a relatively small Paleozoic sedimentary basin in the Hudson Platform area (Figure 1). Akpatok Island is the only location where Paleozoic strata are exposed in the basin.

This basin was explored for hydrocarbon resources in the 1970s at a reconnaissance scale, including drilling a number of shallow drillholes in the offshore area by GSC-Atlantic and a single drillhole on Akpatok Island by Premium Iron Ores Ltd. There were no detailed stratigraphic studies in the basin before GEM-2 launched in 2014. Based on limited data, the previous interpretations were that 1) Akpatok Island is underlain almost entirely by the Akpatok Formation, 2) the Upper Ordovician Amadjuak Formation is exposed only near the shoreline, and 3) the organic-rich interval is located between the Amadjuak and Akpatok formations.

Prior to the Hudson-Ungava project

In order to test whether the organic-rich rocks occur in the Hudson Strait offshore area, the author collected samples (Zhang, 2013b) from the Ordovician short cores obtained from six stations (Figure 1) during two cruises in Hudson Strait by GSC-Atlantic during the 1980s. The short core from one of the six stations contains black shale laminated with limestone; 11 samples were collected from the black shale lamination for Rock-Eval 6 analysis. These samples contain TOC ranging from 0.34% to 12.78% and averaging 2.8%. This was the first time that the petroleum source rock was confirmed to occur in the Hudson Strait Basin but, unfortunately, these source rocks are thermally immature (Zhang, 2013b).

During the Hudson-Ungava project

Akpatok Island is located at the junction between Hudson Strait and Ungava Bay (Figure 1) and is the only location where the Paleozoic rocks are exposed in the Hudson Strait Basin; therefore, it is very important in understanding the Paleozoic geology of the basin. The CNGO played a key role in enhancing knowledge of the Ordovician stratigraphy and petroleum potential on the island.

Work on core collection from Akpatok Island

The Premium Homestead Akpatok F-26 well, drilled on Akpatok Island in 1969, penetrated the Ordovician Ship Point Formation, which is not exposed on the island. The author collected 41 samples from the existing cores from this well for Rock-Eval 6 programmed pyrolysis. The rocks of the Ship Point Formation in the core are thermally immature with poor to fair petroleum source-rock potential (Zhang, 2014).

Geological reconnaissance on Akpatok Island

A one-day geological reconnaissance of Akpatok Island was carried out by the CNGO, led by the author, on August 15, 2014 (Zhang and Mate, 2015). Ten localities were visited, and thirteen and five samples were collected for processing of conodonts and Rock-Eval 6 analysis, respectively. This reconnaissance resulted in

- identification of the organic-rich rocks among frost-shattered rubble of uncertain stratigraphic position;
- recognition that the Ordovician sequence on Akpatok Island contains good to very good petroleum source rocks with average and maximum TOC values of 3.11% and 4.19%, but they are thermally immature; and
- identification of outcrops with workable sections at different elevations across the island.

This reconnaissance provided essential first-hand data for more detailed stratigraphic fieldwork and helped in a preliminary assessment of the hydrocarbon source-rock potential in Ungava Bay and the Hudson Strait (Zhang and Mate, 2015).

Detailed field investigations on Akpatok Island

In 2015, the GSC and the CNGO co-operated in a field investigation on Akpatok Island, led by the author and based on the reconnaissance visit of 2014 (Zhang and Mate, 2015). The detailed fieldwork focused on four selected areas, which cover all the elevations from the shoreline to the top of the island and contain the entire exposed Ordovician sequence. In the four areas, sections were measured and sampled at more than 20 localities. Ninety samples were collected from the entire exposed Ordovician sequence for conodont processing, and some graptolite specimens were collected from the organic-rich rubble. The field and post-field studies (Zhang, 2017a, 2018a, b; Zhang and Riva, 2018; Figure 2) resulted in

- recovering over 22 000 conodont elements from 66 productive samples from both outcrops and rubble at more than 20 localities in four areas;
- establishing four Upper Ordovician conodont zones, namely 1) *Belodina confluens* and *Oulodus velicuspis* interval zones, confined to the Amadjuak Formation and correlated with Edenian and Maysvillian; 2) *Amorphognathus ordovicicus–Plegagnathus dartoni* Concurrent-range Zone, restricted to the Akpatok Formation and correlated with lower Richmondian; and 3) *Rhipidognathus symmetricus* Taxon-range Zone, restricted to the Foster Bay Formation and correlated with upper Richmondian;
- ascertaining the lithostratigraphic units on the island, including the upper Amadjuak Formation and the Akpatok and Foster Bay formations, rather than only the Amadjuak and Akpatok formations, which was especially important, given that nearly the upper half of the island was shown to be underlain by the Foster Bay Formation;
- determining that the stratigraphic position of the organic-rich interval on Akpatok Island is within the lower Foster Bay Formation, rather than between the Amadjuak and Akpatok formations as previously interpreted, based on both conodonts (*Amorphognathus ordovicicus*) and graptolites (*Anticostia decipiens* and *Rectograptus socialis*) recovered from the organic-rich rubble; and
- enabling accurate calculations of the thicknesses of different lithostratigraphic units and substantially revising the geological map of Akpatok Island, based on field observations, paleontological data and stratigraphic analysis, in conjunction with GIS technology.

Stratigraphic position and age of the Ordovician organic-rich intervals in the northern Hudson Bay, Hudson Strait and Foxe basins in view of the graptolites

As mentioned earlier, the organic-rich intervals in the Upper Ordovician succession were found on Southampton, Akpatok and southern Baffin islands, and represent the petroleum source rocks in the northern Hudson Bay, Hudson Strait and Foxe basins. Before the GEM program, these organic-rich intervals were named the Boas River Formation, and their stratigraphic position was interpreted as being between the Bad Cache Rapids and Churchill River groups, or the Amadjuak and Akpatok formations, with an age of Maysvillian (Figure 2).

During the GEM program, the author had paid particular attention to the graptolites preserved in the organic-rich intervals and rubble at the three locations (Zhang and Riva, 2018). The graptolites provide a reliable age assessment for the Upper Ordovician petroleum source rocks in the northern Hudson Bay, Hudson Strait and Foxe basins. These graptolites are characterized by

- *Anticostia lata* and *Anticostia hudsoni* in the lower Red Head Rapids Formation on Southampton Island;
- *Anticostia decipiens* and *Rectograptus socialis* in the lower Foster Bay Formation on Akpatok Island; and
- *Diplacanthograptus spiniferus* and *Amplexograptus praetypicalis* in the lower Amadjuak Formation on southern Baffin Island.

These data suggest that the organic-rich intervals in the northern Hudson Bay and Hudson Strait basins can be correlated with the *Paraorthograptus pacificus* Zone of the upper Katian, and the horizon in the Foxe Basin with the *Diplacanthograptus spiniferus* Zone of the lower Katian (Figure 2). The correlation based on the graptolites strongly supports that based on the conodonts (Zhang, 2011c, 2018a, b, 2019). Use of the Boas River Formation is not deemed appropriate, because it occurs as an organic-rich interbed in different stratigraphic units in different basins; therefore, it is suggested that the Boas River Formation be abandoned as a stratigraphic term (Zhang and Riva, 2018; Zhang, 2019). This was the first time in the history of the study of the northern Hudson Bay, Hudson Strait and Foxe basins that the stratigraphic position and age of the petroleum source rocks were correctly determined based on detailed field investigations and strong paleontological evidence from both conodont and graptolite distributions (Figure 2).

Baffin Bay Basin

Organic-rich black shale from shallow drillholes along the northeastern and southeastern Baffin Shelf

Evaluation of the petroleum potential in the Baffin Bay area was designated as one of the GEM energy-related projects. It is known, from the 1970s, that oil seeps have been found at the sea surface off the Scott Inlet area; however, it has not been confirmed whether the oil seeps originated from Paleozoic source rocks or Mesozoic–Cenozoic source rocks. In an attempt to answer this question, the author accessed the short-core and piston-core collections made by GSC-Atlantic along the northeastern and southeastern Baffin Shelf during the 1970s and 1980s.

Forty-eight samples were collected from short cores and piston cores at 21 stations during six cruises (75009, 77027, 78029, 80028, 82034 and 85027) in the northeastern and southeastern Baffin Shelf area (Figure 1). These samples were analyzed for both Rock-Eval 6 and vitrinite reflectance data collection (Zhang, 2013b). Thirty-four of the 48 samples were from Cretaceous/Paleogene short cores and piston cores. The majority of these samples contain TOC between 1% and 15.82% and hydrogen index (HI) between 23 and 153, which can be evaluated as a good or very good source rock. The HI/oxygen index (OI) and the Tmax values for all the samples from the short cores show that these

Cretaceous/Paleogene source rocks contain immature Type III kerogen, an indication of gas-prone source rock.

The oil seeps and what were considered to be 'oily materials' observed at the sea surface off Scott Inlet are presumed to have originated from mature oil-prone source rocks that contain Type I or Type II kerogen. Regionally, source rocks containing Type I or Type II kerogen have been discovered within Upper Ordovician strata on Southampton Island (Zhang, 2007, 2008a, b), southern Baffin Island (Zhang, 2011d, 2012a, b) and Akpatok Island (Zhang and Mate, 2015). Such rocks were also found to be present on Hall Peninsula (Zhang et al., 2014a, b; see discussion below) and in Hudson Strait (Zhang, 2013b). All of this evidence suggests that the observed oil seeps and oily materials off Scott Inlet may have originated from the Ordovician source rocks, which were then overlain by Cretaceous/Paleogene strata, creating sufficient load to generate oil. Therefore, Zhang (2013b) emphasized that a target for source rocks in the northeastern and southeastern Baffin Shelf area should be the Ordovician source rocks where they have been deeply buried by Cretaceous/Paleogene deposits.

Carbonate xenoliths from Hall Peninsula

From 2013 to 2020, the CNGO conducted a research project in collaboration with the mineral exploration company Peregrine Diamonds (now De Beers Group) to study the carbonate xenoliths collected by the company's drilling campaigns during diamond exploration on Hall Peninsula. Although this xenolith project was not financially supported by the GEM program, its results provide valuable data for both the GEM Baffin Bay Basins and Hudson Bay and Foxe Basins projects.

Hall Peninsula, located on southeastern Baffin Island, hosts the Chidliak kimberlite province. There is no Phanerozoic sedimentary cover in this area, only unconsolidated glacial deposits. However, Late Ordovician and early Silurian conodonts have been recovered from carbonate xenoliths preserved in the Late Jurassic–Early Cretaceous kimberlites. These xenoliths provide a rare opportunity to study the Paleozoic history of the present-day Precambrian country.

A total of 185 carbonate xenolith samples was collected from 36 drillholes in 15 kimberlites, from which more than 2200 well-preserved conodont specimens were recovered. These conodonts are of Late Ordovician and early Silurian age (Zhang and Pell, 2013a, b, 2014, 2016, 2020), thus providing evidence that

- the Upper Ordovician Frobisher Bay, Amadjuak, Akpatok and Foster Bay formations and lower Silurian Severn River Formation were once present on Hall Peninsula;
- the combined thickness of lower Paleozoic strata that were present at the time of kimberlite emplacement is about 270–305 m, and these strata were totally eroded from Hall Peninsula sometime between the Early Cretaceous and today at a minimum erosion rate of 2 m/m.y.; and
- the conodont CAI values of the more than 2200 conodont specimens from Hall Peninsula have a wider range (1.5–8) than anywhere else in Canada and are independent of depth, which is important information for the study of kimberlite-emplacement processes.

Organic-rich black shale xenoliths from Hall Peninsula

A Late Ordovician–early Silurian organic-rich black shale xenolith was discovered from one drillhole (CHI-482-10-DD01) in kimberlite CH-31 on Hall Peninsula. Rock-Eval 6 analysis on the samples from this xenolith shows that it contains average and maximum TOC of 8.04% and 8.96%, with Type II kerogen. The xenolith represents an excellent oil-prone source rock. It provides strong evidence that the natural petroleum seeps in the Baffin Bay area, especially in Cumberland Sound, may have originated from the lower Paleozoic source rocks, rather than from the Cretaceous rocks as previously interpreted. The lower Paleozoic rocks were then overlain by Cretaceous rocks, creating sufficient load to generate oil in the active petroleum system (Zhang et al., 2014a, b).

Boothia Peninsula

The Integrated Geoscience of the Northwest Passage: Boothia Peninsula–Somerset Island activity was part of phase 2 of the GEM program. This project contained three subprojects: Precambrian mapping, Paleozoic stratigraphy and surficial mapping. The author led and performed the field and post-field studies for the Paleozoic stratigraphy subproject on Boothia Peninsula.

Fieldwork in the summer of 2017 (Zhang, 2017b) focused on sampling carbonate rocks within the Cambrian and Ordovician sequence at two locations on the peninsula: Lord Lindsay River and Pasley Bay. The two locations are the type localities of the Netsilik and Franklin Strait formations, named in the 1970s. The type localities of the two formations are located in two different geological settings: that of the Netsilik Formation was not disturbed by structural deformation, but that of the Franklin Strait Formation was overturned by the Boothia Uplift. However, the age of the formations, the relationship between them, and their stratigraphic correlation with the well-established Cambrian and Ordovician units of the Arctic islands have been poorly understood since the 1970s. Resolution of these issues was the focus of this subproject.

The outputs (Zhang, 2017b, 2020a, b, work in progress [Lower and Upper Ordovician conodont biostratigraphy and revised lithostratigraphy in the fault and fold zones of

Boothia Uplift, southwestern Boothia Peninsula, Nunavut]) of this subproject are summarized as follows:

- Thirty-five conodont species were recognized among more than 640 identifiable conodont specimens from 23 conodont-bearing samples, out of 50 samples collected at 12 localities along Lord Lindsay River, the type section of the Netsilik Formation.
- Forty-one conodont species were recognized among nearly 1000 conodont specimens from 39 conodont-bearing samples out of 53 samples collected at Pasley Bay, the type section of the Franklin Strait Formation.
- One upper Cambrian and four Lower Ordovician North American standard conodont zone/subzone–equivalent faunas were recognized from the Lord Lindsay River section, namely the upper Cambrian *Hirsutodontus hirsutus* Subzone-equivalent fauna and the Lower Ordovician *Cordylodus angulatus*, *Rossodus manitouensis*, *Acodus deltatus*/*Oneotodus costatus* and *Oepikodus communis* Zone-equivalent faunas.
- Five Lower Ordovician and four Upper Ordovician North American standard conodont zone–equivalent faunas were recognized from the Pasley Bay section, namely the Lower Ordovician *Cordylodus angulatus*, *Rossodus manitouensis*, *Acodus deltatus/Oneotodus costatus*, *Oepikodus communis* and *Reutterodus andinus,* and the Upper Ordovician *Belodina confluens*, *Oulodus velicuspis*, *Oulodus robustus* and *Amorphognathus ordovicicus* Zone–equivalent faunas.
- In the stratigraphic framework of the Arctic islands, the Netsilik Formation can be correlated with the lower and upper members of the Turner Cliffs Formation and the lower Ship Point Formation; the Franklin Strait Formation can be redefined as the upper part of the lower member and the upper member of the Turner Cliffs Formation and the Ship Point, Thumb Mountain, Irene Bay and Allen Bay (lower member) formations. Therefore, the upper Netsilik and lower Franklin Strait formations are overlapped.
- The preserved Paleozoic strata can be dated as early Age 10, late Cambrian to Richmondian, Late Ordovician, with the strata of Middle and early Late Ordovician missing.
- Tectonically,
  - the exposed upper Cambrian and Lower Ordovician rocks along Lord Lindsay River are the Paleozoic erosional remnants, which are almost undisturbed by regional faults and folds that formed during the late Silurian–Early Devonian Boothia Uplift;
  - the conodonts establish the age of the youngest preserved strata in this area, which provide direct evidence for what part of the Paleozoic strata has been eroded from the Boothia Peninsula after the late Silurian–Early Devonian Boothia Uplift;
  - the stratigraphic occurrence of the Ordovician rocks at the Pasley Bay section supports the tectonic model (i.e., that the Boothia Uplift is a deep-seated, east-dipping thrust block); and
  - the conodont CAI obtained at the Pasley Bay section quantitatively estimates that the folded rocks near the fault zones could have been heated as much as 10°C over the regional burial temperature.

Assisting GSC colleagues in GEM projects and international co-operation

During the years 2008–2020, the author assisted GSC colleagues in their GEM projects (including the Hudson Bay and Foxe Basins, Hudson-Ungava, Baffin Bay Basins, Baffin Island and Baffin Geological Synthesis projects) and contributed to their publications. The outcomes include

- Cretaceous stratigraphy and petroleum potential in the Baffin Bay basins (MacLean et al., 2014);
- Lower Paleozoic stratigraphy in the Baffin Geological Synthesis (Bingham-Koslowski et al., in press);
- Hudson Bay, Hudson Strait and Foxe basins tectono-sedimentary element (Lavoie et al., 2021; Pinet et al., 2021);
- source-rock and reservoir-rock geochemistry in the Hudson Bay Basin (Lavoie et al., 2011; Reyes et al., 2016; Jiang et al., 2018, 2019; Chen et al., 2020);
- geological framework, basin evolution and hydrocarbon system in the Hudson Bay, Hudson Strait and Foxe basins (Lavoie et al., 2013, 2019); and
- bedrock geological mapping on northern Baffin Island (Saumur et al., 2020).

Additionally, international co-operation (Hefter et al., 2017) has helped in tracing the source of ancient reworked organic matter delivered to the North Atlantic Ocean.

Economic considerations

The aim of the CNGO joining the GEM projects related to energy and Paleozoic stratigraphy was to contribute to the evaluation of the presence of favourable hydrocarbon-system elements (source rocks, maturation, reservoirs) and link these in new hydrocarbon plays for the Hudson Bay, Foxe Basin, Hudson Strait and Baffin Bay regions. The extensive fieldwork and post-field studies of Paleozoic stratigraphy, especially the source-rock stratigraphy, in the regions during the years 2007–2020 have contributed significant new data and led to a better understanding of the petroleum potential of the sedimentary basins. These contributions have considerably increased the understanding of regional petroleum systems, which could eventually assist in focusing future exploration activities. Such exploration activities could result in economic hydrocarbon discoveries, the production of which would add a significant

new element to the economic growth in Nunavut and benefit the northern communities.

Acknowledgments

Financial support for all the projects summarized in this paper was provided by phases 1 and 2 of the Geo-mapping for Energy and Minerals program and from the Canadian Northern Economic Development Agency's Strategic Investment Economic Development program, and logistical support was provided from the Polar Continental Shelf Project programs. All of these are greatly appreciated.

The author expresses sincere thanks to

- the Inuit from Coral Harbour, Sanirajak (formerly Hall Beach) and Taloyoak in Nunavut and Kuujjuaq in northern Quebec, and the national and international students for their assistance during the field seasons;
- the staff in Geological Survey of Canada (GSC)–Atlantic, GSC-Calgary, GSC-Ottawa, GSC-Vancouver, the Manitoba Geological Survey, and the Canada–Nova Scotia Offshore Petroleum Board Geoscience Research Centre for their assistance in collecting drillcore and well-cutting samples, processing conodont samples, taking scanning electron microscope conodont photos and running geochemical analyses;
- Peregrine Diamonds Ltd. and De Beers Group for giving the author permission to collect xenolith samples; and
- C.R. Barnes, University of Victoria, for his review of this manuscript.

Natural Resources Canada, Lands and Minerals Sector contribution 20210526

References

Bingham-Koslowski, N., Zhang, S. and McCartney, T. (in press): Lower Paleozoic strata in the Labrador-Baffin Island region, Newfoundland and Labrador and Nunavut; *in* Geological Synthesis of Baffin Island (Nunavut) and the Labrador-Baffin Seaway, L.T. Dafoe and N. Bingham-Koslowski (ed.), Geological Survey of Canada, Bulletin 608.

Chen, Z., Lavoie, D., Mort, A., Jiang, C., Zhang, S., Liu, X., Reyes, J. and Armstrong, D. 2020: Source rock kinetics and petroleum generation history of the Upper Ordovician calcareous shales of the Hudson Bay Basin and surrounding areas; Fuel, v. 270, June 2020, URL <https://doi.org/10.1016/j.fuel.2020.117503>.

Hefter, J., Naafs, A.D.B. and Zhang, S. 2017: Tracing the source of ancient reworked organic matter delivered to the North Atlantic Ocean during Heinrich Events; Geochimica et Cosmochimica Acta, v. 205, p. 211–225.

Jiang, C., Reyes, J., Snowdon, L.R., Milovic, M., Robinson, R., Zhang, S., Armstrong, D. and Lavoie, D. 2018: Cyclopentanones and 2-cyclopenten-1-ones as major products of hydrous pyrolysis of immature organic-rich shales; Organic Geochemistry, v. 122, p. 126–139.

Jiang, C., Zhang, S. and Reyes, J. 2019: Black shale xenolith in a Jurassic-Cretaceous kimberlite and organic-rich Upper Ordovician shale on Baffin Island, Canada: a comparison of their organic matter; Marine and Petroleum Geology, v. 103, p. 202–215.

Lavoie, D., Pinet, N., Dietrich, J., Zhang, S., Hu, K., Asselin, E., Chen, Z., Bertrand, R., Galloway, J., Decker, V., Budkewitsch, P., Armstrong, D., Nicolas, M., Reyes, J., Kohn, B.P., Duchesne, M.J., Brake, V., Keating, P., Craven, J. and Roberts, B. 2013: Geological framework, basin evolution, hydrocarbon system data and conceptual hydrocarbon plays for the Hudson Bay and Foxe basins, Canadian Arctic; Geological Survey of Canada, Open File 7363, 210 p.

Lavoie, D., Pinet, N. and Zhang, S. 2021: Foxe platform and basin tectono-sedimentary element; *in* Arctic Basins, S. Drachev and T. Moore (ed.), The Geological Society of London, Memoir, <https://doi.org/10.1144/M57-2016-27>.

Lavoie, D., Pinet, N., Zhang, S., Reyes, J., Jiang, C., Ardakani, O.H., Savard, M.M., Dhillon, R.S., Chen, Z., Dietrich, J.R., Hu, K., Craven, J.A., Roberts, B., Duchesne, M.J., Brake, V.I., Huot-Vézina, G., Galloway, J.M., McCracken, A.D., Asselin, E., Decker, V. et al. 2019: The Hudson Bay and Strait, Moose River, and Foxe basins: synthesis of the research activities under the Geomapping for Energy and Minerals (GEM) programs 2008–2018; Geological Survey of Canada, Open File 8507, 76 p., URL <https://doi.org/10.4095/314653>.

Lavoie, D., Zhang, S. and Pinet, N. 2011. Hydrothermal dolomites in Hudson Bay platform: preliminary field and geochemical data; Geological Survey of Canada, Open File 7002, 19 p., URL <https://doi:10.4095/289303>.

MacLean, B., Williams, G. and Zhang, S. 2014: New insights into the stratigraphy and petroleum potential of the Baffin shelf's Cretaceous rocks; Bulletin of Canadian Petroleum Geology, v. 63, p. 289–310.

Pinet, N., Lavoie, D. and Zhang, S. 2021: Hudson Strait platform and basins tectono-sedimentary element; *in* Arctic Basins, S. Drachev and T. Moore (ed.), The Geological Society of London, Memoirs, URL <https://doi.org/10.1144/M57-2016-28>.

Reyes, J., Jiang, C., Lavoie, D., Milovic, M., Robinson, R., Zhang, S., Armstrong, D. and Mort, A. 2016: Determination of hydrocarbon generation and expulsion temperature of organic-rich Upper Ordovician shales from Hudson Bay and Foxe basins using modified hydrous pyrolysis, organic petrography, Rock-Eval analysis and organic solvent extraction; Geological Survey of Canada, Open File 8049, 60 p., URL <https://doi.org/10.4095/299254>.

Saumur, B.M., Skipton, D.R., Zhang, S., St-Onge, M.R., Bros, E.R., Acosta-Góngora, P., Kelly, C.J., O'Brien, M.E., Weller, O.M. and Johnston, S.T. 2020: Bedrock geology, Nina Bang Lake, Baffin Island, Nunavut, NTS 37-F west and part of 37-C west; Geological Survey of Canada, Canadian Geoscience Map 404, 1 sheet, scale 1:100 000, URL <https://doi.org/10.4095/314876>.

Zhang, S. 2007: Southampton Island, Nunavut Territory: new discoveries of Ordovician oil shale; Yellowknife Geoscience Forum, 2007, Abstracts, v. 2007, p. 70.

Zhang, S. 2008a: New insight into Ordovician oil shales in Hudson Bay: their number, stratigraphic position, and petroleum potential; Bulletin of Canadian Petroleum Geology, v. 56, p. 300–324.

Zhang, S. 2008b. New insights into Ordovician oil shales, Southampton Island, Nunavut; Canadian Society of Petroleum Geologists Convention, Calgary, Alberta, 2008, URL

<https://geoconvention.com/wp-content/uploads/abstracts/2008/265.pdf> [January 2022].

Zhang, S. 2010: Upper Ordovician stratigraphy and oil shales on Southampton Island – field trip guidebook; Geological Survey of Canada, Open File 6668, 42 p.

Zhang, S. 2011a: Biostratigraphic study in areas lacking outcrops – an example from the Upper Ordovician on Melville Peninsula; Geological Association of Canada–Mineralogical Association of Canada, Joint Annual Meeting, 2011, Abstracts, v. 34, p. 238–239.

Zhang, S. 2011b: Geochemistry data from three oil shale intervals in unit 1, Red Head Rapids Formation (Upper Ordovician) on Southampton Island; Geological Survey of Canada, Open File 6681, 20 p.

Zhang, S. 2011c: Late Ordovician conodont biostratigraphy and the age of oil shale intervals on Southampton Island; Canadian Journal of Earth Sciences, v. 48, p. 619–643.

Zhang, S. 2011d: New understanding of Ordovician stratigraphy and oil shale on southern Baffin Island, Nunavut Territory: preliminary field data; Yellowknife Geoscience Forum, Abstracts, v. 2011, p. 90.

Zhang, S. 2012a: Any source rock potential on southern Baffin Island, Nunavut? – a point of view on Ordovician stratigraphy and oil shale Rock-Eval data; Canadian Society of Petroleum Geologists Convention, Calgary, 2012, URL <https://geoconvention.com/wp-content/uploads/abstracts/2012/009_GC2012_Any_Source_Rock_Potential_Southern_Baffin_Island.pdf> [January 2022].

Zhang, S. 2012b: Ordovician stratigraphy and oil shale, southern Baffin Island, Nunavut – preliminary field and post-field data; Geological Survey of Canada, Open File 7199, 26 p.

Zhang, S. 2013a: Ordovician conodont biostratigraphy and redefinition of the age of lithostratigraphic units on northeastern Melville Peninsula, Nunavut; Canadian Journal of Earth Sciences, v. 50, p. 808–825.

Zhang, S., 2013b: Rock Eval 6 and vitrinite reflectance data from Baffin Island Shelf and Hudson Strait; Geological Survey of Canada, Open File 7341, 32 p., URL <https://doi.org/10.4095/292376>.

Zhang, S. 2014: Rock-Eval 6 data from the Premium Homestead Akpatok F-26 well on Akpatok Island, Nunavut; Geological Survey of Canada, Open File 7627, 23 p., URL <https://doi.org/10.4095/293963>.

Zhang, S. 2017a: New insights into Ordovician stratigraphy and petroleum potential on Akpatok Island and in Ungava Bay; Geological Association of Canada–Mineralogical Association of Canada, Joint Annual Meeting, 2017, Abstracts, v. 40, p. 434.

Zhang, S. 2017b: Report of field activities for Ordovician stratigraphy, Boothia Peninsula, Nunavut – part of the GEM-2 Integrated Geoscience of the Northwest Passage: Boothia Peninsula–Somerset Island Activity; *in S*ummary of Activities 2017, Canada-Nunavut Geoscience Office, p. 13–20, URL <https://m.cngo.ca/wp-content/uploads/Summary_of_Activities_2017-P02-Zhang.pdf> [January 2022].

Zhang, S. 2018a: Conodonts and graptolites as a tool in geo-mapping on Akpatok Island; Canadian Paleontology Conference, Proceedings, v. 15, p. 31–32.

Zhang, S. 2018b: Upper Ordovician conodont biostratigraphy and revised lithostratigraphy and geological map, Akpatok Island, Ungava Bay, Nunavut; Canadian Journal of Earth Sciences, v. 55, p. 52–69.

Zhang, S. 2019: Conodonts as a tool in establishing the age and stratigraphic position of Upper Ordovician petroleum source rock intervals across Hudson Bay Platform, Canada; Geological Society of America, Abstracts with Programs, v. 51, no. 5, no. 88-2, URL <https://gsa.confex.com/gsa/2019AM/webprogram/Paper330999.html> [January 2022].

Zhang, S. 2020a: Upper Cambrian and Lower Ordovician conodont biostratigraphy and revised lithostratigraphy, Boothia Peninsula, Nunavut; Canadian Journal of Earth Sciences, v. 57, p. 1030–1047.

Zhang, S. 2020b: Upper Cambrian and Lower Ordovician conodont biostratigraphy and revised lithostratigraphy, southern Boothia Peninsula, Nunavut; Geoconvention 2020, poster, URL <https://geoconvention.com/wp-content/uploads/abstracts/2020/55690-upper-cambrian-and-lower-ordovician-conodont-biost.pdf> [January 2022].

Zhang, S. and Barnes, C.R. 2007a: Hudson Bay Basin, NE Canada: Late Ordovician–Early Silurian conodont biostratigraphy, thermal maturation, and implications for hydrocarbon generation; Geological Association of Canada–Mineralogical Association of Canada, Joint Annual Meeting, 2007, Abstracts, v. 30, p. 90.

Zhang, S. and Barnes, C.R. 2007b: Late Ordovician–Early Silurian conodont biostratigraphy and thermal maturity, Hudson Bay Basin; Bulletin of Canadian Petroleum Geology, v. 55, p. 179–216.

Zhang, S. and Dewing, K. 2008: Rock-Eval 6 data for four hydrocarbon exploration wells in Hudson Bay and Foxe basins; Geological Survey of Canada, Open File 5872, 25 p., URL <https://doi.org/10.4095/225633>.

Zhang, S. and Hefter, J. 2009: Sea level and paleoenvironment control on Late Ordovician source rocks, Hudson Bay Basin, Canada; AGU Spring Meeting Abstracts, 2009, Abstract CG73B-03, URL <https://ui.adsabs.harvard.edu/abs/2009AGUSMCG73B..03Z/abstract> [January 2022].

Zhang, S. and Hu, K. 2013: Recognition of Devonian hydrocarbon source rocks in Beluga O-23 well, Hudson Bay Basin; Geological Survey of Canada, Open File 7433, 18 p.

Zhang, S. and Lavoie, D. 2013: Studies of Paleozoic stratigraphy and petroleum potential in the Hudson Bay and Foxe basins, Nunavut; *in* Summary of Activities 2012, Canada-Nunavut Geoscience Office, p. 121–130.

Zhang, S. and Mate, D.J. 2015: Geological reconnaissance for Ordovician stratigraphy and petroleum potential, Akpatok Island, Nunavut; *in* Summary of Activities 2014, Canada-Nunavut Geoscience Office, p. 79–88, URL <https://m.cngo.ca/wp-content/uploads/Summary-of-Activities-2014-P10.pdf> [January 2022].

Zhang, S. and Pell, J. 2013a: Conodonts from carbonate xenoliths in Chidliak kimberlites confirm the previous existence of Lower Paleozoic cover on Hall Peninsula, Nunavut and provide temperature estimates; Geological Association of Canada–Mineralogical Association of Canada, Joint Annual Meeting, 2013, Abstracts, v. 36, p. 202–203.

Zhang, S. and Pell, J. 2013b: Study of sedimentary rock xenoliths from kimberlites on Hall Peninsula, Baffin Island, Nunavut; *in* Summary of Activities 2012, Canada-Nunavut Geoscience Office, p. 107–112.

Zhang, S. and Pell, J. 2014: Conodonts recovered from the carbonate xenoliths in the kimberlites confirm the Paleozoic cover on the Hall Peninsula, Nunavut; Canadian Journal of Earth Sciences, v. 51, p. 142–155.

Zhang, S. and Pell, J. 2016: Conodonts and their colour alteration index values from carbonate xenoliths in four kimberlites on Hall Peninsula, Baffin Island, Nunavut; *in* Summary of Activities 2016, Canada-Nunavut Geoscience Office, p. 1–12, URL <https://m.cngo.ca/wp-content/uploads/Summary_of_Activities_2016-P02-Zhang.pdf> [January 2022].

Zhang, S. and Pell, J. 2020: Late Ordovician–early Silurian conodonts and their colour alteration index values from carbonate xenoliths in kimberlite CH-06 on Hall Peninsula, Baffin Island, Nunavut; *in* Summary of Activities 2019, Canada-Nunavut Geoscience Office, p. 1–10, URL <https://m.cngo.ca/wp-content/uploads/Summary_of_Activities_2019-Paper_01.en_.pdf> [January 2022].

Zhang, S. and Riva, J.F. 2018: The stratigraphic position and the age of the Ordovician organic-rich intervals in the northern Hudson Bay, Hudson Strait, and Foxe basins – evidence from graptolites; Canadian Journal of Earth Sciences, v. 55, p. 897–904.

Zhang, S., Creaser, R. and Pell, J. 2014a: Discovery of organic-rich black shale xenolith from kimberlite on the Hall Peninsula, Nunavut and its implication for petroleum potential in Cumberland Sound; Bulletin of Canadian Petroleum Geology, v. 62, p. 125–131, URL <https://doi.org/10.2113/gscpgbull.62.3.125>.

Zhang, S., Creaser, R. and Pell, J. 2014b: Discovery of organic-rich black shale xenoliths from kimberlites, Hall Peninsula, NU – implication for petroleum potential in Cumberland Sound; Geological Association of Canada–Mineralogical Association of Canada, Joint Annual Meeting, 2014, Abstracts, v. 37, p. 296.

Zhang, S., Dewing, K. and Barnes, C.R. 2007: Hydrocarbon potential of the Hudson Bay Basin: new findings from Rock Eval pyrolysis and conodont colour alteration index (CAI) data; Canadian Society of Petroleum Geologists, Gussow Geoscience Conference, 2007, URL <https://www.cspg.org/Gussow/Gussow_Archive/Gussow-Archives.aspx?WebsiteKey=05774a5e-8ef1-49a2-ba4a-1adae6671cad&hkey=c92a974d-b253-4d2e-b6df-88e61db23877&Gussow_Conference_Archives=13#Gussow_Conference_Archives> [January 2022].

Database of the locations of surficial material sample stations in Nunavut

Tommy Tremblay[1] and Serge Basso[2]

[1]*Canada-Nunavut Geoscience Office, Iqaluit, Nunavut, tommy.tremblay@nrcan-rncan.gc.ca*

[2]*Canada-Nunavut Geoscience Office, Iqaluit, Nunavut*

Tremblay, T. and Basso, S. 2022: Database of the locations of surficial material sample stations in Nunavut; *in* Summary of Activities 2021, Canada-Nunavut Geoscience Office, p. 15–20.

Abstract

Data (geochemical, mineralogical and sedimentological) from the analyses of surficial materials in Nunavut, found in various publications and reports, are currently being compiled into a database by the Canada-Nunavut Geoscience Office. This paper presents results of the early processing stage. An initial database was created to include the geographic co-ordinates of all stations where surficial materials were sampled. Associated publications, type of material and survey name are linked to each of the samples. In the future, by adding compilations of the geochemical, mineralogical and sedimentological data for each of the samples, this database will be completed.

Introduction

For Nunavut, an abundance of data are available from online public data repositories but are not fully integrated into a publicly accessible database. In particular, data from geochemical, mineralogical and sedimentological analyses of surficial material samples collected in Nunavut are available in paper and/or digital documents from a variety of sources including the Canada-Nunavut Geoscience Office (CNGO), the Geological Survey of Canada (GSC), academia and the mineral industry. Tremblay and Basso (2021) established a methodology to compile this type of data at the CNGO, partly based on the structure proposed by Adcock et al. (2013), Spirito et al. (2013) and other surveys listed in the Canadian Database of Geochemical Surveys (CDoGS; Natural Resources Canada, 2020). A workflow of three stages was proposed for transforming datasets into directories of spreadsheets (preprocessing), for aggregating the datasets of spreadsheets into relational databases (processing), and for querying and reporting (post-processing) the data. The latter two stages are currently in the initial stages of development using Python and SQLite (SQLite developers, 2020).

This paper presents the process used to compile all samples from preprocessed datasets with the geographic co-ordinates of the sample station, type of material, associated publications and survey name, which will serve as a basis for further inquiries into the data and provide information about the geographic footprint of past/legacy surveys.

Methodology

Data structure

The data structure presented in Tremblay and Basso (2021) has been revised and is shown in Figure 1. The structure shows the various entities and relationships used to capture almost any type of surficial material analytical data. This structure is the basis for the directory of Microsoft® Excel® files and the SQLite database produced in the preprocessing and processing stages, respectively, for a dataset. The nomenclature is briefly recapitulated here and readers can refer to Tremblay and Basso (2021) for more details. Documents of interest are those containing geochemical, mineralogical or sedimentological data; these documents can be published (e.g., CNGO datasets, GSC open files, scientific journals, industry reports, etc.) or unpublished (e.g., analytical data sheets). A survey refers to the geological effort (i.e., sample collection) deployed at a specific time and within a specific region. A sample is the geological material collected in the field and can be described by its name and its affiliation to a survey, and linked to a distinct station name and earth material name. A subsample is named as stated in analytical reports or as reported in documents. Together, metadata types (e.g., method of analysis) and metadata (the value of the metadata; e.g., ICP-MS) characterize specific results. Result types are the quantities or qualities analyzed or observed (e.g., copper concentration) for specific subsamples. Results are the values for result type, subsample and metadata combinations (e.g., 56; Figure 1).

This publication is available, free of charge, as colour digital files in Adobe Acrobat® PDF format from the Canada-Nunavut Geoscience Office website: https://cngo.ca/summary-of-activities/2021/. Il est aussi disponible en français sur https://cngo.ca/fr/.

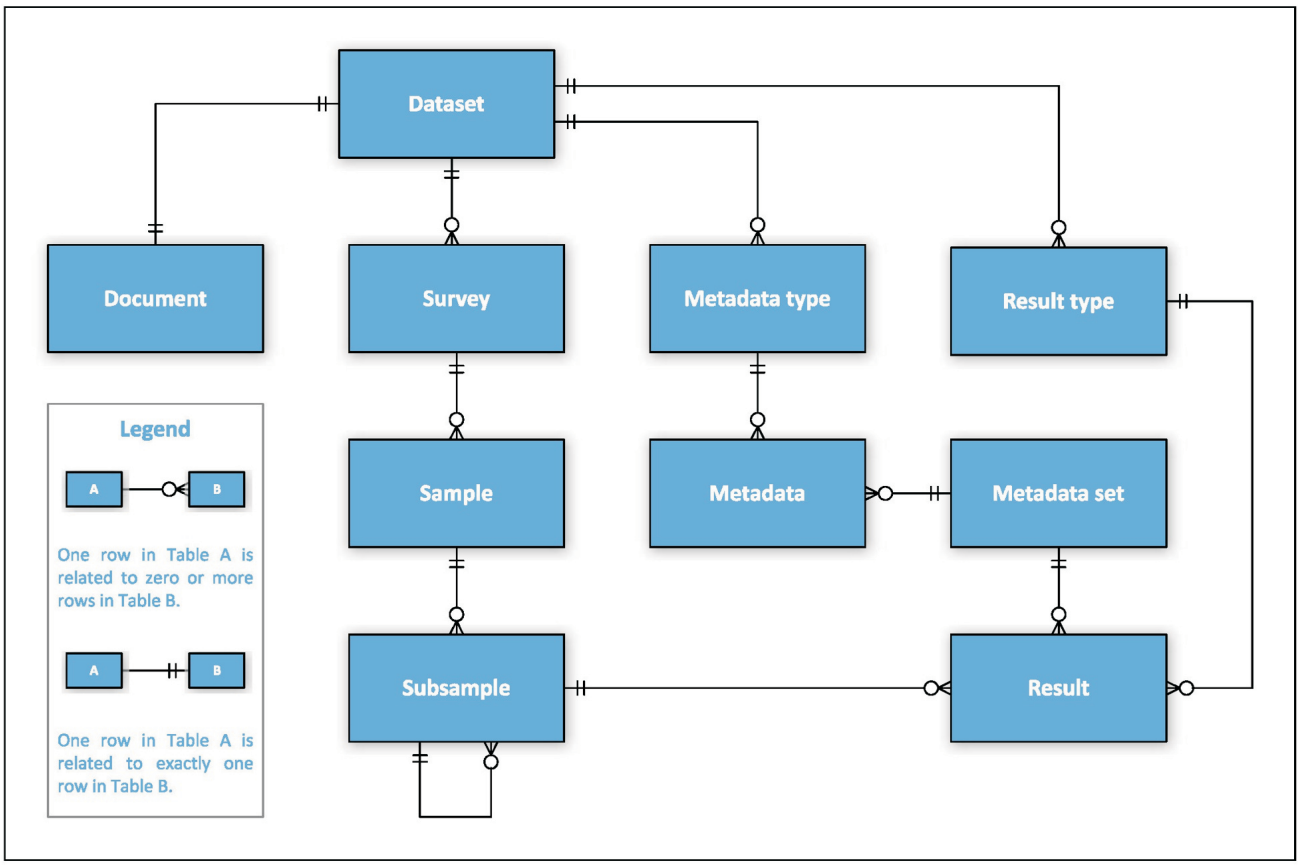

Figure 1: Diagram of data structure for the directory of Microsoft® Excel® files and the SQLite database of analytical data from the surficial materials of Nunavut (modified after Tremblay and Basso, 2021).

Tooling

For the preprocessing stage, the geochemical, mineralogical or sedimentological data from the associated document of a dataset were imported into a directory of Excel files following the methodology described in Tremblay and Basso (2021). A Python package called Geochemistry Dataset (https://github.com/cngo/geochem-dataset/) was developed to provide interfaces that allow users to read datasets in the preprocessed format and read-write datasets in the processed format. Also included in the package is a set of command-line and graphical tools for performing actions on a directory of datasets. Currently, the tools provide the ability to 1) validate datasets in the preprocessed format, and 2) export all samples to a comma-separated value (CSV) file. In development are additional tools to 1) convert datasets from the preprocessed format to the processed format, and 2) combine multiple datasets into a single SQLite database.

Sample extraction from preprocessed datasets

In order to analyze the samples in the preprocessed datasets, the following steps were performed:

1) exporting the samples to a CSV file using the tools in the Geochemistry Dataset package
2) limiting the selection of samples to six earth material types (diamicton, glaciofluvial sediments, gossan, lake sediments, organic material and stream sediments) using R (R Core Team, 2020)

The samples extracted as a result of these procedures are available in Tremblay and Basso (2022)[3]. The samples identified as diamicton are commonly described as till in the documents, and a distinction between till and other diamictons has not been possible for all samples, therefore the term 'diamicton' was chosen to categorize all of the data, including till samples. It should be noted that there may be duplicate samples listed due to more than one dataset (and associated document) referencing the same sample from the same survey.

Results and discussion

Figure 2 shows the locations of surficial material sample stations, categorized into six earth material types. The

[3]*CNGO Geoscience Data Series GDS2022-001, containing the data or other information sources used to compile this paper, is available online to download free of charge at https://cngo.ca/summary-of-activities/2021/.*

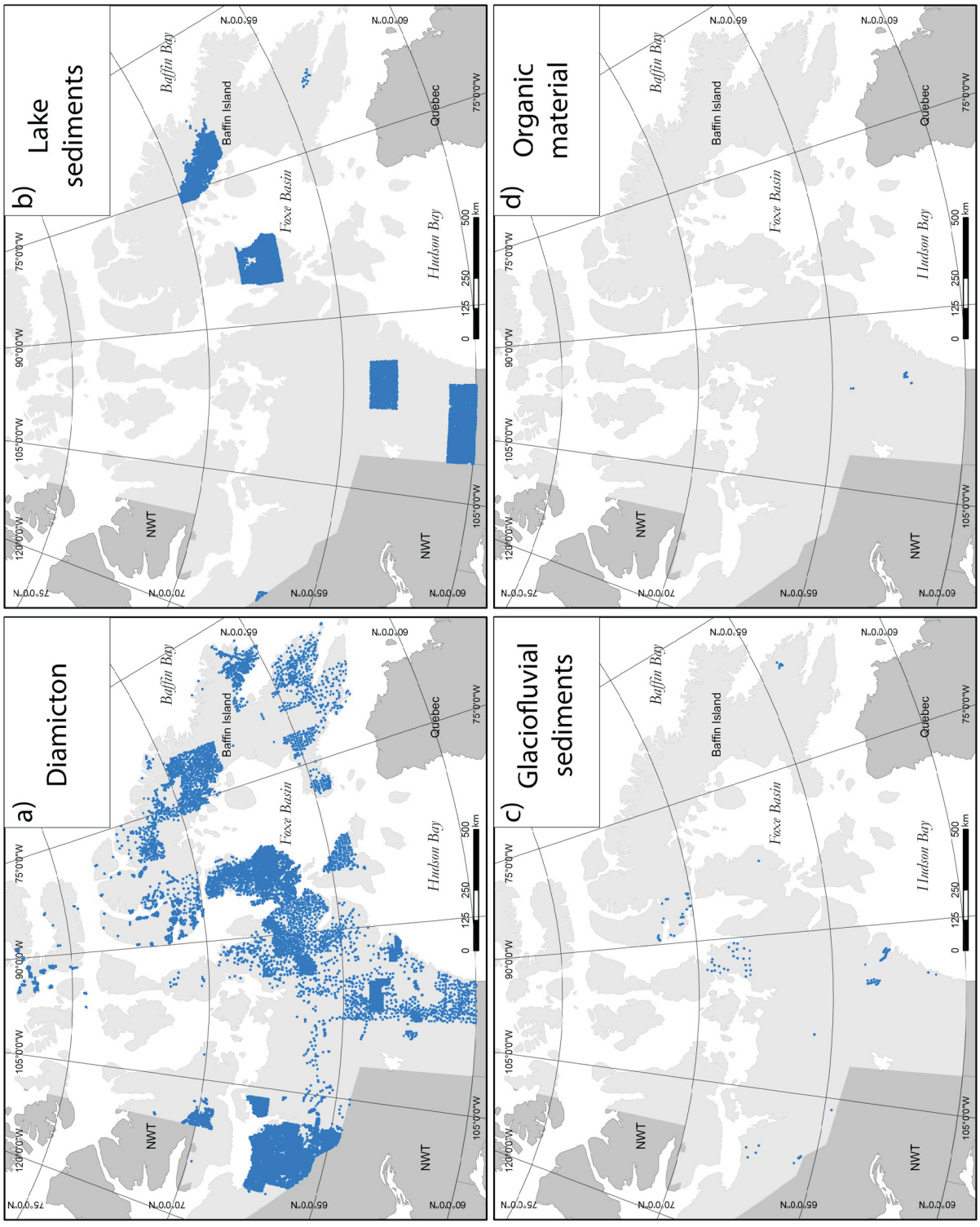

Figure 2: Locations of surficial material sample stations (blue dots) in Nunavut, categorized into earth material type: **a)** diamicton, **b)** lake sediments, **c)** glaciofluvial sediments, **d)** organic material.

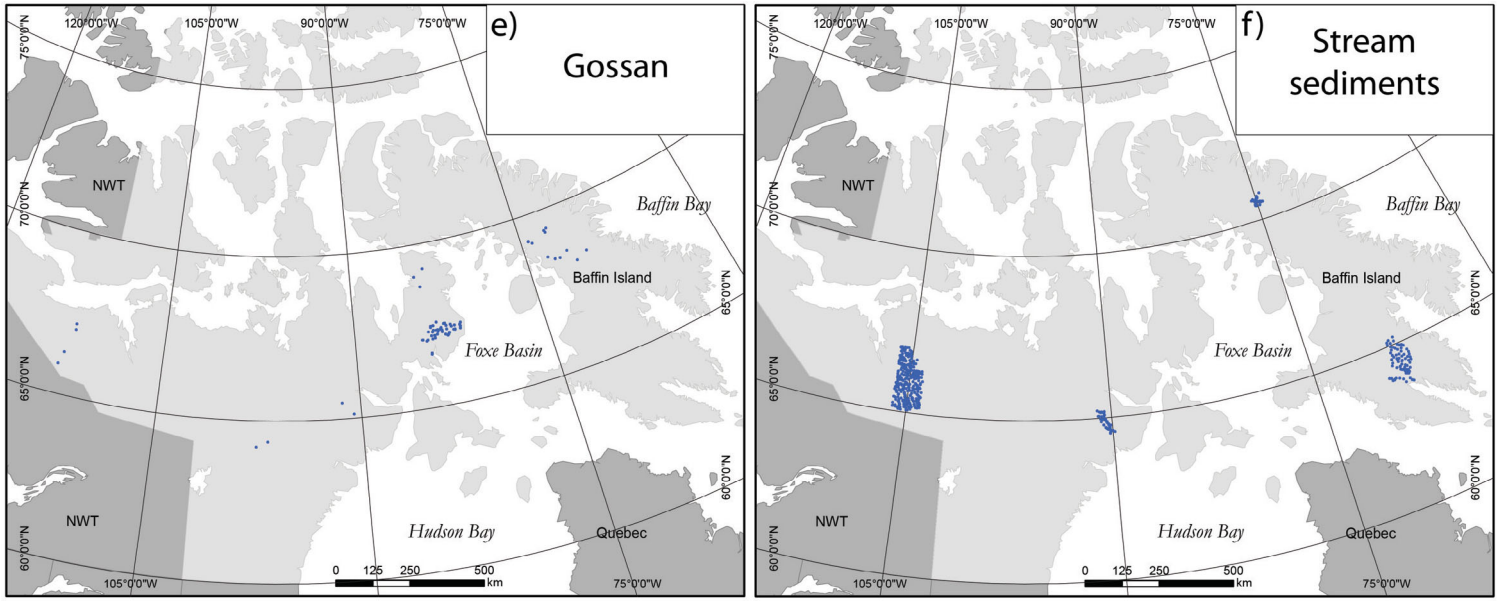

Figure 2 (continued): Locations of surficial material sample stations (blue dots) in Nunavut, categorized into earth material type: **e)** gossan, **f)** stream sediments.

Table 1: Earth material types of samples collected in Nunavut. The organization listed was responsible for the collection of the samples.

	Earth material type							
Organization	Diamicton	Glaciofluvial sediments	Gossan	Lake sediments	Organic material	Stream sediments	Total	Total (%)
CNGO	2437	37	0	17	0	107	2598	5.5
GSC	11 766	221	139	10 224	40	396	22 786	48.6
NTGS	21 222	0	0	0	0	0	21 222	45.2
Others	320	0	0	0	0	0	320	0.7
Total	35 745	258	139	10 241	40	503	46 926	100
Total (%)	76.2	0.5	0.3	21.8	0.1	1.1	100	

Abbreviations: CNGO, Canada-Nunavut Geoscience Office; GSC, Geological Survey of Canada; NTGS, Northwest Territories Geological Survey

density of samples is spatially heterogeneous, with concentrations in west-central and south-central Nunavut and Baffin Island. There are, however, significant gaps evident in the High Arctic islands, parts of central Baffin Island and near the border with the Northwest Territories. From the total number of 46 926 samples compiled (Table 1), 48.6% are from GSC surveys, 45.2% from the Northwest Territories Geological Survey (NTGS; concentrated in western Nunavut, comprising data mostly compiled from mineral exploration assessment reports), 5.5% from CNGO and 0.7% from other sources (e.g., academic institutions; see Tremblay and Basso, 2022). The breakdown of samples by earth material type is diamicton (76.2%), glaciofluvial sediments (0.5%), gossan (0.3%), lake sediments (21.8%), organic material (0.1%) and stream sediments (1.1%).

Steps were taken to detect and remove many inconsistent entries, duplicate entries and omissions within the published data. However, a definitive review of the data has not yet been undertaken to identify wrong co-ordinates, misspelled sample names, undetected duplicates, misinterpretations of the earth material type, missing documents and incomplete definitions of survey titles. Also, a thorough search for unpublished datasets still needs to be undertaken. The initial effort has focused mainly on government-published data and the next step will be to target other sources (e.g., exploration reports, either already compiled [e.g., NTGS data] or noncompiled).

Summary

The initial database of this project, which contains the geographic locations of surficial materials sample stations and associated information, has been released. The next steps will be to complete the final database with a compilation of the geochemical, mineralogical and sedimentological data for each of the samples. This work represents an important step in data management for geoscience in Nunavut and has numerous implications for future data collection and program development that will benefit all interested stakeholders but particularly the mineral exploration industry and those conducting environmental studies.

Economic considerations

The CNGO database of samples with geochemical, mineralogical or sedimentological data can support applied geology projects in Nunavut in many ways. Some of these ways include helping geoscientists to a) find significant geochemical or mineralogical anomalies of specific elements or commodities within a large portion of Nunavut, b) understand the significance of geochemical anomalies found by other surficial sediment sampling surveys, and c) interpret sedimentary transport processes (e.g., glacial, colluvial, alluvial) and glacial systems as an aid to mineral exploration. The compilation of surficial material sample locations is a helpful tool for geoscience data users in Nunavut as it provides quick access to published information and permits a rapid identification of knowledge gaps for better targeting of fieldwork initiatives.

Acknowledgments

This paper benefited from discussions with A. Plouffe, D. Kerr, P.-M. Godbout, I. McMartin, D. Mate, W. Spirito and S. Adcock. Those who assisted with data compilation included R. Bayne, T. Rowe, C. Mayer, I. Randour and C. Gilbert. The authors thank P.-M. Godbout for reviewing the manuscript.

Natural Resources Canada, Lands and Minerals Sector contribution 20210582.

References

Adcock, S.W., Spirito, W.A. and Garrett, R.G. 2013: Geochemical data management – issues and solutions; Geochemistry: Exploration, Environment, Analysis, v. 13, p. 337–348.

Natural Resources Canada 2020: Canadian Database of Geochemical Surveys; Natural Resources Canada, URL <https://geochem.nrcan.gc.ca/cdogs/content/main/home_en.htm> [November 2020].

R Core Team 2020: R: a language and environment for statistical computing; R Foundation for Statistical Computing, Vienna, Austria.

Spirito, W.A., Adcock, S.W. and Paulen, R. 2013: Managing geochemical data: challenges and best practices; *in* New Frontiers for Exploration in Glaciated Terrain, R.C. Paulen and

M.B. McClenaghan (ed.), Geological Survey of Canada, Open File 7374, p. 21–26.

SQLite developers 2020: SQLite; Hipp, Wyrick & Company, Inc., URL <https://www.sqlite.org/appfileformat.html> [November 2020].

Tremblay, T. and Basso, S. 2021: Compiling data from the analysis of surficial materials in Nunavut into a database at the Canada-Nunavut Geoscience Office; *in* Summary of Activities 2020, Canada-Nunavut Geoscience Office, p. 93–100, URL <https://m.cngo.ca/wp-content/uploads/CNGO-SOA2020-Paper-10-Tremblay-and-Basso.en_.pdf> [January 2022].

Tremblay, T. and Basso, S. 2022: Data tables accompanying "Database of the locations of surficial material sample stations in Nunavut"; Canada-Nunavut Geoscience Office, Geoscience Data Series GDS2022-001, Microsoft® Excel® file, URL <https://cngo.ca/summary-of-activities/2021/>.

Studies of the Frobisher Bay half-graben: X-ray diffraction analysis of fault gouges exposed in the Iqaluit area, Baffin Island, Nunavut

Farah Gagnier[1], Benoit M. Saumur[2], Tommy Tremblay[3], Lorraine Lebeau[3], Christian Sasseville[4] and Michel Preda[2]

[1]*Département des sciences de la Terre et de l'atmosphère, Université du Québec à Montréal, Montréal, Québec, gagnier.farah@courrier.uqam.ca*

[2]*Département des sciences de la Terre et de l'atmosphère, Université du Québec à Montréal, Montréal, Québec*

[3]*Canada-Nunavut Geoscience Office, Iqaluit, Nunavut*

[4]*Ministère de l'Énergie et des Ressources naturelles, Direction régionale Nord-du-Québec, Chibougamau, Québec*

Gagnier, F., Saumur, B.M., Tremblay, T., Lebeau, L., Sasseville, C. and Preda, M. 2022: Studies of the Frobisher Bay half-graben: X-ray diffraction analysis of fault gouges exposed in the Iqaluit area, Baffin Island, Nunavut; *in* Summary of Activities 2021, Canada-Nunavut Geoscience Office, p. 21–30.

Abstract

The various Neoproterozoic to Eocene extensional events that have occurred in the Canadian Arctic still give rise to many questions due to a lack of geochronological and structural data. The Frobisher Bay half-graben, which is partially exposed in the Iqaluit area, represents just one of the brittle extension systems found on the southeast Arctic Platform. Recent excavations in Iqaluit have revealed normal faults of the Frobisher Bay system, thus making the sector conducive to geochronological sampling as well as recording of structural data on the kinematics and geometry of the half-graben.

By studying the fault system, it was possible to map the brittle deformation observed in the Iqaluit area, where a conjugate normal-oblique fault system trending northwest and southeast is defined. Samples carefully recovered from fault gouge were analyzed using X-ray diffraction that revealed the presence of a significant amount of illite, an authigenic mineral essential to potassium-argon dating. Chlorite is nevertheless the dominant authigenic mineral in the coarse-grained (0–2 μm) fraction of the analyzed sample. The occurrence of these two authigenic minerals made it possible to determine a temperature interval (220 to 350°C) and to identify propylitic alteration associated with regional hydrothermal processes.

Introduction

The eastern coast of Baffin Island plays a key role in the understanding of the geodynamic evolution of the Canadian Arctic in an extensional setting, particularly with respect to the opening of the Labrador Sea–Baffin Bay brittle deformation corridor in the late Mesozoic to early Cenozoic (Chalmers and Pulvertaft, 2001; Larsen et al., 2009). However, extensional events also occurred before and during the Paleozoic. Therefore, extension age locally associated with the Frobisher Bay half-graben could easily be as early as the Neoproterozoic (Sanford and Grant, 1990, 1998) or as late as the Eocene (Chalmers and Pulvertaft, 2001). The lack of quantitative geochronological data, as well as of mapping data documenting the geometry and kinematics of the brittle faults in the area, gives rise to a number of fundamental questions related to the mechanisms of extension, including those questions regarding the age of the formation and/or the reactivation of the numerous Canadian Arctic fault zones.

The Frobisher Bay half-graben is an extensional kinematics fault zone. The structural and geochronological study of faults in this half-graben could provide geodynamic and temporal constraints on the tectonic evolution of regional extension and exhumation. Recent excavations in Iqaluit have produced fresh exposures of fault surfaces in this half-graben, also exposing fault gouge potentially rich in datable clay minerals such as illite, a potassium-bearing phyllosilicate used in potassium-argon dating (K-Ar; Clauer and Chadhuri, 1995).

This paper outlines mapping done during the summers of 2020 and 2021 in the Iqaluit area, Nunavut, and presents the preliminary mineralogical results from X-ray diffraction analysis of fault gouge recovered along a Frobisher Bay fault exposed in the Iqaluit area. This work provides infor-

This publication is available, free of charge, as colour digital files in Adobe Acrobat® PDF format from the Canada-Nunavut Geoscience Office website: https://cngo.ca/summary-of-activities/2021/. Il est aussi disponible en français sur https://cngo.ca/fr/.

This is a translation of a paper originally submitted in French that can be found in Sommaire des activités 2021.

mation on the type of hydrothermal alteration in the study area as well as first-order mineralogical constraints useful to future geochronological studies. The sample preparation and laboratory analysis procedures specific to clays, which must be followed to obtain the illite concentrates required for K-Ar dating, are also described.

Geological setting

The study area is located in the Frobisher Bay half-graben, which is exposed in the Iqaluit region and controls, at least partially, the geometry of Frobisher Bay. This half-graben crosscuts Paleoproterozoic intrusive units (1.865–1.845 Ga) of the Cumberland batholith (Scott, 1999; Whalen et al., 2010). The roughly 221 000 km^2 Cumberland batholith was formed during the Trans-Hudson Orogen, which involved the collision of two cratonic blocks, the Superior Craton in the southeast and the Rae Craton in the northwest, as well as of many other crustal blocks and volcanic arc terranes. Collision of the Meta Incognita microcontinent with the Rae Craton ended at 1.865 Ga, when post-collisional plutonism leading to the formation of the Cumberland batholith started (St-Onge et al., 2006). The batholith consists mostly of subcrustal felsic granite and continental magmatic arc granite, with minor intrusions of granulite-facies mafic rocks. The southern part of the batholith, in the Iqaluit area, comprises massive or weakly foliated monzogranitic to syenogranitic rocks (Whalen et al., 2010).

Frobisher Bay is located on the eastern margin of the southeast Arctic Platform (Figure 1). During the middle to late Paleozoic, marine sediment deposition on the platform was structurally controlled by several arches that run perpendicular to each other (Sanford and Grant, 2000). Arch orientation appears closely linked to the closely spaced (1 km), pre-existing fault system. These faults were interpreted to predate the late Proterozoic since the basin north of Baffin Island is bounded by northwest-trending faults bordering the late Proterozoic Bylot Supergroup (Sanford and Grant, 1990, 1998). These pre-existing, northwest-trending faults were reactivated many times during the Paleozoic, mainly during the late Silurian as well as during the Cretaceous. Fault reactivation seems to have been the result of basement uplift, which was the cause of late Silurian epeirogenesis, followed by a final episode of major uplift that led to the formation of the Eastern Arctic half-grabens during the Cretaceous (Sanford and Grant, 2000).

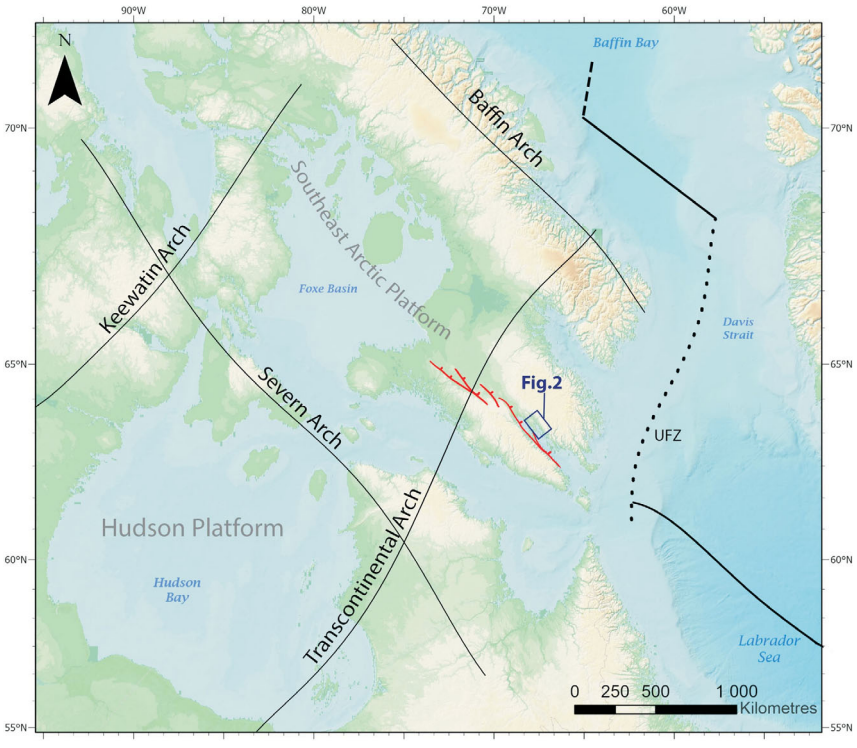

Figure 1: Location of Iqaluit relative to the arches formed during Phanerozoic tectonic events on the southeast Arctic Platform and Hudson Platform (Sanford and Grant, 2000): the red lines represent normal faults that formed the Frobisher Bay half-graben (Sanford and Grant, 1998); the thick black lines indicate the approximate location of earlier openings of the Labrador Sea and Baffin Bay (Chalmers and Pulvertaft, 2001); the dashed line indicates the area of transtensional deformation (Chalmers and Pulvertaft, 2001); and the dotted line indicates the Ungava fault zone (UFZ; Chalmers and Pulvertaft, 2001). The location of Figure 2 is also shown. Background created in ArcGIS Pro. Portions of this figure include intellectual property of Esri® and its licensors and are used under license. Copyright 2021 Esri and its licensors. All rights reserved.

From the late Mesozoic to the late Cenozoic, extension movement led to the formation of the Labrador Sea, Davis Strait and Baffin Bay. Larsen et al. (2009) stated that the ages yielded by West Greenland dyke samples indicate that extension of the proto-Baffin Bay and Labrador Sea started sometime between 223 and 150 Ma. Dyke composition became poorer in silica and richer in alkaline and volatile elements 150 Ma ago, during the Late Jurassic, which would indicate that the rate of extension had increased, leading to the start of rifting in the Labrador Sea at the end of the Cretaceous (Watt, 1969). During the Paleocene, the stress caused by Labrador Sea extension was weakly redirected and extended toward the north, leading to the formation of Baffin Bay. The opening of the Labrador Sea and Baffin Bay, separated by the Hudson Strait, created a transtensional extension coeval with the appearance of the proto-Iceland mantle plume at ca. 62 Ma (Gerlings et al., 2009). The extension of the Labrador Sea and Baffin Bay

would have ended during the mid-Eocene, based on volcanic event ages obtained by Chalmers and Pulvertaft (2001). Given the proximity of Baffin Island to this extension zone, the normal faults found there, including those of the Frobisher Bay half-graben, are considered to have been potentially reactivated during that extension period. However, sedimentation and exhumation rate studies have shown that the Labrador Sea rift had no effect on the southeastern part of Baffin Island. In fact, Creason (2015) suggested that there was no reactivation of the faults bounding the half-grabens from the late Mesozoic to the late Cenozoic since the U-Th-Sm/He apatite and zircon ages, which range from 843 to 75 Ma and from 1067 to 326 Ma, respectively, indicate that cooling occurred slowly due to a slow and constant rate of exhumation.

Sampling strategies and mapping

Site location and sampling were determined based on future work involving K-Ar dating of fault gouge from the Frobisher Bay half-graben as well as obtaining structural and other geochronological data using several different methods (e.g., fission-track analysis). These age data will help characterize the still largely unknown extensional geodynamics of the Iqaluit area.

Sanford and Grant (2000) suggested that the major faults responsible for the geometry of the Frobisher Bay half-graben were northwest-trending normal faults associated with a subordinate population of southeast-trending faults. Fieldwork in the Iqaluit area was mainly done during summer 2021, although preliminary sampling had been undertaken during summer 2020, when a total of 17 sites were visited (Figure 2). During summer 2021, structural measurements of fault planes and joints were documented at 13 sites on the northern shore of the Frobisher Bay half-graben. Compilation of the structural data revealed a system of conjugate normal faults at the local scale, which is consistent with two fault populations observed at the regional scale by Sanford and Grant (2000) and consisting of

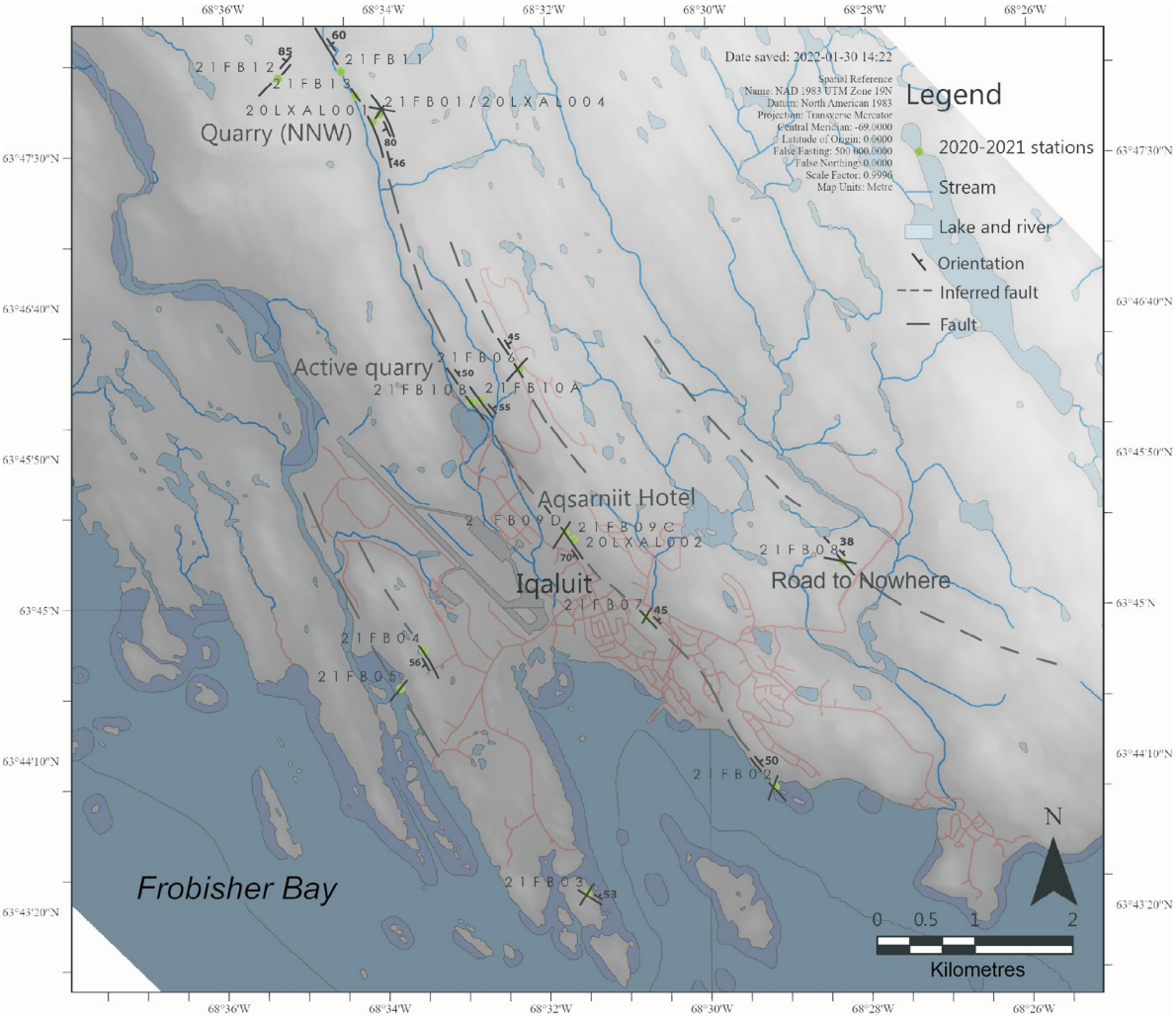

Figure 2: Stations studied and faults recorded in the Iqaluit area during the summers of 2020 and 2021. Background digital elevation model at 1 m resolution from 2010 WorldView images ©DigitalGlobe, Inc. all rights reserved.

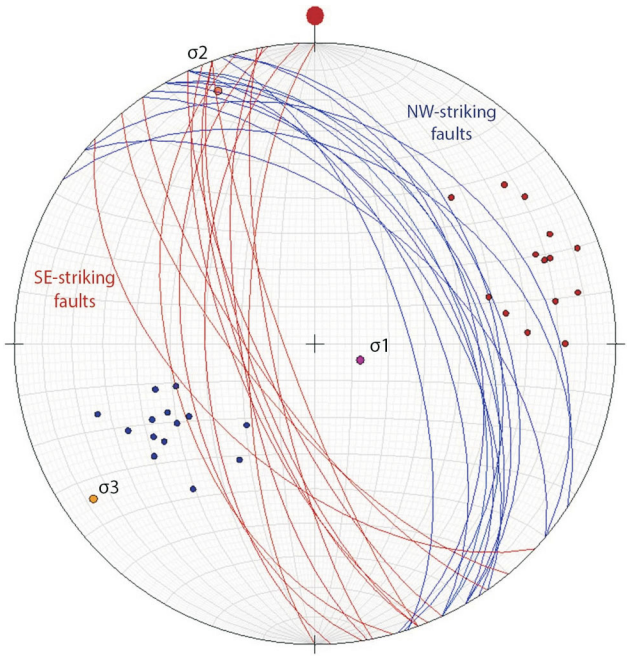

Figure 3: Stereographic projection (lower hemisphere) of the southeast- and northwest-dipping faults, where 1σ represents maximum stress, 2σ intermediate stress and 3σ minimal stress calculated from the data.

a first group of southeast-striking, moderately dipping (70°) faults and a second group of northwest-striking, moderately dipping (50°) faults (Figure 3). Fault striae observed on southeast-striking fault planes at outcrops 21FB01D01 and 21FB09C02 show normal motion with a strike-slip component varying from dextral to sinistral on various fault planes (Figure 4a). The fault striae observed on the northwest-striking fault plane of outcrop 21FB02A01 also show normal motion.

Sampling in this study focused on fault gouge from the Frobisher Bay half-graben resulting from authigenic hydrothermal alteration. A variety of authigenic clay minerals can form in fault gouge (e.g., smectite group, illite, kaolinite group, pyrophyllite, biotite), depending in particular on the composition of the hostrock as well as on temperature conditions at the time the breccia was formed (Fulignati, 2020). The occurrence of authigenic illite, a potassium-rich clay, is important as it is essential to K-Ar dating (Clauer and Chadhuri, 1995), which yields ages corresponding to temperature intervals that can generally reach above 200 to 220°C, and up to 350°C if the illite is a product of K-feldspar or plagioclase alteration (Fulignati, 2020). Preference was thus given to fault gouge that crosscuts syenogranitic rocks during sampling. This sampling method was applied and confirmed for use in K-Ar dating by Sasseville (2009), as part of a study based on the dating of supracrustal faults of the allochthonous Appalachian domain. Sasseville (2009) pointed out that dissolution and precipitation processes in a porous environment, such as cataclastic rocks, favours an open-system and allows input of the chemical elements needed to form authigenic minerals. In far less porous environments, such as shale, the system will be considered closed, which means that the chemical elements, including their inherited radiogenic isotopes, will be partially or completely recycled. Thus, the porosity and permeability factor of rocks determines access and circulation of the authigenic mineral-forming fluids.

Sampling for this study was done exclusively in fault gouge associated with the conjugate fault system related to the Frobisher Bay half-graben; care was taken to recover chip samples that could be analyzed using scanning electron microscopy. Fault gouge sampling, which focused on relatively fresh outcrops in quarries or in areas located near recently constructed buildings, was carried out on secondary faults spatially associated with major faults, whose exposure has been obliterated by recent glacial and fluvial erosion. Of the 13 stations visited in the Iqaluit area in 2021, only four showed fault gouges that could potentially be promising for K-Ar dating: 1) station 21FB01 in a quarry northwest of Iqaluit (Figure 4a, b); 2) station 21FB08 near the 'Road to Nowhere' (Figure 4c); 3) station 21FB09 behind the Aqsarniit Hotel (Figure 5a–c); and 4) station 21FB10 in an active quarry operated by Nunavut Excavating west of Iqaluit (Figure 4d, e). All the faults were in syenogranitic hostrock, except station 21FB10, where the syenogranite was in contact with metagabbro (Figure 4d). The results of preliminary X-ray diffraction (XRD) analysis presented below relate to fault gouge samples recovered in summer 2020 from site 1 in a quarry north-northwest of Iqaluit (sample 20LXAL004A01) from a fault oriented 285°/48°. In addition to this gouge sample, three other samples were also collected from fault breccia (20LXAL001A01, 20LXAL002A01, 20LXAL002A02) to study the mineralogy of the hostrock using thin-section analysis. Samples bearing the prefix 21FB were collected in 2021 and will be used for K-Ar dating in a subsequent study.

Figure 4: Field photographs of fault gouges sampled at stations visited in the Iqaluit area and potentially useful for K-Ar dating (summer fieldwork in 2020 and 2021): **a)** outcrop of samples 21FB01C1g1 and g2 collected from a fault oriented 283°/65° (notebook used for scale measures 19 cm); **b)** outcrop of sample 21FB01D1g collected from a fault oriented 145°/74° (red dotted lines represent two generations of fault striae; pencil used for scale measures 13 cm); **c)** outcrop of sample 21FB08A1b collected from a fault oriented 303°/38° (person used as scale measures 1.83 m); **d)** outcrop of samples 21FB10A1g1 and g2 collected from a fault oriented 325°/55° and showing the contact between a syenogranite (salmon pink) and a metagabbro (grey black; person used for scale measures 1.83 m); **e)** outcrop of sample 21FB10B1g collected from a fault oriented 335°/50° (person used for scale measures 1.83 m).

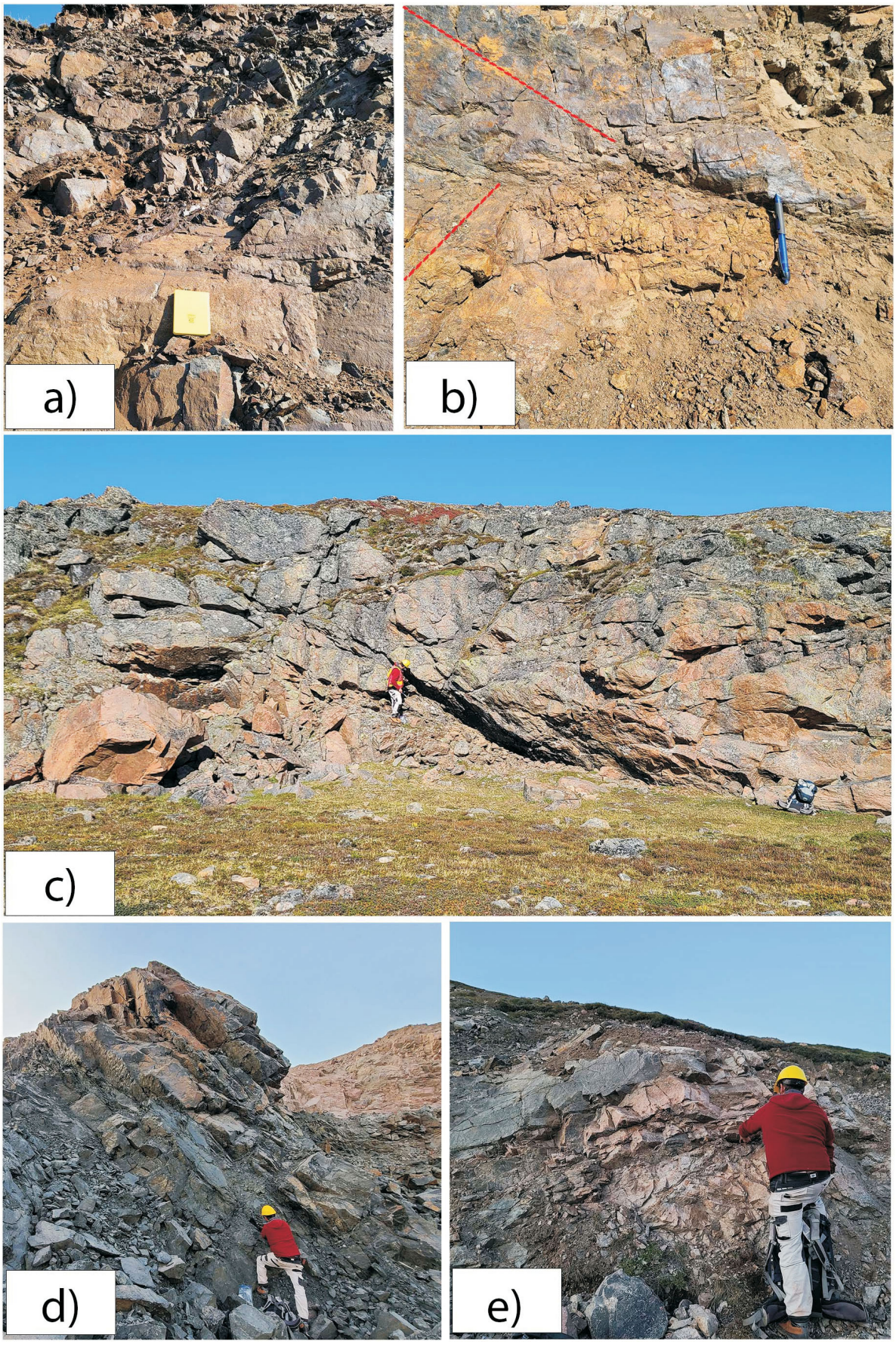
a)
b)
c)
d)
e)

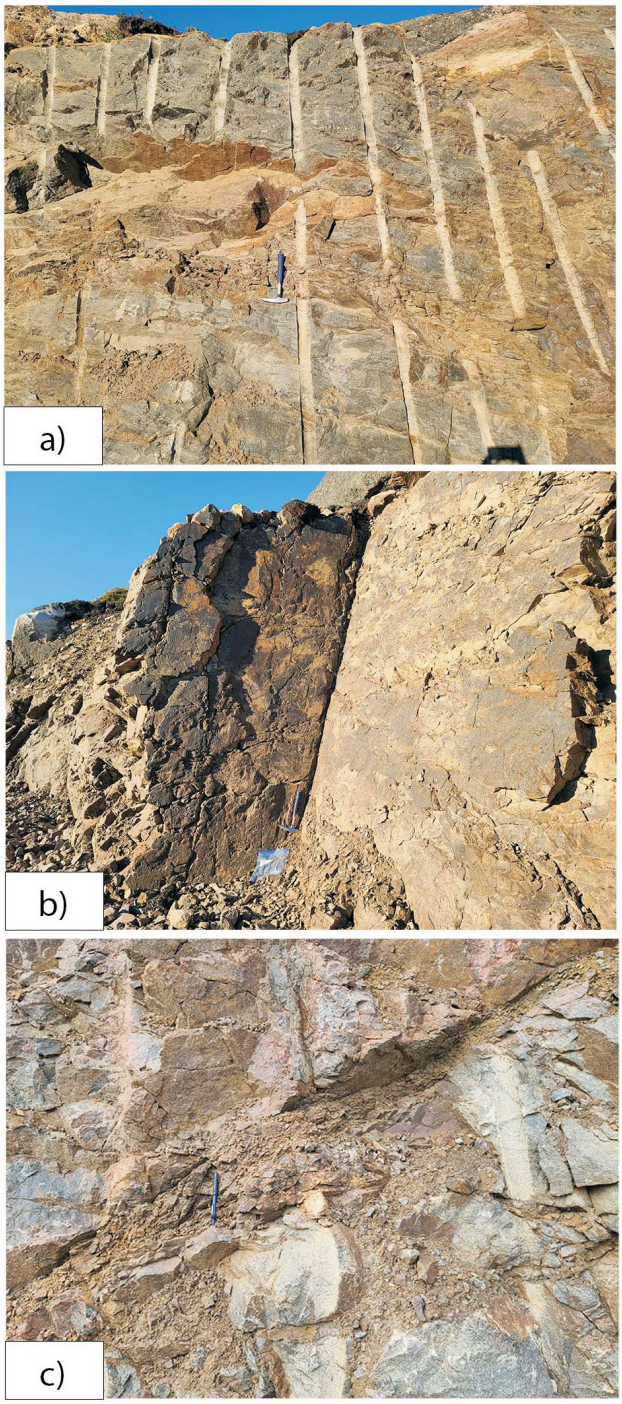

Figure 5: Field photographs of fault gouges sampled behind the Aqsarniit Hotel in Iqaluit and potentially useful for K-Ar dating (summer fieldwork in 2020 and 2021): **a)** outcrop of sample 21FB09C1g collected from a fault oriented 344°/46° (hammer used for scale measures 33 cm); **b)** outcrop of sample 21FB009C2g collected from a fault oriented 160°/70° (hammer used for scale measures 33 cm); **c)** outcrop of sample 21FB09D1g collected from a fault oriented 171°/54° (pencil used for scale measures 13 cm).

X-ray diffraction analysis

Methods

Sample preparation

Analysis using XRD of the coarse-grained (<2 µm) fraction of sample 20LXAL004A01 provided preliminary details on the mineralogy of the Frobisher Bay fault gouge. However, authigenic minerals are usually concentrated in the clay-sized fraction (<0.2 µm) of the fault gouge since the coarse-grained fraction is more easily contaminated by detrital minerals and, hence, yields less reliable ages (Clauer and Chadhuri, 1995). Robinson et al. (1993) suggested the clay-sized fraction can be interpreted as the last mineral growth associated with the tectonic process being studied. Consequently, future investigation of the clay-sized fraction will be of particular importance in determining the timing of movement in the Frobisher Bay half-graben.

Clay-particle separation is a preparatory step to X-ray diffraction analysis and K-Ar dating. Firstly, the fault gouge needs to be crushed while avoiding overgrinding of the coarser mineral fractions that would cause faulty measurement of the potassium relative to argon content in the authigenic mineral fractions, which would yield biased K-Ar ages (Clauer and Chaudhuri, 1995). Grinding the sample with a small amount of water for two minutes, at most, using an electric agate mortar is the conventional method relied upon for geochronological studies involving K-Ar dating, as this method allows minerals to be separated instead of fractured (Sasseville, 2009; Daver, 2017). Washing the samples after grinding them is an essential step since the flocculating effect of the salts prevents total clay suspension. Washing by centrifugal process can be repeated several times before the clays reach a steady state of suspension in the water (Larqué and Weber, 1975). Once the samples have been washed, an initial sieving with ultrapure water is done to recover the <63 µm fraction. A sieve is simply positioned on a beaker of similar circumference and the ground sample is gradually poured through it, then rinsed with ultrapure water to avoid alteration of the clay particles and to recover the <63 µm fraction from the beaker. The <63 µm fraction suspended in the water is then poured through a 20 µm sieve. This requires positioning an agitator-equipped sieve above a cup placed on a magnetic plate. The agitator facilitates passage of the clay particles through the sieve into the cup. The 20 µm suspended fraction can then be recovered and poured into small glass jars, which are three-quarters filled (Steinhauer, 2012). Based on Stokes' law, after one hour and fifty minutes, the first two centimetres will constitute the <2 µm fraction that can then be recovered. The coarse-grained fraction will be used for X-ray diffraction analysis.

The coarse-grained fraction is placed on a thin section in preparation for the diffractometer to provide data. This is achieved by suspending the <2 μm fraction from the fault-gouge sample in a small amount of water and pipetting it delicately onto the thin section, which is then placed in a fume hood until the coarse-grained fraction is completely dry, at which point the thin section is ready for XRD analysis (Steinhauer, 2012).

In addition to the coarse-grained fraction, the mineralogy of the hostrock sample (20LXAL001A01) was also analyzed using whole-rock X-ray powder diffraction. The sample was prepared by grinding it using a cone crusher, and the resulting powder placed compactly on a thin section (Clauer and Chaudhuri, 1995).

X-ray diffraction analysis

The mineralogy of the hostrock as well as the <2 μm fraction from the fault gouge was characterized at the Université du Québec à Montréal using the Siemens D5000 diffractometer with a cobalt X-ray tube.

The spectra produced can be analyzed using standards provided through an internal database (M. Preda, pers. comm., 2021). Sample glycosylation, followed by heating at 300°C for four hours, is required. This step involves placing the sample in a vacuum chamber for 24 hours in a container holding equal proportions of ethylene and glycol. This procedure causes the smectites and certain varieties of vermiculite to swell (Larqué and Weber, 1975). The sample can then be analyzed by XRD to observe the swelling-clay peaks migrate toward greater interreticular distances. Heating at 300°C for four hours allows the smectite and certain varieties of vermiculite to become dehydrated, which assists in the identification of interstratified kaolinite clay minerals. In the section dealing with future work, the heating method is re-evaluated to better meet the criteria of the study.

Results

The XRD data on the mineralogy of hostrock sample 20LXAL001A01 shows 44.6% quartz, 23.5% microcline, 15.2% sanidine, 7.7% clinochlore (chlorite), 7.2% anorthite and 1.4% montmorillonite (diosmectite; Figure 6a). As shown by mineral proportions (Figures 6a, 7), hostrock composition shows less than 10% of mafic minerals but is rich in potassium. Consequently, the hostrock can be interpreted as falling between an alkaline granite and a syenogranite, based on the Streckeisen classification for plutonic igneous rocks. Given the proportions of alkaline feldspar in the hostrocks, it is reasonable to expect that sufficient potassium is present to react to the pressure-solution process and to interact with hydrothermal fluids in areas of high, tectonically induced structural porosity, which occur mainly in brittle fault zones. Therefore, the basic conditions exist to test the proposed hypothesis, which supposes that the potassium-rich composition of the highly porous hostrock lends itself favourably to K-Ar dating, making it possible to determine more precisely the age of the brittle deformation. The fact that the studied hostrock thin sections share a similar mineralogy, which is characterized by the occurrence of chloritization in veinlets and of sericitization within the potassium feldspar (Figure 7a, b), is also relevant.

In the case of fault-gouge sample 20LXAL004A01, only the <2 μm fraction was analyzed using XRD. The peaks of the coarse-grained fraction show 60.2% clinochlore (chlorite), 11.2% montmorillonite (diosmectite), 8.7% sanidine, 7.5% anorthite, 8.8% microcline and 3.7% quartz (Figure 6b). These results reflect rather effective separation of the clay particles since the detrital minerals (potassium feldspar, plagioclase, quartz) represent less than 29% of the coarse-grained fraction of the fault-gouge sample. As illustrated by the high peak at 7.15 nm (Figure 6b), the dominant authigenic mineral is chlorite. Despite the high chlorite concentration of the sample, a much smaller peak at 10 nm shows the presence of a minor quantity of illite (Figure 6b). The fine-grained fraction of such a sample should therefore have a high concentration of illite and, consequently, could be used for K-Ar dating.

At a temperature of approximately 350°C, illite is the product of potassium feldspar and plagioclase alteration (Fulignati, 2020). Chlorite, on the other hand, is the product of the alteration of accessory minerals, such as biotite and hornblende, found in the hostrocks. The occurrence of illite and chlorite indicates that the propylitic-facies hydrothermal alteration process was characterized by temperatures >220°C and <350°C (Fulignati, 2020).

Future work

Where structural data is concerned, a detailed map of the brittle deformation in the Iqaluit area will be produced, highlighting the southeast- and northwest-striking conjugate normal fault system. Many improvements will also be made where future XRD analyses are concerned. Firstly, using an ultracentrifuge, the <0.2 μm fraction will be separated to obtain only authigenic clays and an illite concentrate (Larqué and Weber, 1975). Secondly, the method using oriented paste mounts described in Larqué and Weber (1975) will be applied; this involves suspending the <0.2 μm fraction in water before it is centrifuged and recovered. The fine-grained saturated clay paste recovered is then smeared with a glass knife on the thin section and, ensuring the clays are properly oriented, analyzed using XRD (Larqué and Weber, 1975). Lastly, the heating method will be modified; instead of heating the samples at 300°C for four hours, they will be heated at 500°C for four hours, resulting in the collapse of the peak corresponding to iron-rich chlorite, which is often found interstratified with smec-

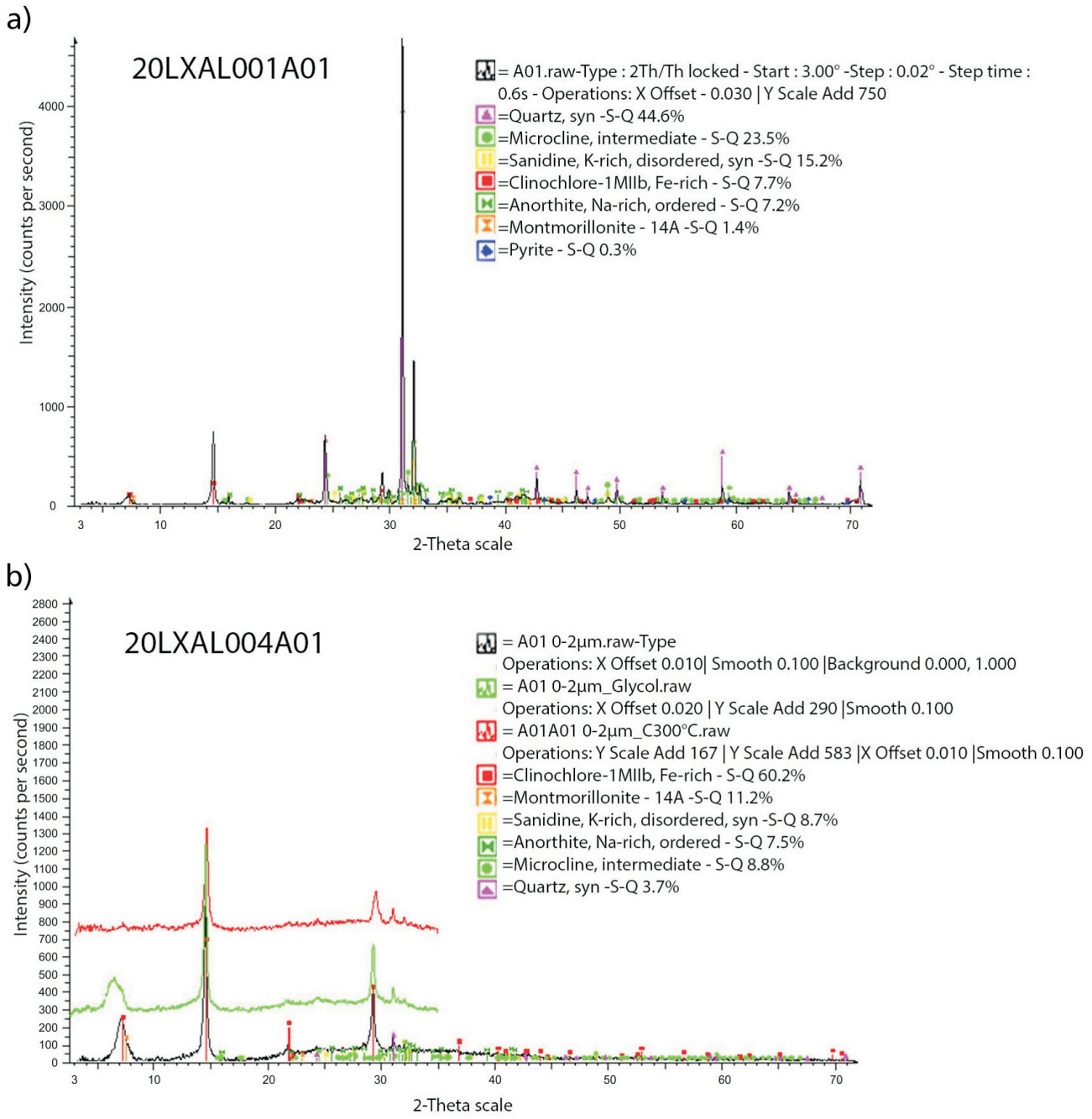

Figure 6: Diagrams of X-ray diffraction analysis results from Iqaluit area samples generated by the Siemens D5000 X-ray diffractometer of the Université du Québec à Montréal: **a)** bulk mineralogical composition of hostrock sample 20XLAL001A01; **b)** coarse-grained fraction (0–2 µm) of fault gouge sample 20XLAL004A01.

tites. Removal of the iron-rich chlorite from the smectites will result in a better resolution, thus allowing more precise semi-quantitative analysis of the crystal structure of the smectites and interstratified illite-smectite–type clays (Clauer and Chaudhuri, 1995).

In addition, the scanning electron microscopy of fault-rock fragments will help determine the mineral phase associated with the potassium as well as the authigenic origin of the minerals <0.2 µm in diameter, which is the fraction required for dating samples using the K-Ar method. This is the preferred method since it provides an accurate geochronometer of supracrustal sequences (Clauer and Chaudhuri, 1995). Furthermore, the loss of approximately 1 µm of argon during irradiation precludes the use of Ar/Ar dating on <0.2 µm fractions (Reuter and Dallmeyer, 1989). Therefore, the sample preparation method for grain-size fractions <0.2 µm is critical to the precision, reproducibil-

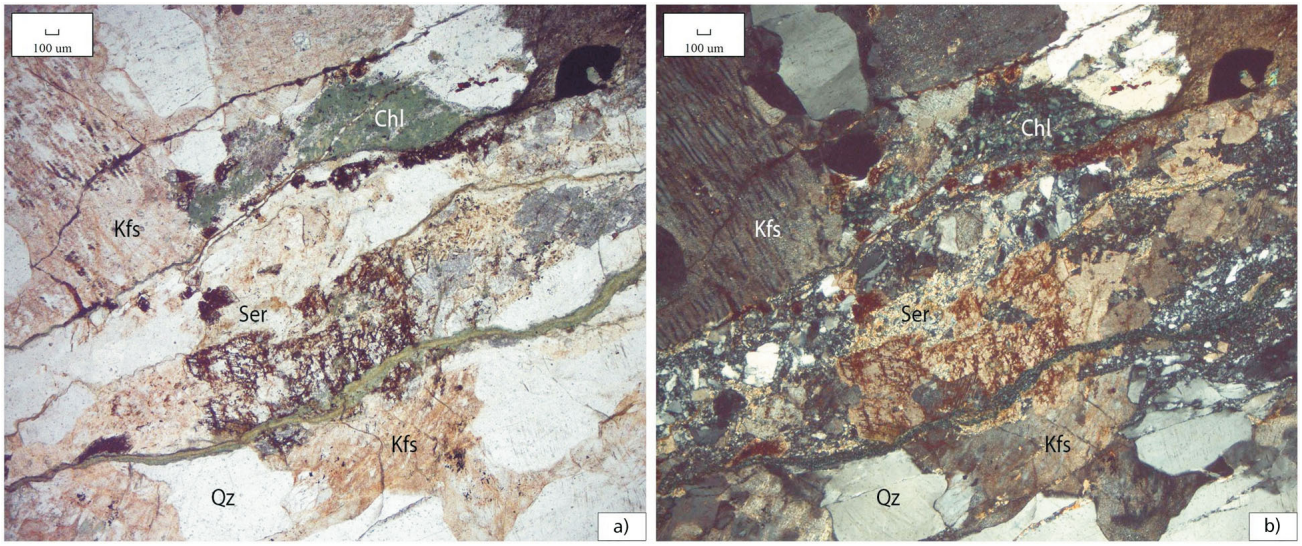

Figure 7: Photomicrograph of a part of the thin section (transmitted light) of sample 20LXAL001A01 collected in the Iqaluit area: **a)** parallel polarization; **b)** cross polarization. Abbreviations: Chl, chlorite; Kfs, potassium feldspar; Qz, quartz; Ser, sericite.

ity, and representativeness of analytical results, as well as to their interpretation and significance. Potassium-argon dating of clays by the lead author will be done at the Universidad Nacional Autonóma de México based on methods outlined in Bonhomme et al. (1975).

Economic considerations

In light of the recent discovery of underground sources of drinking water by Exp Services Inc. during the geotechnical study that preceded the construction of the Aqsarniit Hotel (Exp Services Inc., pers. comm., 2016), a better understanding of the fault system would help constrain the origin and evolution of the local groundwater system. In addition, better understanding of this system is essential to the undertaking of new construction and urban infrastructure.

Where natural resources are concerned, if it can be established that the age of fault activity corresponds to that of the Paleozoic Labrador Sea–Baffin Bay extension event, such a result could lead to a more precise determination of regional exhumation rates and, hence, provide information leading to improved targeting of diamond exploration in the area.

Acknowledgments

This work was undertaken as part of the M.Sc. thesis project of F. Gagnier. The fieldwork benefited from the financial assistance provided by a grant to F. Gagnier from the Northern Scientific Training Program administered by Polar Knowledge Canada as well as a Natural Sciences and Engineering Research Council Discovery Grant (RGPIN-2021-03306) awarded to B.M. Saumur. Support provided by the Canada-Nunavut Geoscience Office, specifically by L. Ham, in the form of fieldwork logistics and financial aid to F. Gagnier is greatly appreciated. The in-kind support provided by Crown-Indigenous Relations and Northern Affairs Canada (CIRNAC) through the loan of a vehicle during fieldwork allowed easy access to the targeted outcrops. In addition, F. Gagnier and B.M. Saumur are most grateful to S. De Beer (CIRNAC) for graciously receiving them upon their arrival in Iqaluit. Critical review by M. Lamothe (Université du Québec à Montréal) and editorial revision by M.-F. Dufour (RnD Technical) greatly improved the quality of this contribution. Finally, the authors thank V. Carnero Bravo (Université du Québec à Montréal) for taking part in preliminary discussions regarding analytical methods.

Natural Resources Canada, Lands and Minerals Sector contribution 20210594

References

Bonhomme, M., Thuizat, R., Pinault, Y., Clauer, N., Wendling A. and Winckler, R. 1975: Méthode de datation potassium-argon: appareillage et technique; Université Louis-Pasteur, Notes Techniques de l'Institut de Géologie, no. 3, 53 p.

Chalmers, J. and Pulvertaft, T. 2001: Development of the continental margins of the Labrador Sea: a review; Geological Society of London, Special Publications, v. 187, p. 77–105, URL <http://dx.doi.org/10.1144/GSL.SP.2001.187.01.05>.

Clauer, N. and Chaudhuri, S. 1995: Clays in Crustal Environment–Isotope Dating and Tracing; Springer Verlag, Heidelberg, Germany, 359 p.

Creason, C.G. 2015: Phanerozoic exhumation history of Hall Peninsula, Baffin Island: insights from apatite and zircon (U-Th-Sm)/He thermochronology and 3D thermokinematic modelling; M.Sc. thesis, Dalhousie University, Halifax, Nova Scotia, 150 p., URL <http://hdl.handle.net/10222/71599> [November 2021].

Daver, L. 2017: Apport de l'analyse des tourmalines et des pyrites à la genèse des gisements orogéniques archéens du district

de Val-d'Or, Abitibi, Canada; M.Sc. thesis, Université du Québec à Montréal, Montréal, Quebec, 177 p.

Fulignati, P. 2020: Clay minerals in hydrothermal systems; Minerals, v. 10, no. 10, p. 919, URL <https://doi.org/10.3390/min10100919>.

Gerlings, J., Funck, T., Jackson, H.R., Louden, K.E. and Klingelhöfer, F. 2009: Seismic evidence for plume-derived volcanism during formation of the continental margin in southern Davis Strait and northern Labrador Sea; Geophysical Journal International, v. 176, no. 3, p. 980–994, URL <https://doi.org/10.1111/j.1365-246X.2008.04021.x>.

Jackson, G.D., Hunt, P.A., Loveridge, W.D. and Parrish, R.R. 1990: Reconnaissance geochronology of Baffin Island, N.W.T.; *in* Radiogenic Age and Isotopic Studies, Report 3, Geological Survey of Canada, Paper 89-3, p. 143, URL <https://doi.org/10.4095/129079>.

Larqué, P. and Weber, F. 1975: Technique de préparation des minéraux argileux en vue de l'analyse par diffraction des rayons X. Mise au point collective; Université Louis-Pasteur, Note technique de l'Institut de Géologie, 33 p.

Larsen, L.M., Heaman, L.M., Creaser, R.A., Duncan, R.A., Frei, R. and Hutchison, M. 2009: Tectonomagmatic events during stretching and basin formation in the Labrador Sea and the Davis Strait: evidence from age and composition of Mesozoic to Palaeogene dyke swarms in West Greenland; Geological Society of London, Journal, v. 166, p. 999–1012, URL <https://dx.doi.org/10.1144/0016-76492009-038>.

Reuter A. and Dallmeyer, R.D. 1989: K-Ar and $^{40}Ar/^{39}Ar$ dating of cleavage formed during very low-grade metamorphism: a review; *in* Evolution of Metamorphic Belts, J.S. Daly, R.A. Cliff and B.W.D. Yardley (ed.), Geological Society of London, Special Publication, v. 43, p. 161–172.

Robinson, A.G., Coleman, M.L. and Gluyas, J.G. 1993: The age of illite cement growth, Village field area, southern North Sea: evidence from K-Ar ages and $^{18}O/^{16}O$ ratios; American Association of Petroleum Geologists, Bulletin, v. 77, p. 68–80, URL <https://doi.org/10.1306/BDFF8B64-1718-11D7-8645000102C1865D>.

Sanford, B. and Grant, A. 1990: New findings relating to the stratigraphy and structure of the Hudson Platform; *in* Current Research, Part D, Geological Survey of Canada, Paper 90-1D, 1990, 218 p., URL <https://doi.org/10.4095/131332>.

Sanford, B. and Grant, A. 1998: Paleozoic and Mesozoic geology of the Hudson and southeast Arctic platforms; Geological Survey of Canada, Open File 3595, scale 1:2 500 000, URL <https://doi.org/10.4095/210108>.

Sanford, B. and Grant, A. 2000: Geological framework of the Ordovician system in the southeast Arctic Platform, Nunavut; *in* Geology and Paleontology of the Southeast Arctic Platform and Southern Baffin Island, Nunavut, A.D. McCracken and T.E. Bolton (ed.), Geological Survey of Canada, Bulletin 557, p. 13–38, URL <https://doi.org/10.4095/211845>.

Sasseville, C. 2009: Géochronologie K-Ar et transfert de matière le long de systèmes de failles et de fractures dans la lithosphère continentale – cas du système de rift Saint-Laurent en relation avec le domaine allochtone des Appalaches, Québec, Canada; Ph.D. thesis, Université Louis-Pasteur, Strasbourg, France, 232 p.

Scott, D.J. 1999: U-Pb geochronology of eastern Hall Peninsula, southern Baffin Island, Canada: a northern link between the Archean of West Greenland and the Paleoproterozoic Torngat Orogen of northern Labrador; Precambrian Research, v. 93, p. 5–26, URL <https://doi.org/10.1016/s0301-9268(98)00095-3>.

St-Onge, M.R., Searle, M.P. and Wodicka, N. 2006: Trans-Hudson Orogen of North America and Himalaya–Karakoram–Tibetan orogen of Asia: structural and thermal characteristics of the lower and upper plates; Tectonics, v. 25, art. TC4006, 22 p., URL <https://doi.org/10.1029/2005TC001907>.

Steinhauer, S. 2012: Protocole sur les procédés de séparation et d'extraction des argiles pour une analyse par diffraction par rayons X; Les cahiers du GEOTOP, unpublished report, Université du Québec à Montréal, 11 p.

Watt, W.S. 1969: The coast-parallel dike swarm of southwest Greenland in relation to the opening of the Labrador Sea; Canadian Journal of Earth Sciences, v. 6, no. 5, p. 1320–1321, URL <https://doi.org/10.1139/e69-133>.

Whalen, J., Wodicka, N., Taylor, B. and Jackson, G. 2010: Cumberland batholith, Trans-Hudson Orogen, Canada: petrogenesis and implications for Paleoproterozoic crustal and orogenic processes; Lithos, v. 117, p. 99–118, URL <https://doi.org/10.1016/j.lithos.2010.02.008>.

Submarine landslides in Pangnirtung Fiord, Baffin Island, Nunavut

Philip Sedore[1], Alexandre Normandeau[2] and Vittorio Maselli[3]

[1]*Department of Earth and Environmental Sciences, Dalhousie University, Halifax, Nova Scotia <sedore.p@dal.ca>*

[2]*Natural Resources Canada, Geological Survey of Canada–Atlantic, Dartmouth, Nova Scotia*

[3]*Department of Earth and Environmental Sciences, Dalhousie University, Halifax, Nova Scotia*

This work is part of the Baffin Bay Geohazards Activity of the Landslides and Marine Geohazards Project of Natural Resources Canada's Public Safety Geoscience Program. This program undertakes research across Canada to support risk reduction from the effects of hazardous natural conditions (i.e., space weather, earthquakes, tsunamis, volcanoes and landslides). The program develops authoritative scientific knowledge and tools to reduce future economic, social and environmental losses from these hazards. Additional funding for this research was provided by Crown-Indigenous Relations and Northern Affairs Canada and the Ocean Frontier Institute through an award from the Canada First Research Excellence Fund.

Sedore, P., Normandeau, A. and Maselli, V. 2022: Submarine landslides in Pangnirtung Fiord, Baffin Island, Nunavut; *in* Summary of Activities 2021, Canada-Nunavut Geoscience Office, p. 31–46.

Abstract

As part of the Geological Survey of Canada's continuing aim to identify the potential marine geohazards in Baffin Bay, this study sought to generate a comprehensive understanding of the distribution, timing and potential triggers of submarine landslides in Pangnirtung Fiord. The high-relief topography of Pangnirtung Fiord is comparable to fiords in Greenland and Alaska, where recent studies have investigated landslide-generated tsunamis. Since the low-lying community of Pangnirtung is situated along the coast of Pangnirtung Fiord, it is ever more critical to understand the submarine-landslide hazard of the area.

The study identified 180 near-surface submarine landslides in Pangnirtung Fiord using multibeam bathymetric and sub-bottom profiler data, along with gravity cores collected in 2019. Morphometric analysis shows that most submarine landslides are relatively small (~0.13 km^2), with elongated failure zones and wide deposits dispersed along the basin floor. Radiometric dating reveals that eight of the eleven dated landslides are younger than 500 years. Landslide-surface roughness was tested as a proxy for age, but the relationship was found to be weak, thus limiting the ability to accurately date all identified landslides. Four broad categories of submarine-landslide triggers were identified and it was shown that at least 53% (96 of 180) of landslides are associated with subaerial sources and, at most, 31% (56 of 180) are shallow-water, non-subaerially influenced. This suggests that triggers of most submarine landslides within Pangnirtung Fiord include rapid flood-water input, subaerial debris flows and sea-ice loading during low tide.

Introduction

Fiords are narrow, submerged, glacially carved valleys flanked by steep, high-relief sidewalls, which are susceptible to subaerial and submarine geological hazards such as landslides and rock avalanches (Syvitski et al., 1987). Landslides may occur as slow or sudden, and potentially catastrophic, downslope movement of rock and sediment (Cruden and Varnes, 1996; Hampton et al., 1996). They have the potential to damage land-based and seabed infrastructure and threaten coastal communities through the generation of displacement waves (i.e., tsunamis) in high-latitude fiords (e.g., Brothers et al., 2016; Gauthier et al., 2017; Higman et al., 2018). In fact, over the last century, eight of the fourteen largest tsunamis recorded worldwide were caused by landslides in fiords (Miller, 1960; Dahl-Jensen et al., 2004; Oppikofer et al., 2009; Gauthier et al., 2017; Higman et al., 2018; Waldmann et al., 2021). Although no landslide-generated tsunami has been documented within the fiords of Baffin Island, the high-relief topography and dynamic sedimentation present similarities to the high-latitude fiords of Alaska, Greenland and Norway, all of which have a history of tsunami generation.

Landslides can be caused by internal stresses; however, seabed sediments need to be preconditioned for failure and an external trigger is often needed to generate downslope movement (Masson et al., 2006). Dynamic fiord sedimen-

This publication is available, free of charge, as colour digital files in Adobe Acrobat® PDF format from the Canada-Nunavut Geoscience Office website: https://cngo.ca/. Il est aussi disponible en français sur https://cngo.ca/fr/.

tation, which often includes high sedimentation rates and coarse-grained layers, can create weak preconditioned surfaces. An increase in shear stress or the development of overpressure in the pore fluid between sediment grains can then provide the necessary triggering mechanism for slope failure (Tappin, 2010; Urlaub et al., 2013; Clare et al., 2016). Numerous processes can trigger submarine landslides, including earthquakes caused by tectonic-plate movement (Kuenen, 1952) and isostatic adjustment (Brooks et al., 2016), wave action (Bea et al., 1983; Prior et al., 1989), sea-ice or iceberg groundings (Normandeau et al., 2021), tides (Johns et al., 1985; Chillarige et al., 1997) and increased river discharge that may promote rapid sediment accumulation and oversteepening of river-delta fronts (Prior and Bornhold, 1989; Bornhold et al., 1994; Girardclos et al., 2007; Clare et al., 2016). Submarine landslides can also be triggered when a subaerial landslide or rock avalanche extends to the water, destabilizing the seabed in shallow water. Subaerial landslides can be triggered by multiple processes, including permafrost thawing, increased precipitation and frost wedging (Gauthier et al., 2017; Higman et al., 2018).

Since 2018, the Geological Survey of Canada (GSC) has sought to identify potential marine geohazards in Baffin Island fiords, including submarine landslides. Seafloor-mapping initiatives reveal that submarine landslides occur within 86% (Bennett et al., 2021) of the mapped fiords (e.g., Broom et al., 2017; Brouard and Lajeunesse 2019; Normandeau et al., 2019; Deering et al., 2019; Bennett et al., 2021); however, their timing and causes are generally poorly understood. To better constrain these critical aspects of submarine landslides within a Baffin Island fiord, multibeam echosounder and sub-bottom profiler data, along with short (<115 cm) gravity cores, and unmanned aerial vehicle (UAV) images were collected in Pangnirtung Fiord in September 2019 aboard the Government of Nunavut Research Vessel (RV) *Nuliajuk* (Figure 1). This paper presents an assessment of submarine-landslide distribution, morphology and timing in Pangnirtung Fiord, and provides insights into possible trigger mechanisms.

A better understanding of submarine geohazards in Baffin Island fiords can help increase public safety for low-lying Arctic communities such as Pangnirtung (population 1481), located along the southeast coast of Pangnirtung Fiord on Baffin Island (Figure 1). All 467 dwellings within the hamlet lie below 60 m asl (metres above sea level), and the airport, fuel-storage tanks, health centre and schools are all below 30 m asl. An assessment of the submarine-landslide hazard in this dynamic fiord environment may help inform the community and protect this low-lying essential infrastructure. Similar assessments throughout the fiords of Baffin Island will be imperative with future development and expansion of essential infrastructure in a rapidly changing Arctic climate.

Regional setting

Pangnirtung Fiord is oriented northeast-southwest, with a length of 43 km, a width of 1–3 km and a maximum water depth of 165 m (Figure 1). In the southwest, the surrounding subaerial landscape features low-relief terrain of glacial till overlying bedrock. The northeastern section of the fiord is surrounded by high-relief terrain rising to 1500 m asl and divided by glacial valleys and cirques. Erosion of the steep fiord side walls that surround the coast has produced talus slopes and debris cones that extend to the shallow intertidal zone. The remaining cirque and alpine glaciers make up ~25% of Pangnirtung Fiord's catchment area (Gilbert, 1978). The bedrock surrounding Pangnirtung Fiord comprises three rock types of the Paleoproterozoic Qikiqtarjuaq dominantly felsic plutonic suite, dated at ca. 1.9–1.88 Ga (Jackson and Sanborn-Barrie, 2014).

Sediment supply to the fiord is sourced from numerous rivers and alluvial fans that drain the 1700 km^2 partially glaciated catchment area (Gilbert, 1978). Two main rivers, the Weasel River at the head of the fiord and the Kolik River across from the Hamlet of Pangnirtung, drain 67% of the catchment area (Figure 1; Gilbert, 1978). Other smaller rivers include Panniqtuup Kuunga (commonly referred to as the Duval River in the literature), which flows through the Hamlet of Pangnirtung, and the Puurusiq River, located to the northeast of the fiord. Although flow-rate measurements are sparse, the winter months see little to no flow, and snowmelt and precipitation in the summer months lead to high and sporadic discharge levels (e.g., average peak discharge of Panniqtuup Kuunga (Duval River) in 1973–1983 was 17.6 m^3/s; Water Survey of Canada, 1983).

Seismic activity surrounding Pangnirtung is concentrated in the northern Labrador Sea, Davis Strait and Baffin Bay, all of which are basins formed through seafloor spreading associated with the rifting of Canada and Greenland in the Late Cretaceous (Basham et al., 1977). Intraplate seismic events in Baffin Bay are caused by postglacial rebound that reactivates faults formed from the original Cretaceous rifting (Stein et al., 1979).

Methods

Hydroacoustic analysis and morphometrics

High-resolution multibeam bathymetric data were collected using a Kongsberg EM2040C. The data were then gridded to 5 m horizontal resolution and exported to Esri® ArcGIS Pro 2.5 to create shaded-relief maps intended for seafloor morphological interpretation (Figure 1). Sub-bottom profiles were acquired using a hull-mounted Knudsen 3260 3.5 kHz sub-bottom profiler (Figure 1). The sub-bottom data were visualized and interpreted using the SegyJp2Viewer developed at the Geological Survey of Canada (Courtney, 2009). Submarine-landslide deposits were

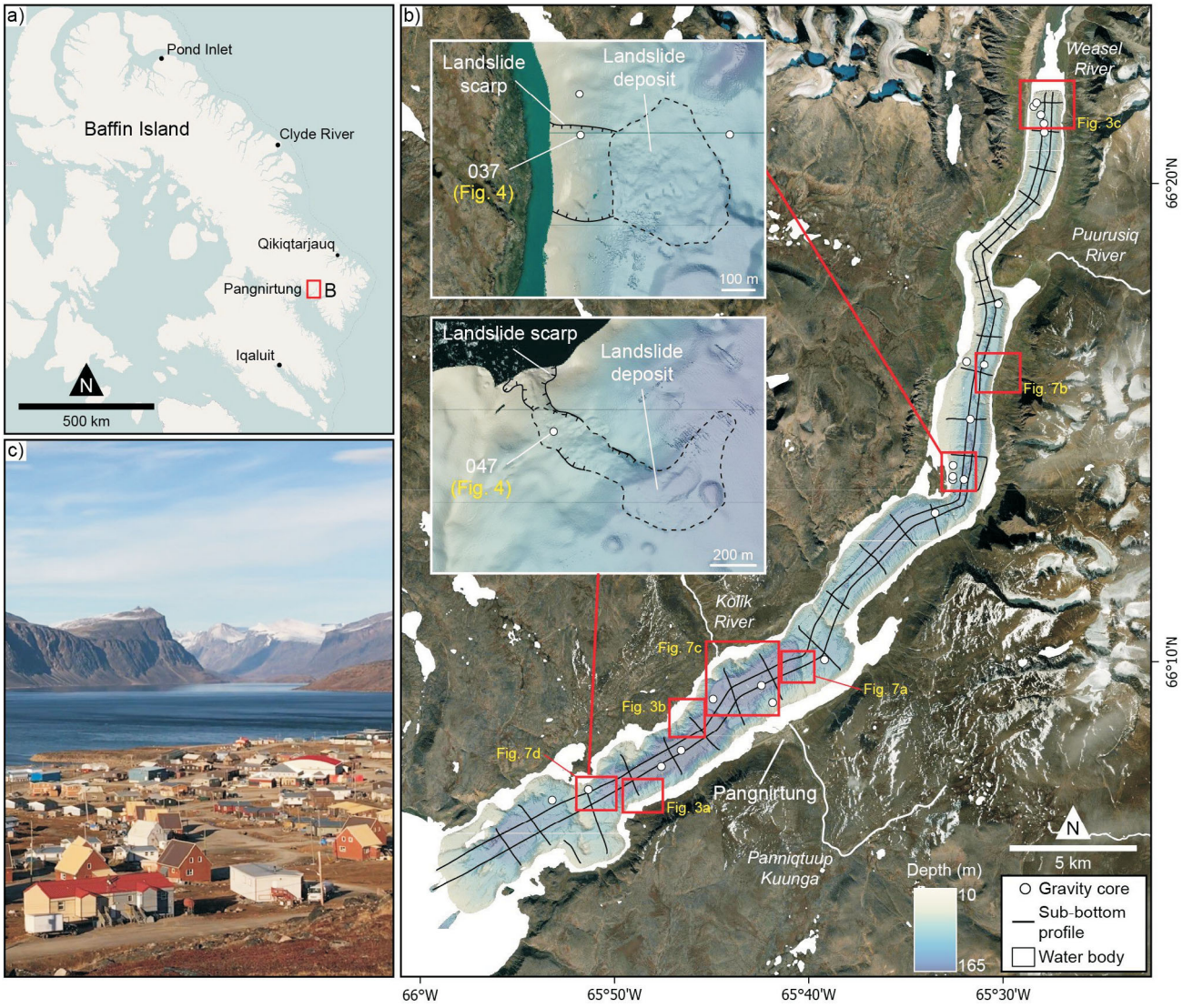

Figure 1: a) Location of Pangnirtung Fiord on eastern Baffin Island, Nunavut. **b)** Multibeam bathymetry of Pangnirtung Fiord, with the locations of gravity-core samples and sub-bottom profiles. Inset is a detailed view of the locations of cores 037 and 047, within mapped landslides. **c)** Photograph of Pangnirtung, facing north. Base map from Maxar Technologies.

identified by integrating bathymetry and sub-bottom data; a fully delineated submarine-landslide features a zone of slope failure including a head scarp, a flow path or transition zone, and a deposit. The relevant morphometric parameters for this study (Table 1) were measured following the standardized procedure outlined in Clare et al. (2019).

Core analysis

Twenty-one sediment gravity cores (Figure 1), ranging in length from 8 to 111 cm, were collected from the RV *Nuliajuk* and processed at the Geological Survey of Canada–Atlantic (GSC-A) facility located at the Bedford Institute of Oceanography (BIO) in Dartmouth, Nova Scotia. Physical and sedimentological properties were measured as an initial interpretation of the depositional processes and to identify landslide deposits. Using a Geotek Multi-Sensor Core Logger (MSCL), whole cores were analyzed for 1) magnetic susceptibility via a Barrington loop sensor (MS2B); 2) bulk density based on the gamma-ray attenuation of the sediment; 3) P-wave velocity based on the travel time of a compressional wave between transducers; and 4) colour reflectance via a Konica Minolta colour spectrophotometer to measure L* (lightness), a* (green to red) and b* (blue to yellow) values.

The cores were then split into a working half and an archive half, and then X-rayed and photographed. Grain-size measurements were completed using a Beckman Coulter LS230 Laser Diffraction Analyzer for grain sizes of 4–2000 µm, and manually sieved and weighed for particles above 1000 µm. Thin sections were also created to aid in characterizing the lithofacies.

Table 1: Descriptions of morphometric parameters used in this study of submarine landslides in Pangnirtung Fiord, eastern Baffin Island.

Parameter	Description
Area (km^2)	Total extent of the landslides and associated scar and flow path
Deposit length (m)	Maximum length of the landslide deposit
Maximum deposit width (m)	Maximum width of the deposit measured perpendicular to the maximum deposit length
Minimum water depth (m)	Water depth measured at the shallowest point of the delineated landslide
Total length (m)	Total length of the landslide from the upper limit of the head scarp to the downslope extent of the landslide
Scar width (m)	Maximum width of the scar
Slope gradient (º)	Measured slope of an adjacent slope outside of the slope failure scar and deposit
Slope gradient at toe (º)	Slope measured directly in front of the toe of the deposit
Elongation	Ratio of the total length to the maximum width of the deposit; a value less than 1 represents a longer width than length, and a value greater than 1 represents a longer length than width

Geochronology

Radiocarbon dates were obtained from shell fragments collected within 10 of the sediment cores (Sedore, M.Sc. in progress [Distribution, timing and potential trigger mechanisms of submarine landslides in Pangnirtung Fiord, eastern Baffin Island, Nunavut]) and analyzed at the A.E. Lalonde Accelerator Mass Spectrometry (AMS) Laboratory at the University of Ottawa (Table 2). The ^{14}C ages were corrected using a local marine reservoir correction (ΔR) of –6 ±58 years, calculated as the average of the 10 nearest shell measurements (Coulthard et al., 2010) and calibrated using the Marine20 calibration curve in Calib 8.2 (Heaton et al., 2020). Heaton et al. (2020) do not recommend this model for high latitudes (higher than 40–50°N), but presently there is not a better model. The ^{210}Pb and ^{137}Cs radioisotope activities for four sediment gravity cores were used to calculate sedimentation rates within the fiord. Subsamples were taken within the top 30 cm of the cores at 1–2 cm intervals (Pourchet and Pinglot, 1989; Bronk Ramsey, 2008) and analyzed at the Laboratory for the Analysis of Natural and Synthetic Environmental Toxins (LANSET) at the University of Ottawa. Sedimentation rates were calculated using the 'serac' R package developed by Bruel and Sabatier (2020) and the Constant Flux Constant Sedimentation (CFCS) model (Krishnaswamy et al., 1971). This model assumes that the ^{210}Pb activity in the

Table 2: Radiocarbon dating information, including core number, lab number, sample depth, radiocarbon age and uncertainty, and calibrated age and total uncertainty for cores 015, 017, 020, 030, 034, 037, 041, 043, 047 and 048 from Pangnirtung Fiord, eastern Baffin Island.

Core	Lab number	Sample depth (cm)	Radiocarbon age (yr BP)	Uncertainty (yr BP)	Calibrated age (cal. yr BP; ΔR = –6±58)	Uncertainty (yr BP)
015	UOC-13995	38–39	722	26	165	165
017	UOC-13996	68	697	24	145	145
020	UOC-13997	20	>Modern		>Modern	
020	UOC-13998	41–43	183	24	>Modern	
020	UOC-13999	49–51	>Modern		>Modern	
030	UOC-14000	72	1129	25	540	150
034	UOC-14001	2–3	>Modern		>Modern	
037	UOC-14002	3-5	>Modern		>Modern	
041	UOC-14003	49–51	899	25	325	175
043	UOC-14004	40–41	1733	25	1110	170
047	UOC-14005	0-1	>Modern		>Modern	
047	UOC-14006	22–25	4181	25	4060	230
048	UOC-14007	2-3	1362	25	745	165

newly deposited sediment has been constant throughout time; however, bioturbation, which is a prevalent process occurring throughout the hemipelagic sediments within the fiord, will affect the measured ^{210}Pb and ^{137}Cs activities. The CFCS model is the simplest model, with other models requiring porosity measurements that were not recorded during sampling.

The morphological and sedimentological characterizations of the submarine landslides were used to determine the intervals of interest. The ages of the submarine-landslide deposits were constrained through a combination of radiocarbon ages and the ^{210}Pb/^{137}Cs activity–derived sedimentation rates. In cores with only radiocarbon dates available, the sedimentation rates in the sediment cores were calculated through manual age-depth modelling. For these calculations, the instantaneous landslide deposits were excluded. Using these sedimentation rates (Sedore, M.Sc. in progress), the absolute ages of the instantaneous landslide deposits were calculated based on their depth in the cores and subbottom profiles using linear interpolation.

Surface roughness

The standard deviation (SD) of the bathymetric position index (BPI) was used to calculate the surface roughness for the delineated landslide deposits using ArcGIS Pro 2.5. The BPI is a measurement of the relative position of a pixel (2 m resolution) compared to the surrounding neighbourhood of pixels (Lundblad et al., 2006). The BPISD expresses the surface roughness for each landslide deposit, as a highly variable topographic surface will have a larger standard deviation than a smoother topographic surface. Under the assumption that older, buried landslides will have a smoother surface than recently deposited landslides, this measurement can be used as a proxy for the landslide's relative age when compared to other landslides. The surface roughness of the landslide deposits is also influenced by the type of landslide, the run-out distance, the slope and the sediment type. A linear regression was used to test the validity of this method for Pangnirtung Fiord submarine landslides, comparing the BPISD value to the absolute ages of landslides determined from radiometric dating. From this, an age for each landslide was calculated based on the BPISD and then compared to the absolute age of the landslide (Sedore, M.Sc. in progress).

Results and discussion

Distribution, morphology and sedimentology of submarine landslides

The high-resolution bathymetric data reveal 180 partially or fully delineated submarine landslides throughout Pangnirtung Fiord. Failure zones are identified in areas of high seafloor gradients (>4º), demonstrating an association between slope failure and high-relief sections of the fiord, such as the subaqueous fiord sidewalls and glacial sills (Figure 2). Conversely, no distinct slope failures are observed in areas with a low gradient (0–4º). Most landslide deposits are mapped along the relatively flat basin floor and, in some instances, crosscut other landslide deposits. Not every landslide deposit can be linked to its head scarp due to mapping limitations that prevent imaging the seafloor in shallow water. Due to this, the minimum water-depth measurement is a truncated distribution that should normally extend to 0 m but instead is restricted at about 10–30 m to 0 m (Figure 2). Considering this mapping limitation, at least 62% of mapped landslides have their head scarps at a water depth of less than 40 m.

Morphometric parameters were measured for the submarine landslides, and descriptive statistics can be summarized to provide the morphometrics of a typical submarine landslide in Pangnirtung Fiord (Figure 2). Most submarine-landslide deposits have an area less than 0.13 km^2 (lower quartile (Q1) = 0.03 km^2 and upper quartile (Q3) = 0.13 km^2), while the minimum water depth of the landslides varies from 3 to 132 m (mean = 38 m). The maximum scar width (Q1 = 98 m, Q3 = 260 m) and total length of deposit (Q1 = 310 m, Q3 = 637 m) can be used to calculate the elongation parameter for each landslide deposit. The elongation value of most deposits is above 1 (Q1 = 1.4, Q3 = 3.4), indicating a long and narrow feature oriented toward the downslope gradient. The slope gradient measured adjacent to the slope failure zone (Q1 = 9.5º, Q3 = 5º) is meant to provide insight into the unfailed slope angle; however, slope measurements within the failure zones show little deviation from the slope-gradient parameter. The mean slope of <1º at the toe of the landslides demonstrates the flow of the landslides to the flat basin floor.

The various morphologies and surface expressions of mapped submarine landslides in the geophysical datasets represent distinct landslide processes, including debris avalanches and debris flows (Figure 3). Debris avalanches are made up of unsorted sediment and rock that move rapidly downslope and do not appear to have distinct lateral bathymetric constraints (i.e., into an underwater channel; Hungr et al., 2001). Within Pangnirtung Fiord, the debris avalanches have a wide failure zone with distinct side scarps. The associated deposits are blocky and rough, with transverse compressional ridges. Debris flows are distinguished from debris avalanches by flowing through confined channels developed along the submarine slope from repeated failures. Generally, debris-flow deposits are lobe shaped and have a smoother appearance. Multiple debris-flow deposits can be identified at the base of these channels or gullies. Side scarps are not as distinct and the failure zones are narrower, creating an elongated landslide. Turbidity currents are inferred from the distinct sediment waves at the head of the fiord (Normandeau et al., 2019), as well as from potential turbidites in both sediment cores and

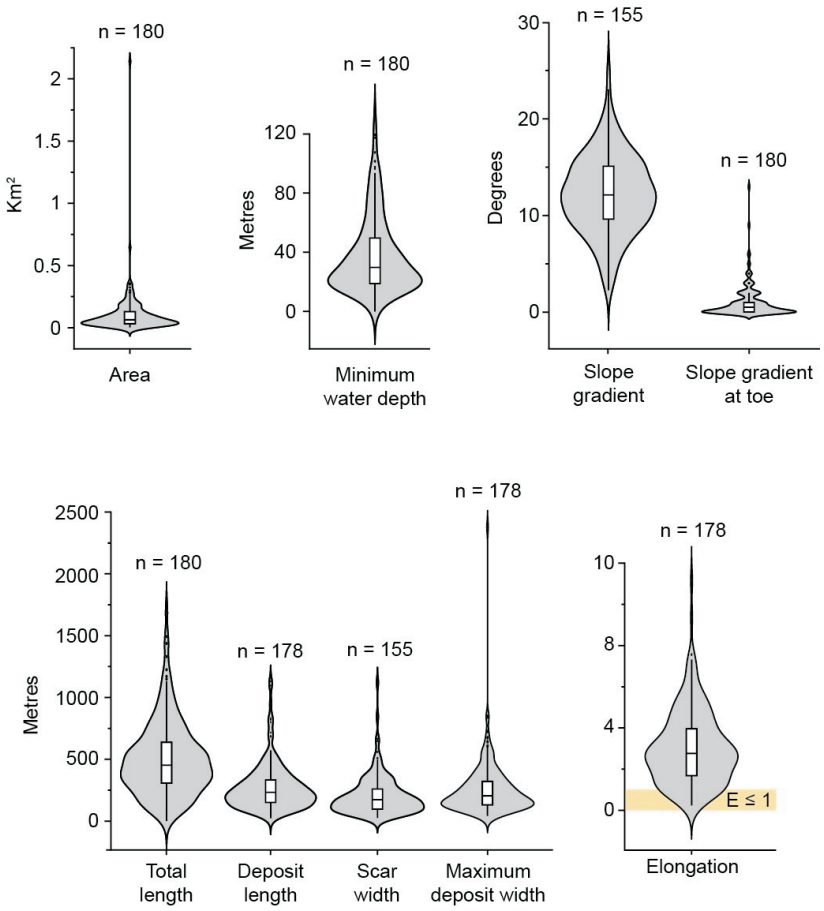

Figure 2: Violin plots of the morphometric parameters for the submarine landslides identified within Pangnirtung Fiord, eastern Baffin Island, including area, minimum water depth, slope gradient, slope gradient at toe, total length, deposit length, scar width, maximum deposit width, and elongation (parameters are defined in Table 1).

the sub-bottom profiles downslope of the fiord-head delta (Figure 3).

Photographs, X-radiographs and physical properties of 14 gravity cores (Sedore, M.Sc. in progress) were used to describe the landslide deposits, as well as discern the dominant lithological facies found in the fiord. The main lithofacies of interest to this study is identified at the top of cores 037 and 047 that were collected within the failure zones of two landslides along the steeply sloped (~20º and ~7º, respectively) submarine fiord sidewalls (Figure 4). These intervals, consisting of coarse-grained sand and a minor proportion of gravel, are interpreted as landslide deposits. These deposits have a lower magnetic susceptibility, and generally a higher but variable bulk density, than the hemipelagic sedimentation found in most cores. The landslide deposits are assumed to be thicker downslope from the coring position; however, these intervals capture remnant sediments associated with the mapped landslides. In core 037, the fining-upward sequence within the top 10 cm was caused by slow sediment settling at the sediment-water interface during the core extraction process; however, coarse-grained sand, gravel and shell fragments are still interpreted as a part of the landslide deposit. These upper intervals of cores 037 and 047 have erosive contacts with the underlying sediment that makes up the rest of the cores (Figure 4).

The underlying facies features wavy-parallel–laminated, dark grey clayey silt with intervals of very fine grained sand and granules identified in the X-radiograph images. These intervals, distinguished by their colour from the rest of the cored sediment, are interpreted as older postglacial sediments. To capture these older sediments in the short sediment cores, there must have been high erosion rates from submarine landslides along the fiord sidewall that removed thick sequences of postglacial hemipelagic sedimentary cover. Additionally, landslide deposits are also identified by fine- to coarse-grained sandy-silt laminations interpreted as turbidites associated with the respective landslide. The coarser grain size of these laminations distinguishes them from the surrounding dark grey or olive grey, highly bioturbated clay and silt with minor occurrences of very fine grained sand and granules. This surrounding lithofacies is interpreted to represent the background hemi-

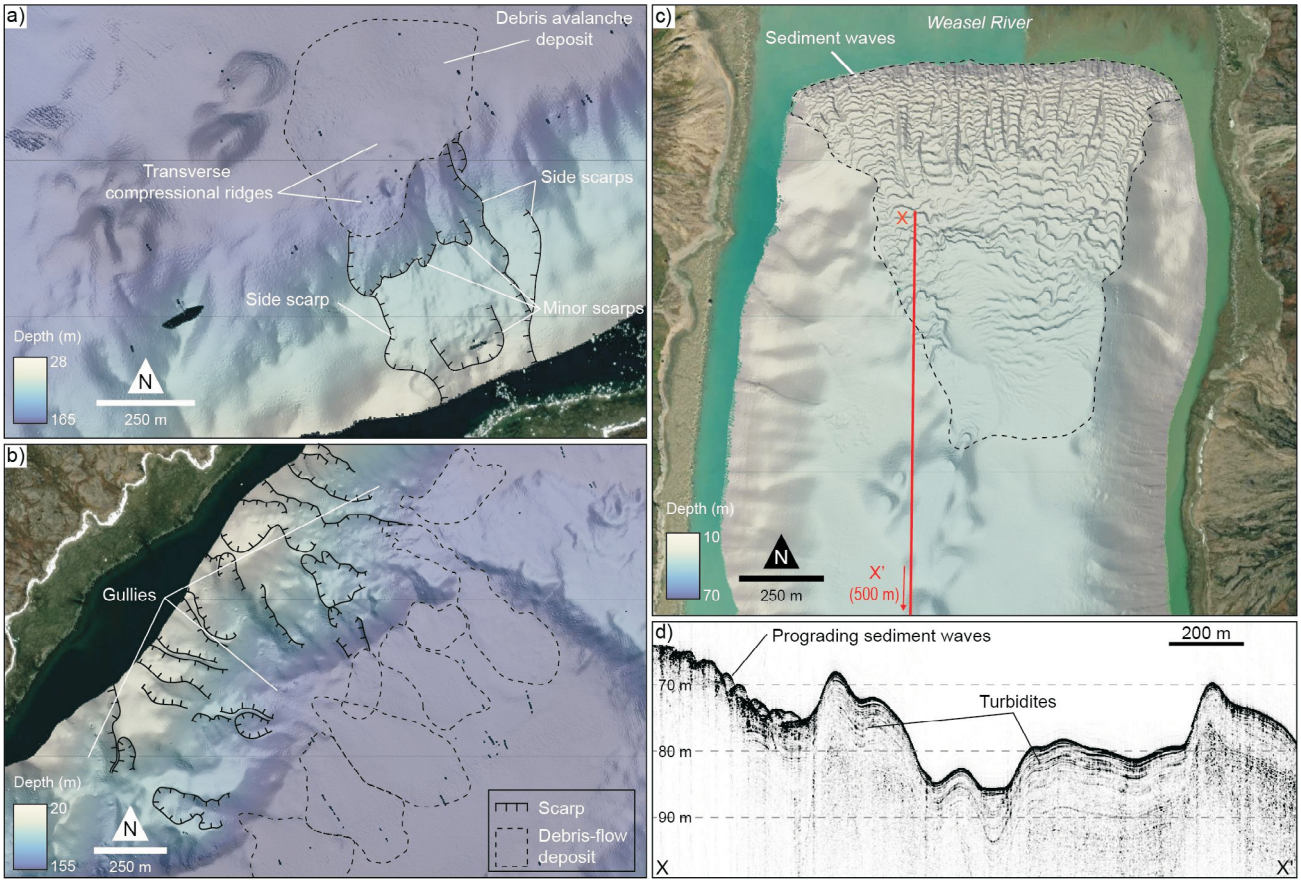

Figure 3: Example of **a)** debris avalanche; **b)** debris flow; **c)** sediment waves identified at the fiord-head delta; and **d)** turbidites and sediment waves identified in a sub-bottom profile acquired near the fiord-head delta. See Figure 1 for locations in Pangnirtung Fiord, eastern Baffin Island. Base map from Maxar Technologies.

pelagic sedimentation within the fiord that also incorporates ice-rafted debris.

Timing of submarine landslides

Using sedimentation rates derived from ^{14}C dating and ^{210}Pb and ^{137}Cs activities (Table 3), the ages of 11 landslides were calculated: eight occurred within the last 500 years with four of these found to be modern events (post-1950). Two examples of these modern landslides are captured in cores 037 and 047 (Figure 4). In core 047, an additional radiocarbon date of 4060 ±230 cal. yr BP (Table 2) at 22 cm depth from within a landslide deposit demonstrates the erosive nature of these landslides to incorporate this older material. The oldest landslide deposit is dated to approximately 4000 yr BP using the sedimentation rates determined from an overlying sediment core and an overburden height of 3 m estimated from sub-bottom data. The largest landslide, which the authors have tentatively named the Kolik River landslide, has an overburden height of approximately 1 m, and is tentatively dated to 1500–2000 yr BP. Future analysis of a sediment core collected in 2021 will precisely date this event. The modern ages of most landslides indicate that there has been recent landslide activity in the fiord, suggesting that these processes are still active and being caused by modern triggering mechanisms. There is a bias toward modern landslides in this study because only short sediment cores were collected; therefore, many buried landslide deposits identified in the multibeam echosounder data are excluded from this analysis. The exclusion of these buried landslide deposits and insufficient sub-bottom profile resolution to differentiate multiple landslides prevent accurate estimates of landslide recurrence in the fiord.

Strupler et al. (2019) found that, in a study of submarine landslides in Lake Zurich, Switzerland, dating based on BPISD can produce a first-order assessment of landslide ages, distinguishing between recent landslides that occurred within the last 150 years and sub-recent landslides. In Pangnirtung Fiord, there is an insufficient number of absolute landslide ages to validate the BPISD as a similar proxy for first-order landslide age. Of the landslide deposits dated in this study (Figure 5), recent landslides (cores 030, 037, 047 and 048 in Table 3) have a wider range of BPISD values than older deposits (cores 034, 041 and 043 in Table 3). The intervals tentatively interpreted as landslides in cores 015, 017 and 020 are not included in this BPISD analysis due to low confidence in the correct interpretation of the landslide

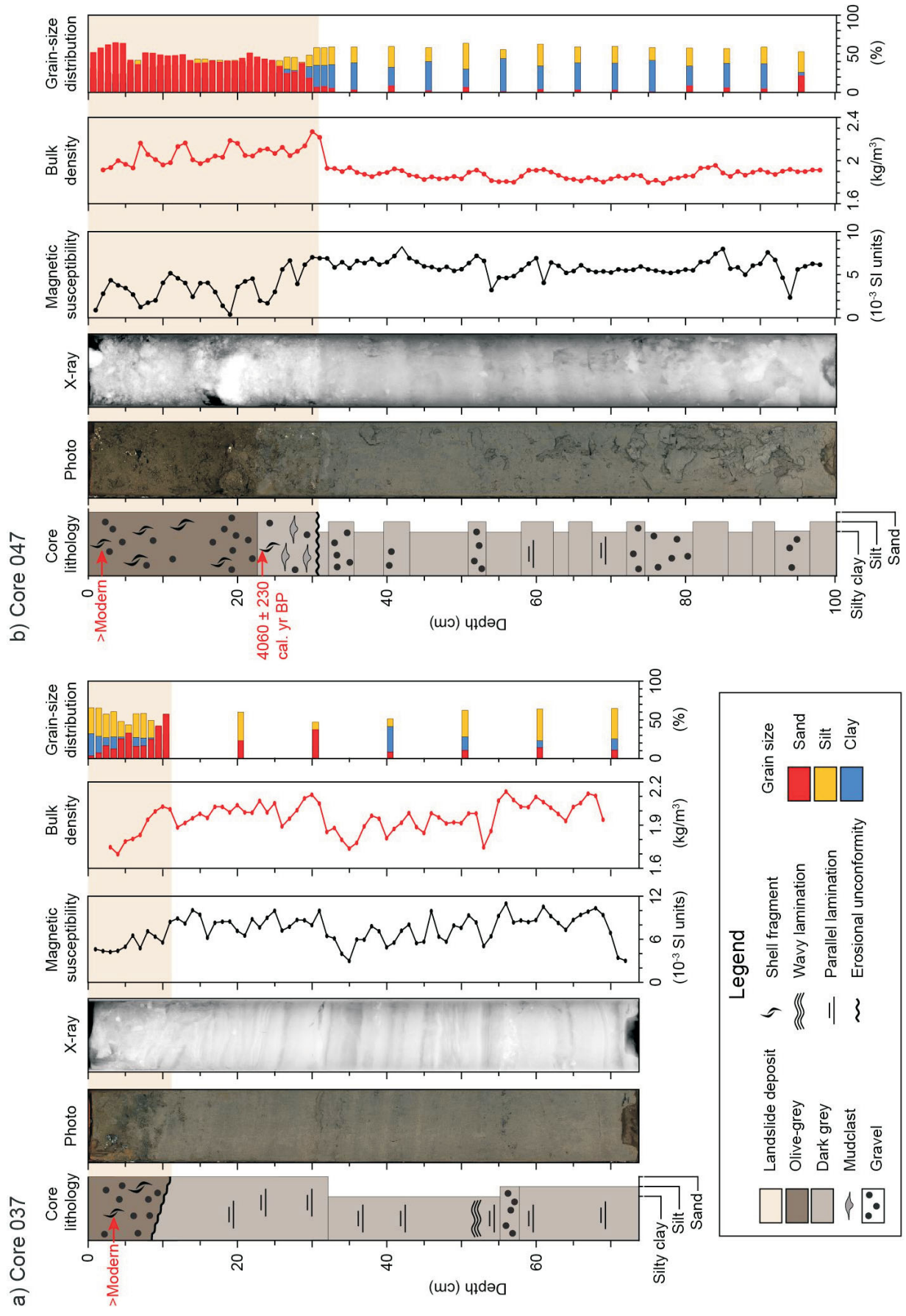

Figure 4: Lithological interpretations, photographs, X-radiographs, physical properties (magnetic susceptibility, bulk density), radiocarbon-dating results (see Table 2) and grain-size data of cores **a)** 037, and **b)** 047. See Figure 1 for core locations in Pangnirtung Fiord, eastern Baffin Island.

interval, as they are located near the fiord-head delta. The landslide interval identified in core 031 is also not included, as artifacts in the bathymetric data prevent accurate surface-roughness analysis. The wide range of BPISD values in recent landslides is reflected by large differences between the absolute and calculated ages of the deposits. In older deposits, their calculated age is a more accurate representation of their absolute age. However, this does not result in a sufficient differentiation of BPISD values to enable the use of surface roughness of the landslides as a proxy for landslide age.

The large range of landslide surface-roughness values is most likely caused by the different types of landslides identified in the fiord, along with variations in slope and landslide run-out (total length). Additionally, possible variations in overburden sedimentation rates, not captured in the dating results from this study, may cause less accurate age predictions of submarine landslides. Despite this conclusion, the surface-roughness analysis suggests that landslide deposits near each other with different relative surface-roughness values may be asynchronous, allowing for a semiquantitative interpretation of the sequence of events (Sedore, M.Sc. in progress).

Trigger mechanisms of submarine landslides

Based on the morphometric parameters, the spatial distribution and the relationship with the subaerial environment (Figure 6), the submarine landslides in Pangnirtung Fiord were grouped into four categories that reflect their possible trigger mechanisms. As an initial discerning factor, the 'minimum water depth' measured parameter, referring to the initiation depth of a submarine landslide, differentiates the mapped landslides into deep-water and shallow-water triggers. The shallow-water triggers are then subdivided based on the submarine landslide's relationship to the subaerial environment. From this, four categories of trigger mechanisms emerge: 1) deep water; 2) shallow water, subaerial debris-flow influenced; 3) shallow water, fluvially influenced; and 4) shallow water, non-subaerially influenced (Figure 7).

Table 3: Landslide interval ages calculated from ^{14}C dating and $^{210}Pb/^{137}Cs$ activities, Pangnirtung Fiord, eastern Baffin Island. Abbreviation: SAR, sediment accumulation rate.

Core	Dating method	Sample interval	Landslide interval depth (cm)	Calibrated age (cal. yr BP)	SAR (cm^2/yr)	Landslide age (cal. yr BP)
015	^{14}C	38–39	20–24	165	0.1834	109
017	^{14}C	68	36–39	145	0.4324	83
020	^{14}C	49–51	51–60	>Modern	-	0
030	$^{210}Pb/^{137}Cs$	-	10–18	-	0.09723	43
031	$^{210}Pb/^{137}Cs$	-	9–28	-	0.07946	58
034	$^{210}Pb/^{137}Cs$	-	300†	-	0.07946	3775
037	^{14}C	3–5	0–9	>Modern	-	0
041	$^{210}Pb/^{137}Cs$	-	100†	-	0.06161	1625
043	^{14}C	40–41	100†	1110	0.0358	2795
047	^{14}C	22–25	0–31	4060	-	0
048	^{14}C	2–3	0–22	745	-	0‡

†Landslide interval depth calculated from sub-bottom profiles.

‡Radiocarbon age is likely older material incorporated into a modern landslide interval.

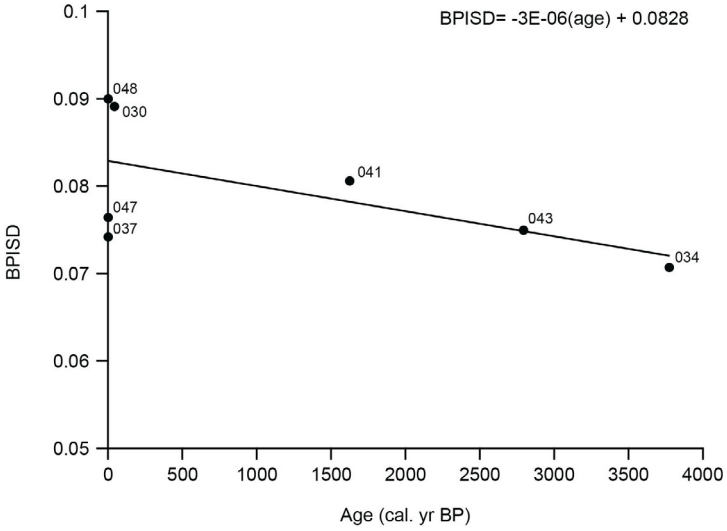

Figure 5: Standard deviation of the bathymetric position index (BPISD) plotted against the ages of the landslide deposits in Pangnirtung Fiord, eastern Baffin Island. Landslides are identified based on their respective core number (see Table 3). The trendline represents the calculated ages of the landslides (R^2 = 0.364).

Deep-water trigger mechanisms

Submarine landslides initiated in deep water (e.g., Figure 7a) constitute 15% of the mapped landslides and are not likely to have a shallow-water or subaerial trigger (Figure 6). The failure zones are identified along the middle of sills where the shallowest possible head scarp is far deeper than wave or tidal influence and far enough away from the fiord sidewalls and major sediment inputs that subaerial and fluvial triggers likely have no influence. Many of these landslides appear to be the result of slope failures in recessional moraine sediments and have numerous scarps over a wide failure area. The most probable triggers for these deeper water landslides are most likely a combination of seismicity induced by isostatic rebound during the retreat of the glaciers in Pangnirtung Fiord and the oversteepening of slopes. Oversteepening of slopes can act as a preconditioning factor, leaving sediment susceptible to seismic triggers (Clare et al., 2016).

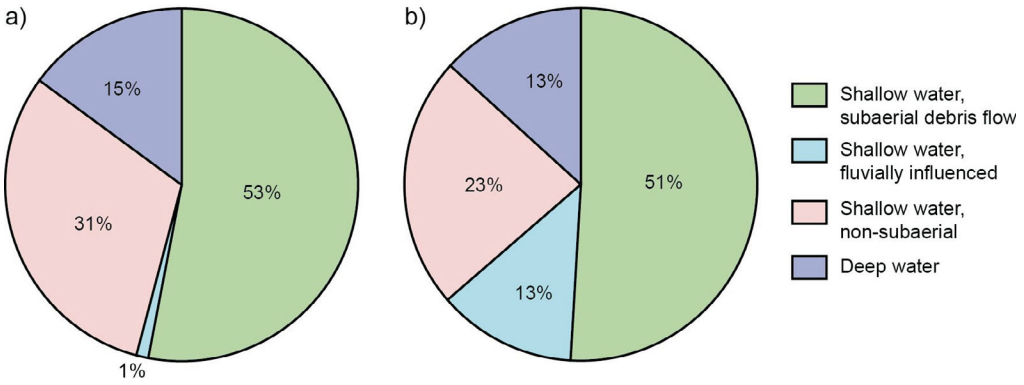

Figure 6: Proportion of interpreted triggering mechanisms of submarine landslides in Pangnirtung Fiord, eastern Baffin Island based on **a)** number of landslides, and **b)** total area of landslides in each trigger classification.

Shallow-water, subaerial debris-flow trigger mechanisms

Subaerial debris flows have been suggested as a potential trigger mechanism of shallow submarine landslides (Bellwald et al., 2016; Deering et al., 2019). Sudden rapid colluvial and alluvial outwash into the shallow water would increase the pore pressure and potentially increase shear stress in the shallow-water sediments. Deering et al. (2019) suggested that subaerial slope failures are a contributing triggering mechanism for most submarine landslides identified in Frobisher Bay, Baffin Island. In Pangnirtung Fiord, the shallow minimum water depth of most landslide failure zones also suggests a possible subaerial influence. Conclusive evidence of a connection between the subaerial environment and submarine landslides in the fiord is shown in satellite imagery from 2019 overlain by the multibeam bathymetry (Figure 7b). A subaerial debris fan clearly extends to the intertidal zone and three submarine landslides are visible downslope; however, no head scarp is mapped in the bathymetry, only side scarps and a transition zone. Three likely head scarps are distinguished in the satellite imagery downslope from the debris fan by their concave shape created at the cusp of the intertidal zone. The proximity of the submarine-landslide head scarps to the subaerial debris fan demonstrates a clear connection between subaerial debris flows and submarine-landslide occurrence. Based on ^{210}Pb geochronological data, the middle landslide, with the highest surface-roughness value, occurred in the early 20th century.

Building on these initial findings, subaerial susceptibility modelling of Pangnirtung Fiord (Normandeau et al., 2022) can be used to understand which of the other submarine landslides were potentially triggered by subaerial debris flows. Normandeau et al. (2022) employed subaerial-landslide susceptibility modelling at the scale of the fiord to identify potential source and propagation areas for subaerial debris-flow hazards following the steps of Horton et al. (2013). The Figure 8 inset shows the results of subaerial susceptibility debris-flow modelling for the subaerial debris-flow example shown in Figure 7b. The area classified as a potential zone for 'large torrents', shaded black, is upslope of the submarine landslides with a clear subaerial connection. This example demonstrates that this subaerial debris-flow susceptibility modelling can be used to determine the number of submarine landslides potentially triggered by subaerial processes. Examining the entire fiord, Figure 8 presents the relative probability of the modelled subaerial landslides entering the fiord, as well as the location of the submarine-landslide deposits identified in the bathymetry. Those landslides located directly downslope of the modelled subaerial debris flows make up 53% of submarine landslides (Figure 6). Overall, this classification of submarine landslides presents a definitive relationship between submarine landslides and the subaerial environment, and illustrates the impact subaerial debris flows have as a major triggering mechanism of submarine landslides in Pangnirtung Fiord.

Shallow-water, fluvial trigger mechanisms

Landslides located downslope of fluvial sources account for 1% of the mapped landslides in the fiord; however, they represent 13% of the total area of all submarine landslides in Pangnirtung Fiord (Figure 6). The largest landslide (2.1 km^2), the Kolik River landslide, was identified downslope from the Kolik River (Figure 7c). Failure scarps are mapped within the bathymetric coverage, but the head scarp is likely in shallower waters, outside the mapping area. A potential head scarp or portion of a head scarp is identified in satellite imagery (Figure 7c). The associated landslide deposit features large blocks that create an undulating surface texture. Delta collapse was the likely cause of the Kolik River landslide, similar to that of a submarine landslide in Lake Brienz, Switzerland (Girardclos et al., 2007). Elevated discharge rates in the Kolik River or an earthquake may be responsible for the delta collapse. There are ongoing efforts to determine the tsunamigenic potential of this landslide.

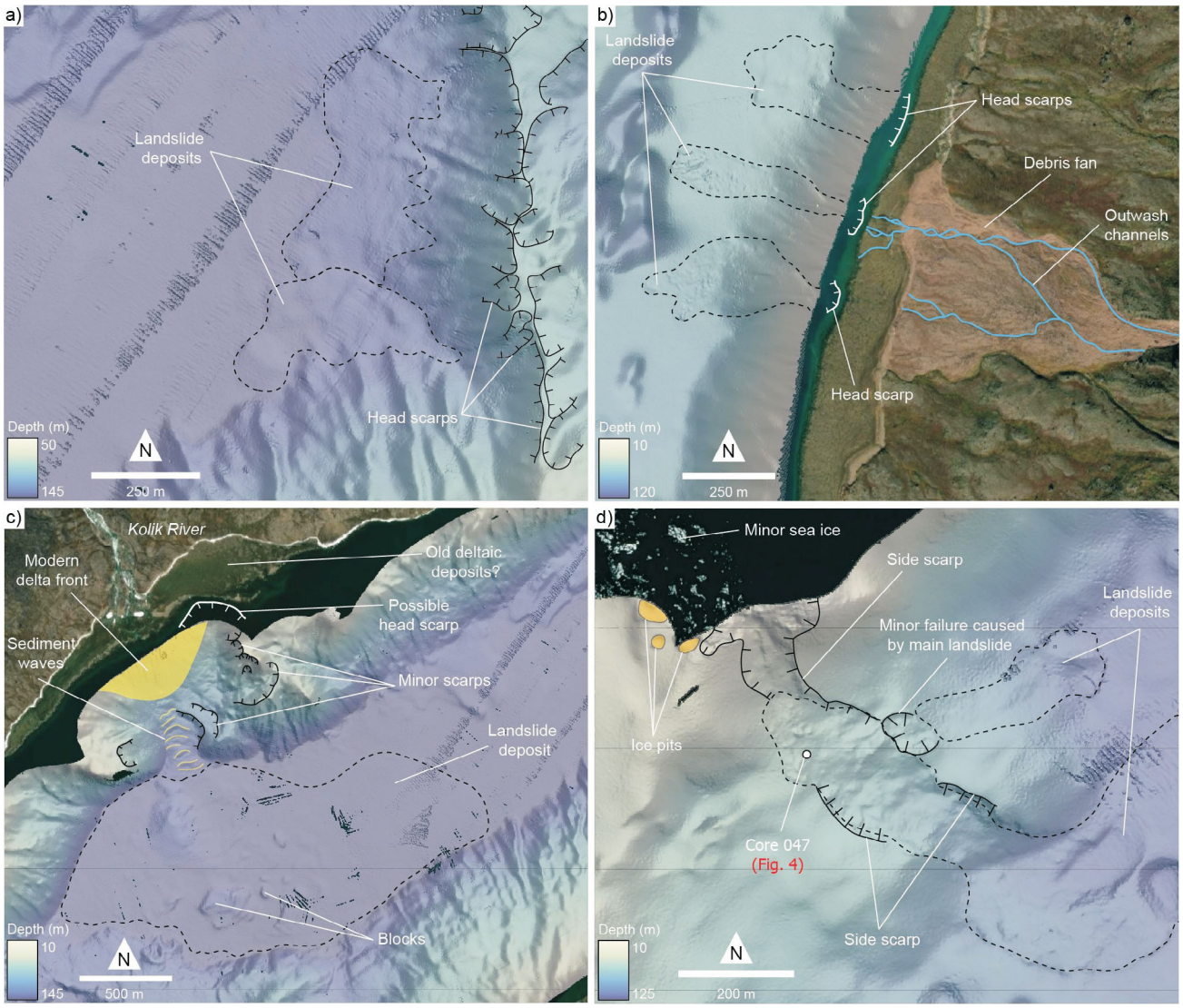

Figure 7: Examples of detailed landslide mapping in Pangnirtung Fiord, eastern Baffin Island: **a)** landslide triggered by deep water; **b)** submarine landslide influenced by shallow-water debris flow; **c)** shallow-water, fluvially influenced submarine landslide at the mouth of the Kolik River; **d)** shallow-water, non-subaerially influenced submarine landslide. See Figure 1 for locations. Base map from Maxar Technologies.

Shallow-water, non-subaerial trigger mechanisms

Thirty-one percent of landslides (Figure 6) are initiated in shallow water but do not have an obvious relationship to a subaerial trigger (Figure 7d). Like the previous classification, the head scarps are identified in shallow water or the assumed head scarps are too shallow to map; however, these landslides do not occur downslope of an area modelled to be susceptible to subaerial landslides. In addition, these landslides are also generally elongated, suggesting a point-source trigger. Likely point-source triggers for these slides include sea-ice and iceberg groundings, wave action and tides. Earthquakes are a possible trigger mechanism, although they would likely cause a wider area of sediment to fail, thus presenting lower elongation values, which is not supported by the morphometric measurements (Figure 2). These mechanisms may also trigger the previously described submarine landslides with perceived connections to fluvial output and subaerial debris flows. These subaerial debris flows and rivers transport sediment to the marine environment, preconditioning the slopes for failure, with these shallow-water, non-subaerially influenced mechanisms ultimately triggering a landslide.

Economic considerations

Both submarine and subaerial landslides are known natural hazards in fiords that can affect coastal communities. Landslide-generated displacement waves of sufficient height can inundate coastal areas and damage low-lying infrastructure. The existence of high-relief fiord sidewalls and mapped subaerial and submarine landslides in Pangnirtung Fiord provide the necessary elements seen in previous Arctic displacement-wave locations (e.g., Brothers et al., 2016;

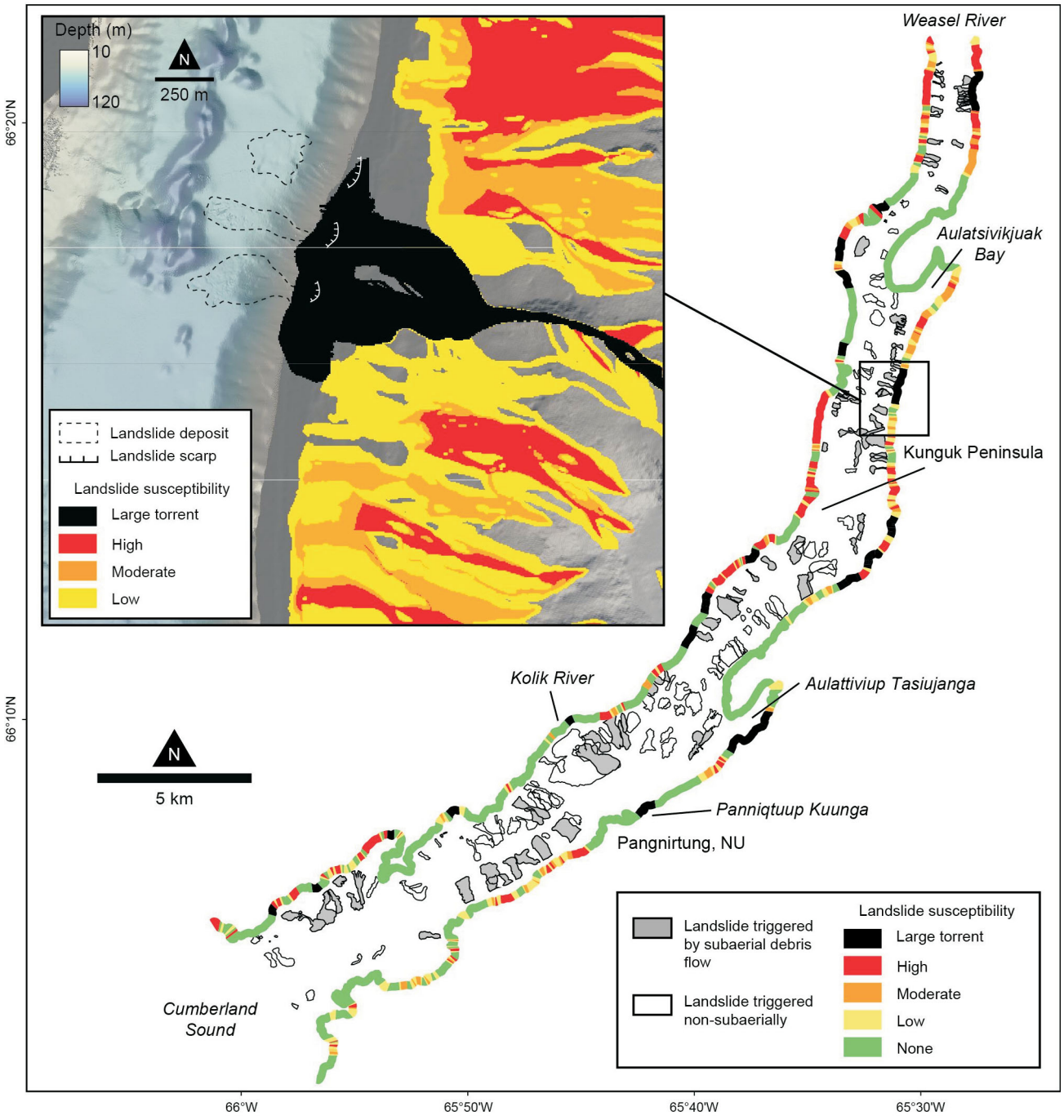

Figure 8: Relative probability of modelled subaerial debris flows (Normandeau et al., 2022) extending to the coast, superimposed on mapping of submarine landslides in Pangnirtung Fiord, eastern Baffin Island. Inset: shallow-water submarine landslides influenced by subaerial debris flows shown in Figure 7b, overlain by results of subaerial debris-flow susceptibility modelling. Digital elevation model created from DigitalGlobe imagery and funded under National Science Foundation awards 1043681, 1559691 and 1542736.

Gauthier et al., 2017; Higman et al., 2018). Without consideration of seafloor-sediment dynamics, submarine landslides can also damage seafloor infrastructure. Proposed seafloor fibre-optic Internet cables may connect the community of Pangnirtung to high-speed Internet, which will help with economic growth. However, submarine landslides remain a possible threat to damage seafloor cables, which would involve costly and lengthy repairs. Mapping the seafloor and understanding the landslide hazards that may affect this infrastructure is a crucial step when planning routes and depths at which cables are buried.

Conclusions

Landslides are proven geological hazards in high-latitude fiords, potentially causing tsunamis and damaging essen-

tial infrastructure. This study sought to provide an evaluation of the distribution, timing, and trigger mechanisms of submarine landslides and associated geohazards for Pangnirtung Fiord. Results of radiometric dating, combined with an analysis of the surface roughness of the landslide deposits, indicate that most landslides occurred within the last 500 years and at least five have occurred since 1900.

This attempt to discern the cause of these submarine landslides produced four categories of triggers. The most abundant trigger mechanism is interpreted as subaerial debris flows entering the sea, causing a rapid influx of sediment and water, and triggering submarine landslides. An examination of subaerial debris flows shows that there is a clear relationship between the distribution of submarine landslides and the surrounding subaerial environment. This relationship demonstrates the need to integrate an evaluation of the subaerial environment when addressing geohazards in the high-relief fiords of Baffin Island. Although most submarine landslides do not appear to have the capacity to initiate a tsunami, ongoing work is focusing on determining the tsunamigenic potential of the largest submarine landslide, the Kolik River landslide (Figure 7c).

Acknowledgments

The authors thank the Captain, officers, crew and scientific staff onboard the RV *Nuliajuk*, and the Hamlet of Pangnirtung. Thanks also go to T. Tremblay of the Canada-Nunavut Geoscience Office for the insightful and detailed review. Financial support for this study was provided by Crown-Indigenous Relations and Northern Affairs Canada, the Government of Nunavut Fisheries and Sealing Division, the Public Safety Geoscience Program of Natural Resources Canada and the Ocean Frontier Institute through an award from the Canada First Research Excellence Fund. Finally, thank you to K. Regular of the Marine Institute and L. Broom, O. Brown, J. Higgins, K. Jarrett, K. Jenner and G. Philibert of the Geological Survey of Canada–Atlantic.

Natural Resources Canada, Lands and Minerals Sector contribution 20210542

References

Basham, P.W., Forsyth, D.A. and Wetmiller, R.J. 1977: The seismicity of northern Canada; Canadian Journal of Earth Sciences, v. 14, no. 7, p. 1647–1667, URL <https://doi.org/10.1139/e77-140>.

Bea, R., Wright, S., Sircar, P. and Niedoroda, A.W. 1983: Wave induced slides in South Pass Block 70, Mississippi Delta; ASCE Journal of Geotechnical Engineering, v. 109, no. 4, p. 619–644, URL <https://doi.org/10.1061/(ASCE)0733-9410(1983)109>.

Bellwald, B., Hjelstuen, B.O., Sejrup, H.P. and Haflidason, H. 2016: Postglacial mass movements and depositional environments in a high-latitude fjord system – Hardangerfjorden, western Norway; Marine Geology, v. 379, p. 157–175, URL <http://dx.doi.org/10.1016/j.margeo.2016.06.002>.

Bennett, R., Normandeau, A. and Campbell, D.C. 2021: Preliminary assessment of the distribution of submarine slope failures in Baffin Island fiords, Nunavut; *in* Summary of Activities 2020, Canada-Nunavut Geoscience Office, p. 73–80, URL <https://cngo.ca/summary-of-activities/2020> [October 2021].

Bornhold, B.D., Ren, P. and Prior, D.B. 1994: High-frequency turbidity currents in British Columbia fjords; Geo-Marine Letters, v. 14, p. 238–243, URL <https://doi.org/10.1007/BF01274059>.

Bronk Ramsey, C. 2008: Radiocarbon dating: revolutions in understanding; Archaeometry, v. 50, p. 249–275, URL <https://doi.org/10.1111/j.1475-4754.2008.00394.x>.

Brooks, G.R. 2016: Evidence of late glacial paleoseismicity from submarine landslide deposits within Lac Dasserat, northwestern Quebec, Canada; Quaternary Research (United States), v. 86, p. 184–199, URL <https://doi.org/10.1016/j.yqres.2016.06.005>.

Broom, L.M., Campbell, D.C. and Gosse, J.C. 2017: Investigation of a Holocene marine sedimentary record from Pond Inlet, northern Baffin Island, Nunavut; *in* Summary of Activities 2017, Canada-Nunavut Geoscience Office, p. 93–104, URL <https://cngo.ca/summary-of-activities/2017/> [October 2021].

Brothers, D.S., Haeussler, P.J., Liberty, L., Finlayson, D., Geist, E., Labay, K. and Byerly, M. 2016: A submarine landslide source for the devastating 1964 Chenega tsunami, southern Alaska; Earth and Planetary Letters, v. 438, p. 112–121, URL <https://doi.org/10.1016/j.epsl.2016.01.008>.

Brouard, E. and Lajeunesse, P. 2019: Submarine geomorphology of the northeastern Baffin Island fiords and cross-shelf troughs; Journal of Maps, v. 15, no. 2, p. 662–676, URL <https://doi.org/10.1080/17445647.2019.1647302>.

Bruel, R. and Sabatier, P. 2020: *serac*: An R package for ShortlivEd RAdionuclide chronology of recent sediment cores; Journal of Environmental Radioactivity, v. 225, p. 106449, URL <https://doi.org/10.1016/j.jenvrad.2020.106449>.

Chillarige, A.R.V., Morgenstern, N.B., Robertson, P.K. and Christian, H.A. 1997: Seabed instability due to flow liquefaction in the Fraser River delta; Canadian Geotechnical Journal, v. 34, p. 520–533, URL <https://doi.org/10.1139/T97-019>.

Clare, M.A., Hughes Clarke, J.E., Talling P.J., Cartigny, M.J.B. and Pratomo, D.G. 2016: Preconditioning and triggering of offshore slope failures and turbidity currents revealed by most detailed monitoring yet at a fjord-head delta; Earth and Planetary Science Letters, v. 450, p. 208–220, URL <https://doi.org/10.1016/j.epsl.2016.06.021>.

Clare, M., Chaytor, J., Dabson, O., Gamboa, D., Georgiopoulou, A., Eady, H., Hunt, J., Jackson, C., Katz, O., Krastel, S., León, R., Micallef, A., Moernaut, J., Moriconi, R., Moscardelli, L., Mueller, C., Normandeau, A., Patacci, M., Steventon, M., Urlaub, M. et al. 2019: A consistent global approach for the morphometric characterization of subaqueous landslides; Subaqueous Mass Movements, Geological Society of London, Special Publications, v. 477, p. 455–477, URL <https://doi.org/10.1144/SP477.15>.

Coulthard, R., Furze, M.F.A., Pieńkowski, A.J., Nixon, F.C. and England, J.H. 2010: New marine ΔR values for Arctic Canada; Quaternary Geochronology, v. 5, no. 4, p. 419–434, URL <https://doi.org/10.1016/j.quageo.2010.03.002>.

Courtney, B. 2009: SegyJp2 Viewer Version 1.0 software; Geological Survey of Canada, Natural Resources Canada, available

at URL <https://ge0mlib.com/software.htm> [January 2022].

Cruden, D.M. and Varnes, D.J. 1996: Landslide types and processes, National Academy of Sciences, Transportation Research Board, Special Report, v. 247, p. 36–75.

Dahl-Jensen, T., Larsen, L.M., Pedersen, S.A.S., Jepsen, H.F., Nielsen, T., Von Platen-Hallermund, F. and Weng, W. 2004: Landslide and tsunami, 21 November 2000 in Paatuut, West Greenland; Natural Hazards, v. 31, p. 277–287, URL <https://doi.org/10.1023/B:NHAZ.0000020264.70048.95>.

Deering, R., Bell, T., Forbes, D.L., Campbell, C. and Edinger, E. 2019: Morphological characterization of submarine slope failures in a semi-enclosed fjord, Frobisher Bay, eastern Canadian Arctic; Subaqueous Mass Movements, v. 477, p. 367–376, URL <https://doi.org/10.1144/SP477.35>.

Gauthier, D., Anderson, S.A., Fritz, H.M. and Giachetti, T. 2017: Karat Fjord (Greenland) tsunamigenic landslide of 17 June 2017: initial 3D observations; Landslides, v. 15, p. 327–332, URL <https://doi.org/10.1007/s10346-017-0926-4>.

Gilbert, R. 1978: Observations on oceanography and sedimentation at Pangnirtung Fiord, Baffin Island; Maritime Sediments, v. 14, no. 1, p. 1–9, URL <https://doi.org/10.4138/1952>.

Girardclos, S., Schmidt, O.T., Sturm, M., Ariztegui, D., Pugin, A., and Anselmetti, F.S. 2007: The 1996 AD delta collapse and large turbidite in Lake Brienz; Marine Geology, v. 241, p. 137–154, URL <https://doi.org/10.1016/j.margeo.2007.03.011>.

Hampton, M.A., Lee, H.J. and Locat, J. 1996: Submarine landslides; Springer Geology, v. 34, p. 33–59, URL <https://doi.org/10.1007/978-3-319-57852-1_13>.

Heaton, T., Köhler, P., Butzin, M., Bard, E., Reimer, R., Austin, W.E.N., Ramsey, C.B., Grootes, P.M., Hughen, K.A., Kromer, B., Reimer, P.J., Adkins, J., Burke, A., Cook, M.S., Olsen, J. and Skinner, L. 2020: Marine20 – the marine radiocarbon age calibration curve (0–55,000 cal. BP); Radiocarbon, v. 62, no. 4, p. 779–820, <https://doi.org/10.1017/RDC.2020.68>.

Higman, B., Shugar, D.H., Stark, C.P., Ekström, G., Koppes, M.N., Lynett, P., Dufresne, A., Haeussler, P.J., Geertsema, M., Gulick, S., Mattox, A., Venditti, J.G., Walton, M.A.L., McCall, N., Mckittrick, E., MacInnes, B., Bilderback, E.L., Tang, H., Willis, M.J., Richmond, B. et al. 2018: The 2015 landslide and tsunami in Taan Fiord, Alaska; Nature: Scientific Reports, v. 8, art. 12993, URL <https://doi.org/10.1038/s41598-018-30475-w>.

Horton, P., Jaboyedoff, M., Rudaz, B., and Zimmermann, M. 2013: Flow-R, a model for susceptibility mapping of debris flows and other gravitational hazards at a regional scale; Natural Hazards and Earth System Sciences, v. 13, p. 869–885, URL <https://doi.org/10.5194/nhess-13-869-2013>.

Hungr, O., Evans, S.G., Bovis, M.J. and Hutchinson, J.N. 2001: A review of the classification of landslides of the flow type; Environmental and Engineering Geoscience, v. 7, p. 221–238, URL <https://doi.org/10.2113/gseegeosci.7.3.221>.

Jackson, G.D. and Sanborn-Barrie, M. 2014: Geology, Pangnirtung Fiord, Nunavut; Geological Survey of Canada, Canadian Geoscience Map 4, 1:100 000 scale, URL <https://doi.org/10.4095/288928>.

Johns, M.W., Prior, D.B., Bornhold, D.B., Coleman, J.M. and Bryant, W.R. 1985: Geotechnical aspects of a submarine slope failure, Kitimat Fjord, British Columbia. Marine Geotechnology, v. 6, p. 243–279, URL <https://doi.org/10.1080/10641198609388190>.

Krishnaswamy, S., Lal, D., Martin, J.M. and Meybeck, M. 1971: Geochronology of lake sediments; Earth and Planetary Science Letters, v. 11, p. 407–414, URL <https://doi.org/10.1016/0012-821X(71)90202-0>.

Kuenen, P.H. 1952: Estimated size of the Grand Banks turbidity current; American Journal of Science, v. 250, p. 874–884, URL <https://doi.org/10.2475/ajs.250.12.874>.

Lundblad, E.R., Wright, D.J., Miller, J., Larkin, E.M., Rinehart, R., Naar, D.F., Donahue, B.T., Anderson, S.M. and Battista, T. 2006: A benthic terrain classification scheme for American Samoa; Marine Geodesy, v. 29, p. 89–111, URL <https://doi.org/10.1080/01490410600738021>.

Masson, D.G., Harbitz, C.B., Wynn, R.B., Pedersen, G. and Løvholt, F. 2006: Submarine landslides: processes, triggers and hazard prediction; Philosophical Transactions of the Royal Society, A: Mathematical, Physical and Engineering Sciences, v. 364, p. 2009–2039, URL <https://doi.org/10.1098/rsta.2006.1810>.

Miller, D.J. 1960: Giant waves in Lituya Bay, Alaska; U.S. Geological Survey, Professional Paper 354-C, URL <http://pubs.er.usgs.gov/publication/pp354C> [January 2022].

Normandeau, A., Blais-Stevens, A., Horton, T., Oppikofer, T., Sedore, P. and Maselli, V. 2022: Landslide susceptibility in Pangnirtung Fiord, Nunavut; Geological Survey of Canada, Open File 8843, 1 poster.

Normandeau, A., Dietrich, P., Hughes Clarke, J., Van Wychen, W., Lajeunesse, P., Burgess, D. and Ghienne, J.F. 2019: Retreat pattern of glaciers controls the occurrence of turbidity currents on high-latitude fjord deltas (eastern Baffin Island); Journal of Geophysical Research: Earth Surface, v. 124, p. 1559–1571, URL <https://doi.org/doi:10.1029/2018JF004970>.

Normandeau, A., MacKillop, K., Macquarrie, M., Richards, C., Bourgault, D., Campbell, D.C., Maselli, V., Philibert, G. and Hughes Clarke, J. 2021: Submarine landslides triggered by iceberg collision with the seafloor; Nature Geoscience, v. 14, p. 599–605, URL <https://doi.org/10.1038/s41561-021-00767-4>.

Oppikofer, T., Jaboyedoff, M., Derron, M.H. and Bilkra, L.H. 2009: Geometric back-analysis of ancient rockslides in Tafjord (Norway); Geophysical Research Abstracts, EGU General Assembly 2009, v. 11, EGU 2009-7647, URL <https://ui.adsabs.harvard.edu/abs/2009EGUGA.11.7647O/abstract>.

Pourchet, M., Pinglot, J.F. and Marie, A.M. 1989: Cesium-137 and lead-210 in alpine lake sediments: measurements and modeling of mixing process; Journal of Geophysical Research, v. 94, no. C9, p. 12761–12770. URL <https://doi.org/10.1029/JC094iC09p12761>.

Prior, D.B. and Bornhold, B.D. 1989. Submarine sedimentation on a developing Holocene fan delta; Sedimentology, v. 36, p. 1053–1076, URL <https://doi.org/10.1002/9781444304473.ch34>.

Strupler, M., Anselmetti, F.S., Hilbe, M. and Strasser, M. 2019: Quantitative characterization of subaqueous landslides in Lake Zurich (Switzerland) based on a high-resolution bathymetric dataset; Geological Society of London, Special Publications, v. 477, p. 399–412, URL <https://doi.org/10.1144/SP477.7>.

Stein, S., Sleep, N.H., Geller, R.J., Wang, S. and Kroeger, G.C. 1979: Earthquakes along the passive margin of eastern Canada; v. 6, p. 537–540, URL <https://doi.org/10.1029/GL006i007p00537>.

Syvitski, J., Burrell, D.C. and Skei, J.M. 1987: Fjords: processes and products; Arctic and Alpine Research, v. 20, no. 3, URL <https://doi.org/10.1007/978-1-4612-4632-9>.

Tappin. D.R. 2010: Submarine mass failures as tsunami sources – their climate control; Philosophical Transactions of the Royal Society A: Mathematical, Physical and Engineering Sciences, v. 368, no. 1919, p. 2417–2434. URL <https://doi.org/10.1098/rsta.2010.0079>.

Urlaub, M., Talling, P.J. and Masson, D.G. 2013: Timing and frequency of large submarine landslides: implications for understanding triggers and future geohazard; Quaternary Science Reviews, v. 72, p. 63–82, URL <https://doi.org/10.1016/j.quascirev.2013.04.020>.

Waldmann, N., Vasskog, K., Simpson, G., Chapron, E., Støren, E.W.N., Hansen, L., Loizeau, J., Nesje, A. and Ariztegui, D. 2021: Anatomy of a catastrophe: reconstructing the 1936 rock fall and tsunami event in Lake Lovatnet, western Norway; Frontiers in Earth Science, v. 9, p. 1–18, URL <https://doi.org/10.3389/feart.2021.671378>.

Water Survey of Canada 1983: Daily discharge graph for Duval River near Pangnirtung (10UF001) [NU]; Water Survey of Canada, URL <https://wateroffice.ec.gc.ca/report/historical_e.html?stn=10UF001> [October 2021].

Geotechnical characterization of a submarine landslide in Southwind Fiord, Baffin Island, Nunavut

Meaghan Macquarrie[1], Kevin MacKillop[2] and Alexandre Normandeau[1]

[1]*Natural Resources Canada, Geological Survey of Canada–Atlantic, Dartmouth, Nova Scotia*

[2]*Natural Resources Canada, Geological Survey of Canada–Atlantic, Dartmouth, Nova Scotia, kevin.mackillop@nrcan-rncan.gc.ca*

This work is part of the Baffin Bay Geohazards Activity of the Landslides and Marine Geohazards Project of Natural Resources Canada's Public Safety Geoscience Program (PSGP). This program undertakes research across Canada to support risk reduction from the effects of hazardous natural conditions (i.e., space weather, earthquakes, tsunamis, volcanoes and landslides). The program develops authoritative scientific knowledge and tools to reduce future economic, social and environmental losses from these hazards. Additional funding for this research was provided by the Government of Canada's Program of Energy Research and Development (PERD), Crown-Indigenous Relations and Northern Affairs Canada, ArcticNet and the Ocean Frontier Institute.

Macquarrie, M., MacKillop, K. and Normandeau, A. 2022: Geotechnical characterization of a submarine landslide in Southwind Fiord, Baffin Island, Nunavut; *in* Summary of Activities 2021, Canada-Nunavut Geoscience Office, p. 47–56.

Abstract

Most eastern Baffin Island communities are located in the near-shore areas of fiords in Baffin Bay, where submarine landslides represent a significant geohazard for offshore infrastructure and for coastal communities. Fiords have long been known for the occurrence of a wide variety of mass-wasting processes and have been designated as one of the major submarine landslide areas. Geotechnical characterization is an important component in developing a better understanding of the engineering behaviour of the marine sediments and constraining seabed slope stability analysis. Southwind Fiord, eastern Baffin Island, contains numerous slope failures identified from 2018 and 2019 multibeam bathymetry surveys and was chosen for detailed seabed sampling in 2018 as a test site to understand the occurrence and triggers of such events. A comprehensive geotechnical testing program was undertaken on sediments from two piston cores collected offshore Southwind Fiord: one from a reference seabed site, and one from a site within a slope failure. The geotechnical test data were used to characterize the geotechnical properties of the seabed sediments, and to evaluate slope stability and seabed foundation conditions within the fiord. The sediments within the two sites identify as low- to high-plasticity, normally consolidated clayey silts. The compressibility of the sediments is moderate to high, ranging from 0.36 to 0.73. Based on the data presented in this paper, the sediments have a low hydraulic conductivity (average of 6.0×10^{-9} m/s), typical for clayey silt, and the Mohr-Coulomb failure criteria (effective cohesion and angle of friction) average 0.6 kPa and 31.3°. An infinite slope stability analysis suggests the sediments are stable under gravitational loading up to a critical slope angle of 20°.

Introduction

Since 2009, the Geological Survey of Canada (GSC) has undertaken a research project to study marine geohazards in Baffin Bay, Nunavut. Slope instability resulting in slope failure and landslides, particularly within fiords extending into Baffin Bay, represents one of the major potential geohazards in the region, such that their understanding and some degree of predictability is important. Fiords are known for a variety of mass-wasting processes and have been designated a major submarine landslide area (Hampton et al., 1996). Slope stability evaluation involves delineating the linkage between failure-triggering mechanisms, the geotechnical properties of the seabed sediments, and their geology and geomorphology.

Baffin Bay forms an elongated ocean basin, 1300 km in length and 450 km wide, which connects northward to the Arctic Ocean and southward to the Labrador Sea and North Atlantic Ocean. Baffin Island's offshore contains inner fiords, which trap most of the sediment brought in by rivers and have steep side walls. Southwind Fiord on Baffin Island, Nunavut (Figure 1), was selected as a test site for a detailed geohazards assessment because it contains a large number of submarine slope failures, which have been identified from multibeam bathymetric surveys carried out in 2018 and 2019 (Normandeau et al., 2021).

A detailed seabed sampling program was initiated in Southwind Fiord in 2018, with the objective of characteriz-

This publication is available, free of charge, as colour digital files in Adobe Acrobat® PDF format from the Canada-Nunavut Geoscience Office website: https://cngo.ca/summary-of-activities/2021/. Il est aussi disponible en français sur https://cngo.ca/fr/.

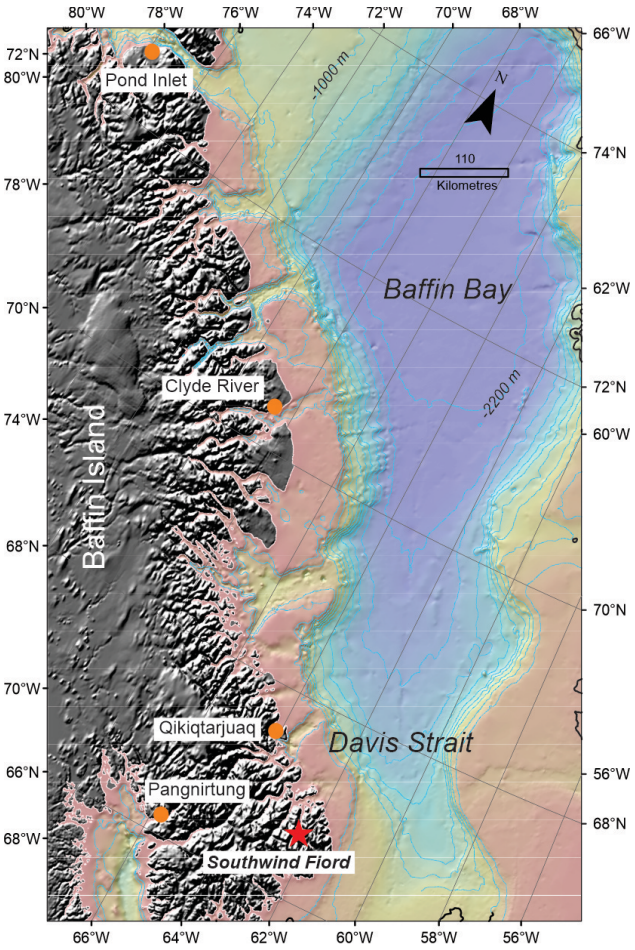

Figure 1: Location of Southwind Fiord (red star), eastern Baffin Island, Nunavut. Orange dots indicate the main coastal communities in the area. The bathymetric contour interval (blue lines) is 200 m. Bathymetry is from the General Bathymetric Chart of the Oceans (GEBCO; GEBCO Compilation Group, 2014). The digital elevation model (DEM) is from 2012 (unpublished Canadian Hydrographic Service data).

ing the engineering behaviour of the sediments. This characterization is used in this paper to evaluate the sediments' response to environmental loading (including authigenic activity). The geotechnical properties that were analyzed include the following:

- Bulk density, water content and void ratio: these are elementary properties that characterize the in situ state of the sediment.
- Grain size analysis and Atterberg limit tests: these were used to determine the sediment's classification, representative of its engineering properties—including permeability, compressibility and strength.
- Consolidation: defined as the compression of sediments following the application of loads and used to measure the sediment's compressibility, hydraulic conductivity and maximum past geological stress.
- Shear strength: this includes the sediment properties (friction angle and cohesion) that characterize its ability to withstand external loading, including construction loads as well as environmental loads from seismic activity, iceberg impacts and rock falls that extend into the fiord.

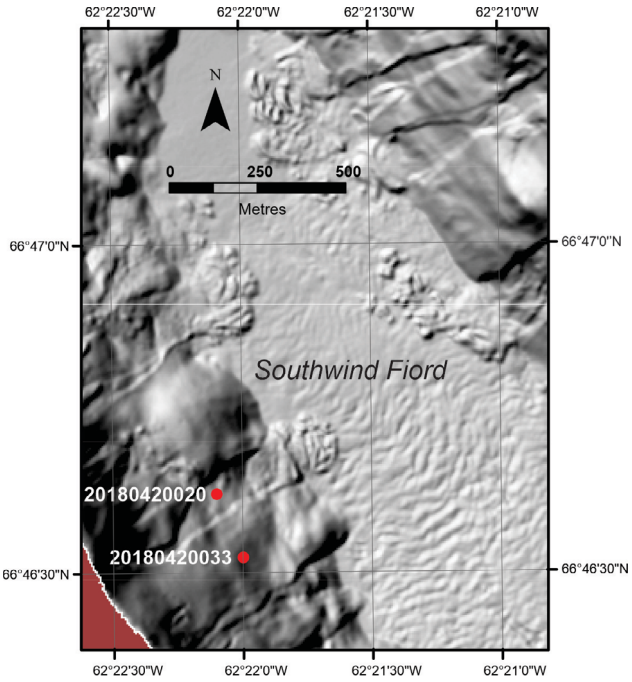

Figure 2: Location of piston cores taken in 2018 in Southwind Fiord (eastern Baffin Island) and used for this study. Core 20180420033 is from a representative seabed site, core 20180420020 is from a slope failure site. The background image is from Ocean Mapping Group (2014).

This paper presents a geotechnical characterization of seabed sediments from Southwind Fiord using results of laboratory tests on samples of sediment from two piston cores collected in 2018: one core from a representative seabed site (core 20180420033, hereinafter referred to as core 33), and one core taken at a past slope failure site within the study area (core 20180420020, hereinafter referred to as core 20; Figure 2).

Methods

Core sampling

Piston cores were collected in 2018 from the Canadian Coast Guard Ship *Hudson* (Normandeau et al., 2021) using the AGC long-coring system and processed at the Geological Survey of Canada–Atlantic Division's (GSC-A) marine core processing and sedimentology laboratory. Bulk density measurements (determined from gamma-ray attenuation) were performed at 1 cm intervals using Geotek Ltd.'s whole-core Standard Multi-Sensor Core Logger (MSCL-S).

Whole-core subsamples of 15 to 25 cm length of undisturbed sediment were obtained from the piston cores for

consolidation and triaxial testing. Prior to taking whole rounds, the sample quality was evaluated using X-ray images, which identified areas of core disturbance, and presence of dropstones and biogenic shells.

Core sections not selected for consolidation and triaxial testing were split, X-rayed, photographed under high resolution and described visually. Undrained shear strength measurements were obtained every 5 to 10 cm using an automated miniature vane shear (MV) apparatus, following ASTM D4648 (ASTM D4648/D4648M, 2010). Remoulded undrained shear strength measurements were taken at 20 to 30 cm intervals. Water content, unit weight and void ratio were determined from constant-volume samples. Water content was corrected for a salt content of 35 parts per trillion (ppt). Constant-volume samples were taken at the locations of the MV measurements and at other locations of interest. Atterberg limits (ASTM D4318, 2010) and grain size were determined on representative samples and used to classify the sediments according to the Unified Soil Classification System (USCS; ASTM D2487, 2011). The grain-size distribution was determined using a Beckman Coulter, Inc. LS230 multi-frequency laser at the GSC-A marine core processing and sedimentology laboratory.

The geotechnical test results from the GSC-A marine core processing and sedimentology laboratory were compiled into geotechnical profiles with the various sediment properties presented as a function of depth. The profiles include down-core plots of X-ray analyses, core photographs, grain size, MSCL-S bulk density, natural water content, plastic and liquid limits, and MV undrained shear strength.

Consolidation testing

Consolidation tests reproduce gravitational compaction in a controlled environment to simulate a sediment's response to vertical loading. Consolidation results in the expulsion of water from the sediment and a corresponding decrease in volume. The compressibility (C_c) and rate of consolidation are used in seabed foundation design and depend on the sediment's composition, grain-size distribution, permeability (k) and stress state, described by the overconsolidation ratio (OCR).

The compressibility (C_c), hydraulic conductivity, and OCR of the sediments were measured on four samples in standard incremental loading consolidation tests with a load increment ratio of 0.5, following ASTM D2435 (ASTM D2435/D2435M, 2011). Two samples were from the reference seabed site and two from within the slope failure site. The preconsolidation stress (P'_c) was determined using Casagrande's method (Casagrande, 1936). The effective overburden stress (σ'_v) was calculated by integrating the MSCL-S bulk density results with depth.

The consolidation system used was GDS Instrument's (GDS) back-pressured constant rate of strain cell (CRS) system, consisting of a CRS consolidation cell for 6.35 cm diameter samples, a 50 kilonewton (kN) load frame, a GDS 1 MPa standard pressure/volume controller, a 25 mm linear displacement transducer, a 2 MPa pore pressure transducer, 2 kN submersible load cell, 16-bit data acquisition system, computer and GDSLAB software.

Triaxial testing

The shear strength of a sediment is the maximum resistance it displays against failure and is controlled by its effective stress. The strength characteristics of seabed sediment are paramount in evaluating seabed foundation conditions and various triggering mechanisms for slope stability analysis. The most common failure criteria applied to a sediment is the Mohr-Coulomb failure criteria, defined as,

$$\tau_f = c' + \sigma'_n \tan \phi'$$

where τ_f is the drained shear strength at failure, c' is the effective cohesion, σ'_n is the effective normal stress, and ϕ' is the effective internal angle of friction.

Factors that affect Mohr-Coulomb strength parameters include grain size, angularity of the particles, relative density and stress history. The effect of stress history on the undrained shear strength of fine-grained sediments can be characterized using Ladd and Foott's (1974) 'stress history and normalized soil engineering properties' (SHANSEP) method. A comprehensive analysis of the sediments' undrained shear strength using the SHANSEP method includes the determination of the ratio of undrained strength (S_u) to the vertical effective stress (σ'_v) for several stress state (OCR) values and is presented as

$$\frac{S_u}{\sigma'_v} = S(OCR)^m$$

where S is the S_u/σ'_v ratio for normally consolidated soils and m is a soil constant. For simplicity, S will be used to represent the S_u/σ'_v ratio for normally consolidated soils (OCR = 1) for the remainder of the paper.

The Mohr-Coulomb stress parameters, c' and ϕ', and S values were determined from isotropically consolidated undrained (CIU) triaxial tests following ASTM D4767 (ASTM D4767, 2011). In this test method, the sediment sample is fully consolidated under a load and is then subjected to a compressive axial stress without allowing drainage. The S values were determined at consolidation loads of 2.5 to 4 times the preconsolidation stress (Ladd and Foott, 1974). The measured S values were used to obtain continuous profiles of undrained shear strength for normally consolidated clays (OCR = 1).

The triaxial system used was a GDS computer-controlled hydraulic stress path triaxial testing system consisting of a 50 mm Bishop & Wesley–type triaxial cell, three GDS 2 MPa pressure/volume controllers, a 5 kN submersible load cell, pore pressure transducer, linear displacement transducer, a data acquisition system, a computer and GDSLAB software.

Slope stability

The limit equilibrium methods are most commonly used to assess the slope stability in a marine environment. The limit equilibrium analysis evaluates a well-defined body on a slope as if it is about to fail and determines the shear stress induced under various trigger mechanisms. The shear stresses are then compared to the soil's shear strength to determine the factor of safety (FS), with the slope considered to be unstable if the FS is equal to or less than 1.

$$FS = \frac{Sediment\ \ Strength\ \ (Available\ \ Shear\ \ Strength)}{Trigger\ \ Mechanisms\ \ Stress\ \ (Driving\ \ Force)}$$

The infinite slope method was used for the slope stability analysis. It assumes the failure surface is parallel to the slope, the slope is planar, of infinite length and is significantly greater than the failure thickness. The minimum FS and critical slope angle were calculated for the length of each core. The triggering mechanism investigated was gravitational loading. The gravitational force is considered to be parallel to the slope and is equal to the effective weight of the soil and the sediments' shear strength.

Results

Soil classification

The seabed sediments from the two sites are similar in character and consist of inorganic clayey silts of low to high plasticity (categories ML and MH, respectively, of the USCS; Figure 3). The three samples near the bottom of core 33 are of low plasticity and plot within Zone B of Seed et al. (2003), suggesting the potential for liquefaction. The sediments are considered to be inactive (the 'activity' of a clay may be defined as the ratio of its plasticity index to its clay fraction; Skempton, 1953), with an activity similar to the value for illite. The water content is consistent in the upper core depths and then shows a steady decrease with depth, corresponding with an increase in the MSCL-S bulk density (Figures 4, 5). The water content is higher than the liquid limit, suggesting underconsolidated sediments. Table 1 summarizes the physical properties of the sediments.

Consolidation characteristics

The compressibility (C_c), hydraulic conductivity (k) and stress history of the sediments were determined from the results of four back-pressured consolidation tests (Figure 6). The sediments exhibit very similar consolidation (e-log effective stress) curves. The compressibility (C_c) of the sediments is intermediate to high, ranging from 0.36 to 0.73 (Table 2). There is good correlation between the initial void ratio (e_o) and the compressibility values (Figure 7), indicative of silts to clayey silts of low sensitivity (Holtz and Kovacs, 1981). The recompression (C_r) values range from 0.10 to 0.18 and are approximately 25% of the compressibility.

The overconsolidation ratio (OCR) calculated from the four tests, using Casagrande's (1936) method, indicate the sediments are normally consolidated, with the exception of the sediments in the upper depths of the slope failure site (core 20). The high OCR value of 2.8 is considered to be in a zone of apparent overconsolidation (Gourvenec and White, 2010). The sediments have a low hydraulic conductivity (k) at the estimated in situ stress. The k values range from 1.0×10^{-8} to 8.4×10^{-9} m/s (Table 2), typical for clayey silt.

Strength

Results of the triaxial tests are presented in Table 3. The effective friction angles (ϕ') range from 27.6° to 33.8°. The failure envelopes show low cohesion (c') intercepts, ranging from 0.0 to 2.4 kPa. Skempton's (1954) pore pressure parameter at failure (A_f) is consistent for the five samples tested, ranging from 0.40 to 0.48. The c' and A_f values are

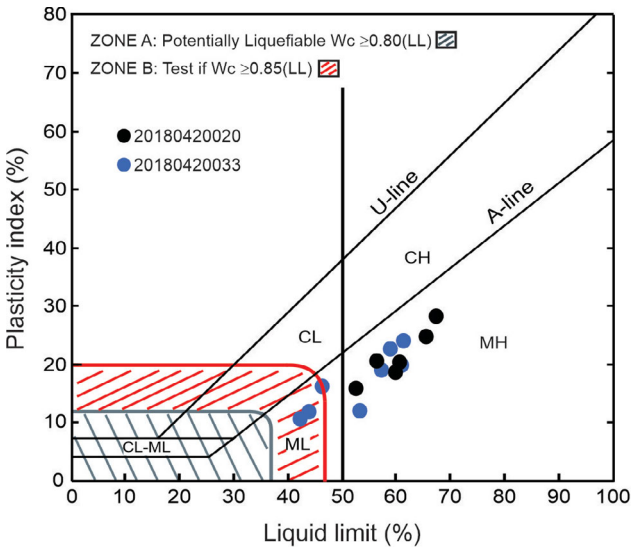

Figure 3: Plasticity chart showing the Atterberg limits for cores 20180420020 and 20180420033 from Southwind Fiord, eastern Baffin Island (modified after Seed et al., 2003). The A-line separates clay-like (C) sediments from silty (M) sediments. The U-line indicates the upper plasticity index and liquid limit values for all sediments. The chart is further subdivided on the basis of low (L) and high (H) liquid limits. Seed et al. (2003) used the sediments' water content (Wc), plasticity index and liquid limit (LL) to identify sediments that are potentially susceptible to cyclic liquefaction (Zone A), sediments requiring further testing to evaluate liquefiable potential (Zone B) and sediments not susceptible to liquefaction (Zone C; areas of the chart not designated as Zone A or B).

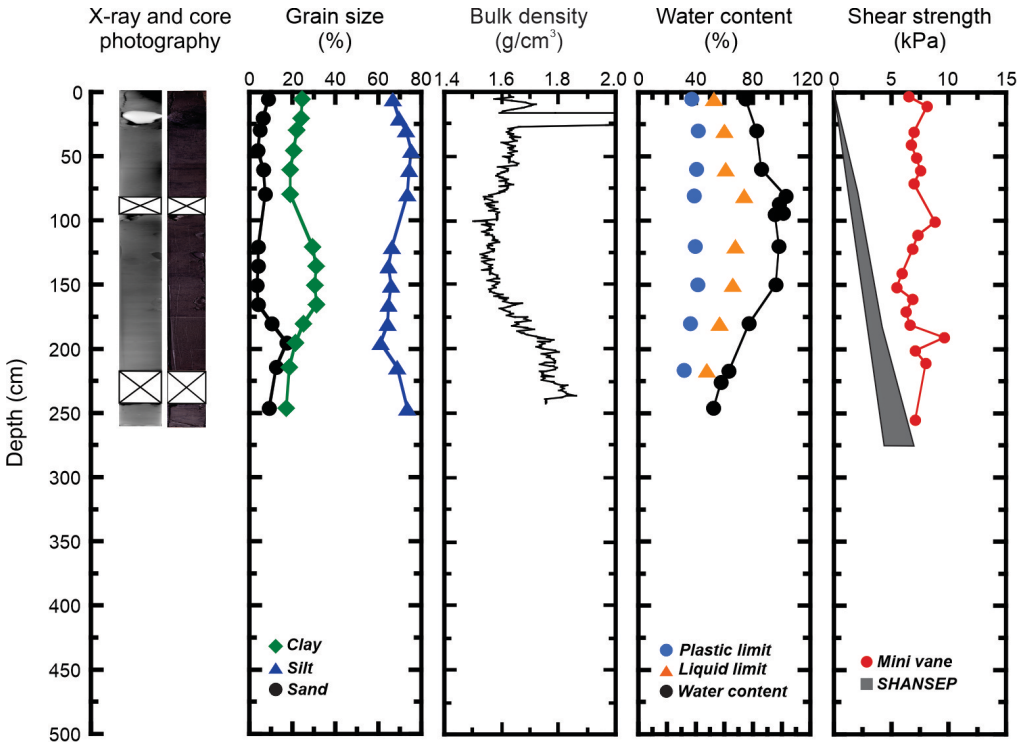

Figure 4: Geotechnical profile for core 20180420020, from the slope failure site at Southwind Fiord, eastern Baffin Island. Abbreviations: Mini vane, miniature vane shear-strength measurements; SHANSEP, stress history and normalized soil engineering properties (Ladd and Foott, 1974).

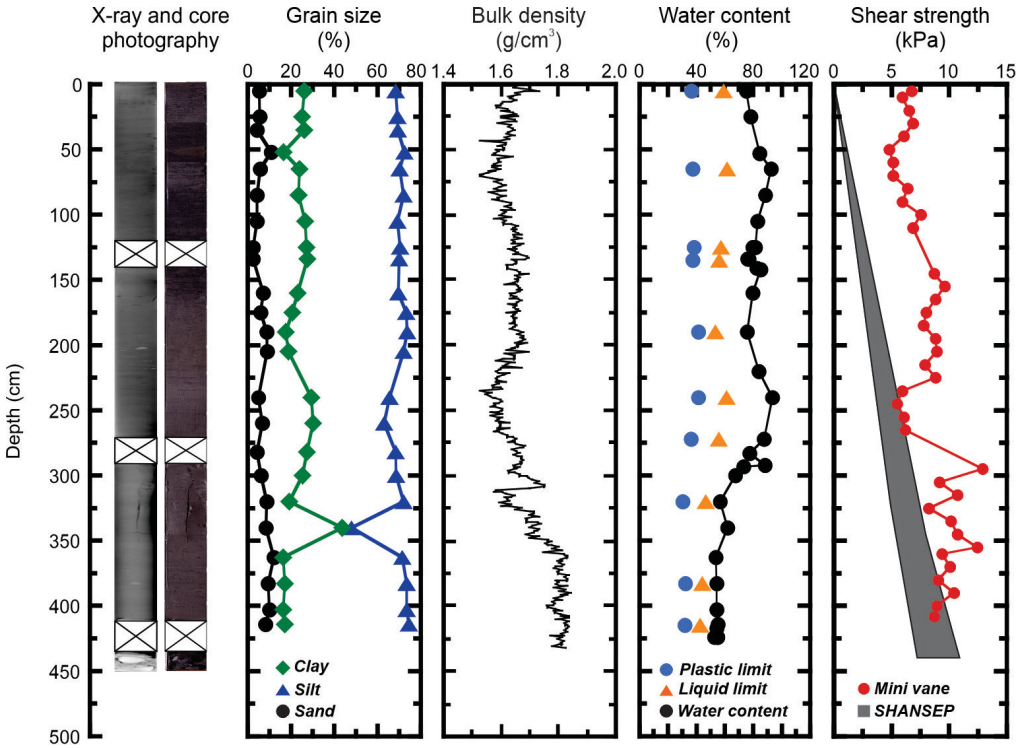

Figure 5: Geotechnical profile for core 20180420033, from the representative seabed site at Southwind Fiord, eastern Baffin Island. Abbreviations: Mini vane, miniature vane shear-strength measurements; SHANSEP, stress history and normalized soil engineering properties (Ladd and Foott, 1974).

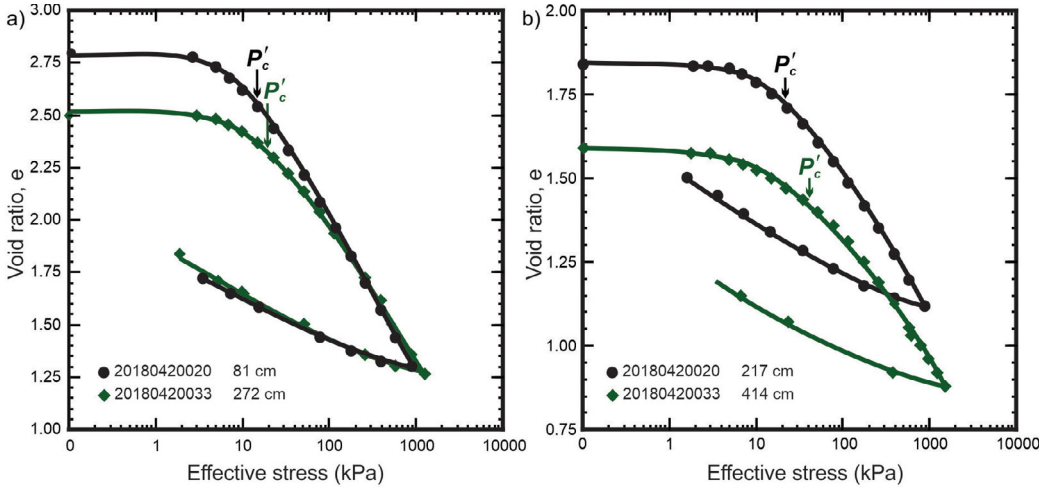

Figure 6: Results of consolidation tests on four samples from cores 20180420020 (core 20) and 20180420033 (core 33) at depths of **a)** 81 cm (core 20) and 272 cm (core 33), and **b)** 217 cm (core 20) and 414 cm (core 33), from Southwind Fiord, eastern Baffin Island. 'P'_c' is the preconsolidation stress.

Table 1: Summary of the physical properties of the sediments from the piston cores sampled. Core 20180420020 is from the slope failure site, core 20180420033 is from the representative seabed site at Southwind Fiord, eastern Baffin Island. The bracketed numbers show the range of values, unbracketed numbers are the average values. Abbreviations: MH, high-plasticity clayey silt; ML, low-plasticity clayey silt; USCS, Unified Soil Classification System.

Core number	Silt (%)	Clay (%)	Liquid limit (%)	Plasticity index (%)	Activity	Grain density (g/cm^3)	USCS classification
20180420020	69 (61–75)	24 (17–31)	60 (48–74)	22 (16–35)	0.85	2.80	MH
20180420033	70 (48–74)	24 (16–44)	54 (42–62)	18 (11–24)	0.68	2.86	ML,MH

Table 2: Summary of consolidation test results on four samples from cores 20180420020 (from the slope failure site) and 20180420033 (from the representative seabed site), from Southwind Fiord, eastern Baffin Island. Abbreviations: Max, maximum; MH, high-plasticity clayey silt; ML, low-plasticity clayey silt; OCR, overconsolidation ratio; USCS, Unified Soil Classification System.

Core number	Depth (cm)	Void ratio	Grain density (g/cm^3)	Compression index (C_c)	Expansion index (C_r)	Max past stress (kPa)	OCR	Hydraulic conductivity (m/s)	USCS classification
20180420020	79.5–82	2.80	2.80	0.73	0.18	15.0	2.8	8.40×10^{-9}	MH
20180420020	215.5–218	1.64	2.86	0.40	0.14	21.0	1.6	2.57×10^{-9}	ML
20180420033	270.5–273	2.50	2.88	0.61	0.17	19.5	1.2	1.03×10^{-8}	MH
20180420033	413–415.5	1.57	2.83	0.36	0.10	40.0	1.6	2.85×10^{-9}	ML

indicative of normally consolidated sediments (Holtz and Kovacs, 1981). The SHANSEP normally consolidated undrained strength ratios (S) vary from 0.29 to 0.39. The CIU triaxial tests yield similar failure envelopes for all samples tested (Figure 8).

The miniature laboratory vane (MV) shear-strength data are shown in Figures 4 and 5. The MV data present little increase with depth for core 20, and a slight increase for core 33. Normalizing the undrained shear strength using the effective overburden indicates the shear strengths from the two cores are similar with depth (Figure 9). The sensitivity, defined as the ratio of undisturbed to remoulded strengths, was similar for both cores, ranging from 1.4 to 10.27 with an average of 4.52, and is indicative of low- to medium-sensitivity sediments.

Slope stability

Gravity is a mechanism for general downslope movement causing slopes to fail or sediments to consolidate under their own weight. A factor of safety (FS) was calculated for undrained conditions and total stress conditions using the slope angle (β) obtained from the multibeam bathymetry data, effective overburden stress (σ'_v) calculated from the MSCL-S bulk density and down-core depth, and the undrained shear strength of the sediments using both the MV data (S_u) and the SHANSEP values (S). The FS was calculated using Morgenstern's (1967) basic infinite slope analysis equation:

$$FS = \frac{2}{\sin 2\beta} \frac{S_u}{\gamma' h}$$

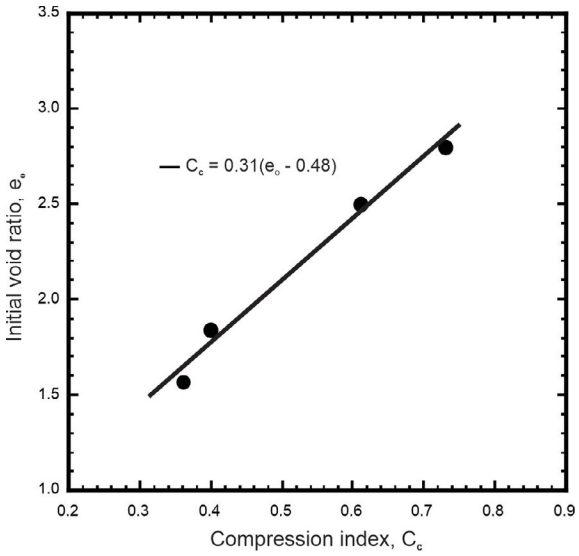

Figure 7: Initial void ratio versus compression index for the four consolidation tests on sediment samples from cores 20180420020 and 20180420033, from Southwind Fiord, eastern Baffin Island.

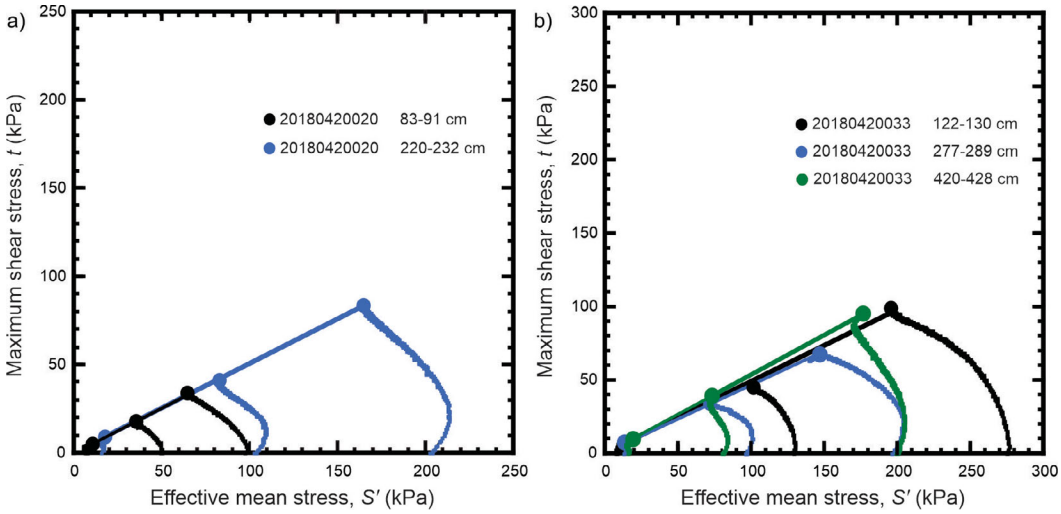

Figure 8: Stress path and failure envelopes for seabed sediments sampled in cores 20180420020 (core 20) and 20180420033 (core 33) from Southwind Fiord, eastern Baffin Island. **a)** Results for samples from core 20 at depths of 83–91 cm and 220–232 cm. **b)** Results for samples from core 33 at depths of 122–130 cm, 277–289 cm and 420–428 cm.

Table 3: Summary of triaxial test results on five samples of seabed sediment from cores 20180420020 (from the slope failure site) and 20180420033 (from the representative seabed site), from Southwind Fiord, eastern Baffin Island. Abbreviations: A_f, Skempton's (1954) pore pressure parameter at failure; MH, high-plasticity clayey silt; ML, low-plasticity clayey silt; *S*, normalized undrained shear strength ratio; USCS, Unified Soil Classification System.

Core number	Depth (cm)	Void ratio	Water content (%)	Grain density (g/cm^3)	Friction angle (°)	Cohesion (kPa)	*S*	A_f	USCS classification
20180420020	83–91	2.66	98.38	2.80	33.8	0.0	0.30	0.44	MH
20180420020	220–232	1.64	57.80	2.86	31.2	0.1	0.34	0.48	ML
20180420033	121.5–129.5	2.22	80.53	2.83	31.2	0.0	0.29	0.40	MH
20180420033	277–289	2.17	77.50	2.88	27.6	2.4	0.29	0.45	MH
20180420033	420–428.5	1.46	52.62	2.83	32.7	0.4	0.39	0.45	ML

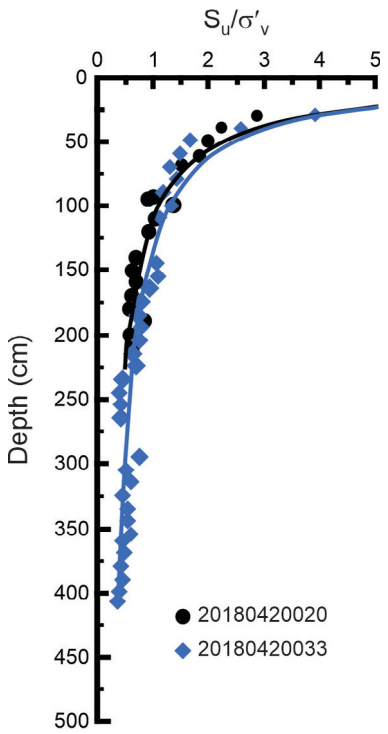

Figure 9: The effective overburden (σ'_v) and shear strength (S_u) versus depth for the seabed sediments in cores 20180420020 and 20180420033 from Southwind Fiord, eastern Baffin Island.

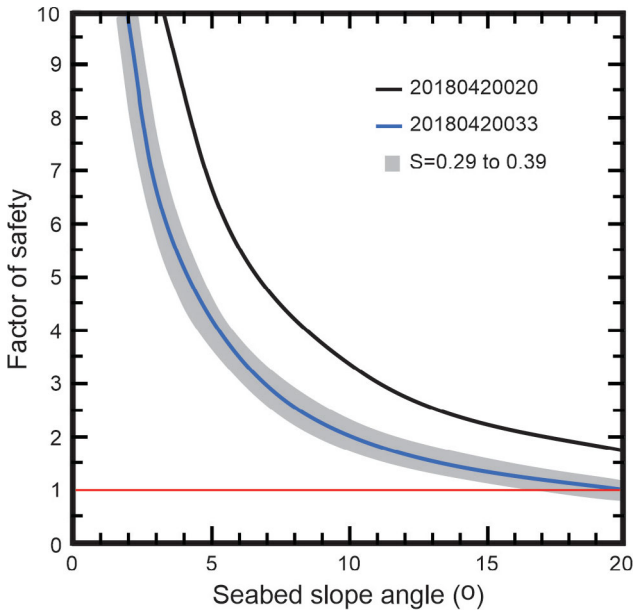

Figure 10: Factor of safety calculated for various slope angles for cores 20180420020 and 20180420033 from Southwind Fiord, eastern Baffin Island. Abbreviation: *S*, normalized undrained shear-strength ratio, based on Ladd and Foott's (1974) 'stress history and normalized soil engineering properties' method.

The FS calculated at all MV measurement depths varied down core, while the FS calculated using *S* values was consistent with depth. It should be noted that the FS calculated using the MV data is high in the upper 3 m of sediments in both cores sampled due to the high S_u and low σ'_v values. Therefore, sites with limited core recovery will present as very stable. The slope angles used were 4.6° and 13.9° for cores 20 and 33, respectively. The minimum FS determined using the MV data was 4.6 for core 20 and 2.1 for core 33. Using the SHANSEP minimum (0.29) and maximum (0.39) values, the minimum and maximum FS for core 20 were 2.3 and 3.1, and for core 33 were 1.2 and 1.7. The FS calculated for various slope angles is presented in Figure 10. The slope stability analysis indicates that the sediments are stable under gravitational loading for slope angles up to 20°, indicating an additional triggering mechanism is required to fail the sediments.

Economic considerations

The sustainability of communities located on the shores of fiords on Baffin Island requires an understanding of the engineering behaviour of the sediments offshore of the fiords. Seabed geotechnical properties are used in this paper to develop a geotechnical characterization of the engineering behaviour of the seabed sediments in Southwind Fiord, Baffin Island, in order to assess seabed foundation conditions and constrain slope stability analysis. This characterization is paramount in making decisions about existing and future seabed infrastructure development. Submarine landslides can destroy existing seafloor infrastructure and have the potential to generate tsunamis, thus impacting near-shore communities, as happened in Karrat Fjord, Greenland, in 2017. Therefore, understanding the physical properties of the seafloor is essential to making informed decisions about infrastructure development, such as subsea communication cables, and public safety of Nunavut communities located near the coast of Baffin Bay.

Conclusions

A comprehensive geotechnical testing program was conducted on two cores collected in Baffin Bay offshore Southwind Fiord, Baffin Island. The two cores targeted reference seabed sediments and sediments from the site of a slope failure. The geotechnical data presented in this paper include density from multi-sensor core logging, water content, Atterberg limits, consolidation and triaxial test results. The geotechnical characterization includes

- the sediments are uniform between the reference and slope failure sites, consisting of inorganic clayey silts and silts of low to high plasticity;
- the compressibility, permeability and effective friction angles are typical of marine clayey silt;

- the sediments are normally consolidated, characteristic of young sediments with minimum geological history; and
- the upper 3.5 m of the sediments are stable under gravitational loading, with a critical slope angle of approximately 20°.

Acknowledgments

The authors thank the officers, crew and scientific staff on board Canadian Coast Guard Ship *Hudson* during the 2018 field program. The authors also thank D. Ouettelle for her critical review of the paper. Financial support for this study was provided by the Government of Canada's Program of Energy Research and Development, ArcticNet and Crown-Indigenous Relations and Northern Affairs Canada.

Natural Resources Canada, Lands and Minerals Sector contribution number 20210518

References

ASTM D2435/D2435M 2011: One-dimensional consolidation properties of soils; ASTM International, West Conshohocken, Pennsylvania, URL <https://doi.org/10.1520/D2435_D2435M-11>.

ASTM D2487 2011: Classification of soils for engineering purposes (Unified Soil Classification System); ASTM International, West Conshohocken, Pennsylvania, URL <https://doi.org/10.1520/D2487-11>.

ASTM D4318 2010: Liquid limit, plastic limit, and plasticity index of soils; ASTM International, West Conshohocken, Pennsylvania, URL <https://doi.org/10.1520/D4318-10>.

ASTM D4648/D4648M 2010: Laboratory miniature vane shear test for saturated fine-grained clayey soil; ASTM International, West Conshohocken, Pennsylvania, URL <https://doi.org/10.1520/D4648_D4648M-10>.

ASTM D4767 2011: Consolidated undrained triaxial compression test for cohesive soils; ASTM International, West Conshohocken, Pennsylvania, URL <https://doi.org/10.1520/D4767-11>.

Casagrande, A. 1936: The determination of pre-consolidation load and its practical significance; Discussion D-34 *in* Proceedings of the First International Conference on Soil Mechanics and Foundation Engineering, June 22–26, Cambridge, Massachusetts, v. III, p. 60–64.

GEBCO Compilation Group 2014: GEBCO 2014 Grid; International Hydrographic Organization and Intergovernmental Oceanographic Commission (of UNESCO), URL <https://www.gebco.net/> [June 2014].

Gourvenec, S. and White, D. 2010: Gulf of Guinea deepwater sediments: geotechnical properties, design issues and installation experiences; *in* Frontiers in Offshore Geotechnics II, CRC Press, Boca Raton, Florida, p. 59–86.

Hampton, M.A., Lee, H.J. and Locat, J. 1996: Submarine landslides; Reviews of Geophysics, v. 34, p. 33–59.

Holtz, R.D. and Kovacs, W.D. 1981: An Introduction to Geotechnical Engineering; Prentice-Hall, Inc., Englewood Cliffs, New Jersey, 733 p.

Ladd, C. and Foott, R. 1974: New design procedure for stability of soft clays; Journal of the Geotechnical Engineering Division, American Society of Civil Engineers, v. 100, issue 7, p. 763–786.

Morgenstern, N.R. 1967: Submarine slumping and the initiation of turbidity currents; *in* Marine Geotechnique, A.F. Richards (ed.), University of Illinois Press, p. 189–220.

Normandeau, A., MacKillop, K., Macquarrie, M., Philibert, G. and Bennett, R. 2021: Southwind Fiord, Baffin Island, Nunavut: a natural laboratory to explore modern turbidity currents, submarine landslides and iceberg scouring in an Arctic environment; *in* Summary of Activities 2020, Canada-Nunavut Geoscience Office, p. 81–92, URL <https://m.cngo.ca/wp-content/uploads/CNGO-SOA2020-Paper-09-Normandeau-et-al.en_.pdf> [January 2022].

Ocean Mapping Group 2014: 2014 multibeam sonar data collected from the M/V Nuliajuk; Ocean Mapping Group, University of New Brunswick, Fredericton, New Brunswick, URL <http://www.omg.unb.ca/> [September 2014].

Seed, R.B., Cetin, K.O., Moss, R.E.S., Kammerer, A.M., Wu, J., Pestana, J.M., Riemer, M.F., Sancio, R.B., Bray, J.D., Kayen, R.E. and Faris, A. 2003: Recent advances in soil liquefaction engineering: a unified and consistent framework; 26th Annual ASCE Los Angeles Geotechnical Spring Seminar, April 30, 2003, Long Beach, California, 71 p.

Skempton, A.W. 1953: The colloidal "activity" of clays; *in* 3rd International Conference on Soil Mechanics and Foundation Engineering, August 16–27, 1953, Switzerland, v. 1, p. 57–61.

Skempton, A.W. 1954: The pore-pressure coefficients A and B; Géotechnique, v. 4, p. 143–147.

Community water quality data across Nunavut: an introduction to available data for community water supplies

James Elliott[1], Meredith G. Clayden[2], Kayla Clouter[3], Sarah Collins[3], Tommy Tremblay[4] and Michele LeBlanc-Havard[2]

[1]*Department of Environment, Government of Nunavut, Iqaluit, Nunavut, jelliott@gov.nu.ca*

[2]*Department of Environment, Government of Nunavut, Iqaluit, Nunavut*

[3]*Department of Community and Government Services, Government of Nunavut, Iqaluit, Nunavut*

[4]*Canada-Nunavut Geoscience Office, Iqaluit, Nunavut*

Elliott, J., Clayden, M.G., Clouter, K., Collins, S., Tremblay, T. and LeBlanc-Havard, M. 2022: Community water quality data across Nunavut: an introduction to available data for community water supplies; *in* Summary of Activities 2021, Canada-Nunavut Geoscience Office, p. 57–68.

Abstract

There are several existing stressors for managing Arctic drinking water systems including water availability, staffing challenges and logistical issues. Managing these systems will likely become more difficult due to impacts of climate change, such as changes in the timing and quantity of precipitation, chemical release from thawing permafrost and altered runoff regime. The Government of Nunavut's Department of Community and Government Services collects water quality data from drinking water sources one to four times a year in keeping with applicable regulations. Work is being done to consolidate this data, which will inform the design of broader water quality monitoring, as the Government of Nunavut prepares for expanded water management responsibilities.

A more regular schedule of data collection would help establish temporal and seasonal trends in water quality. Future work could also better characterize permafrost conditions and assess links between surficial geology and water quality. For example, in 2016, the concentration of salts increased in Sanikiluaq's drinking water source, reaching levels above the chloride aesthetic objective. The authors hypothesize that frozen salty water trapped in marine sediments was released from thawing permafrost due to an increase in the annual average air temperature. Developing longer term baseline data on water quality and other geotechnical characteristics of community source watersheds can help identify changes as they happen and mitigate potential risks associated with climate change.

Introduction

Providing an adequate supply of drinking water in remote northern communities has always been challenging (Medeiros et al., 2017). Arctic water supplies have been identified as vulnerable to the effects of climate and efforts have been made to quantify this (Alessa et al., 2008; Harper et al., 2020). With the increased awareness of water security issues in the Arctic (Medeiros et al., 2017), baseline data are required for each community's primary and alternative water sources so that changes in quality and quantity can be detected and adaptively managed.

In Nunavut, drinking water is supplied entirely by surface water. The majority of drinking water in the territory comes from lakes, however, some communities draw their water from creeks, rivers or glacial meltwater. While all communities use chlorine disinfection to treat their water, some communities also have secondary treatments such as filtration and/or ultraviolet (UV) disinfection (Table 1).

Many communities are small in population and may not have access to specialized tradespeople or equipment within the community, which can affect operation and maintenance of drinking water infrastructure and prolong repairs of vital parts of the drinking water system (Figure 1). Staffing and planning of operations can also be a challenge for communities, and therefore ongoing access to training on operating water system infrastructure is required.

Environmental factors that affect drinking source water quality and quantity

Climate change will present additional challenges to providing drinking water in Nunavut. Climate-driven hydrological regime changes are directly affecting the water

This publication is available, free of charge, as colour digital files in Adobe Acrobat® PDF format from the Canada-Nunavut Geoscience Office website: https://cngo.ca/summary-of-activities/2021/. Il est aussi disponible en français sur https://cngo.ca/fr/.

Table 1: Water source and water treatment technology used at selected Nunavut communities, with the population in 2016 (Statistics Canada, 2019). Abbreviation: UV, ultraviolet.

Community	Population	Water source	Treatment type
Arctic Bay	868	Marcil Lake	Chlorine disinfection
Arviat	2657	Wolf creek*	Chlorine disinfection, filtration, UV disinfection
Baker Lake	2069	Baker Lake	Chlorine disinfection, filtration, UV disinfection
Cambridge Bay	1766	Water lake*	Chlorine disinfection, filtration, UV disinfection
Chesterfield Inlet	437	Puiqsuk lake*	Chlorine disinfection
Clyde River	1053	Emirtavik lake*	Chlorine disinfection
Coral Harbour	891	Post River	Chlorine disinfection, filtration
Gjoa Haven	1324	Swan lake* (official name Swan Lakes)	Filtration, chlorine disinfection
Grise Fiord	129	Glacial meltwater	Chlorine disinfection
Igloolik	1682	South lake* (official name Mianiqsivik)	Chlorine disinfection, filtration
Iqaluit	7740	Lake Geraldine*	UV disinfection, filtration, chlorine disinfection
Kimmirut	389	Fundo Lake	Chlorine disinfection
Kinngait	1441	T lake* (official name Imiqtarvik)	Chlorine disinfection
Kugaaruk	933	Kugajuk River	Filtration, UV disinfection, chlorine disinfection
Kugluktuk	1491	Coppermine River	Coagulation/flocculation (seasonal), filtration, UV disinfection, chlorine disinfection
Naujaat	1082	Nuviq Laktujuq lake* (official name Nuviqłuktujuq)	Chlorine disinfection, filtration
Pangnirtung	1481	Duval river* (official name Panniqtuup Kuunga)	Chlorine disinfection, filtration
Pond Inlet	1617	Water lake reservoir* and Salmon creek*	Chlorine disinfection
Qikiqtarjuaq	598	Tulugak river*	Chlorine disinfection
Rankin Inlet	2842	Nipissar lake* (official name Nipissak Lake) and Lower Landing lake*	Chlorine disinfection
Resolute	198	Char Lake	Chlorine disinfection
Sanikiluaq	882	Sanikiluaq lake*	Chlorine disinfection
Sanirajak	848	Water Supply lake*	Chlorine disinfection
Taloyoak	1029	Canso Lake	Chlorine disinfection, filtration
Whale Cove	435	Fish lake*	Chlorine disinfection

*Unofficial name used in the Government of Nunavut's water licenses issued by the Nunavut Water Board

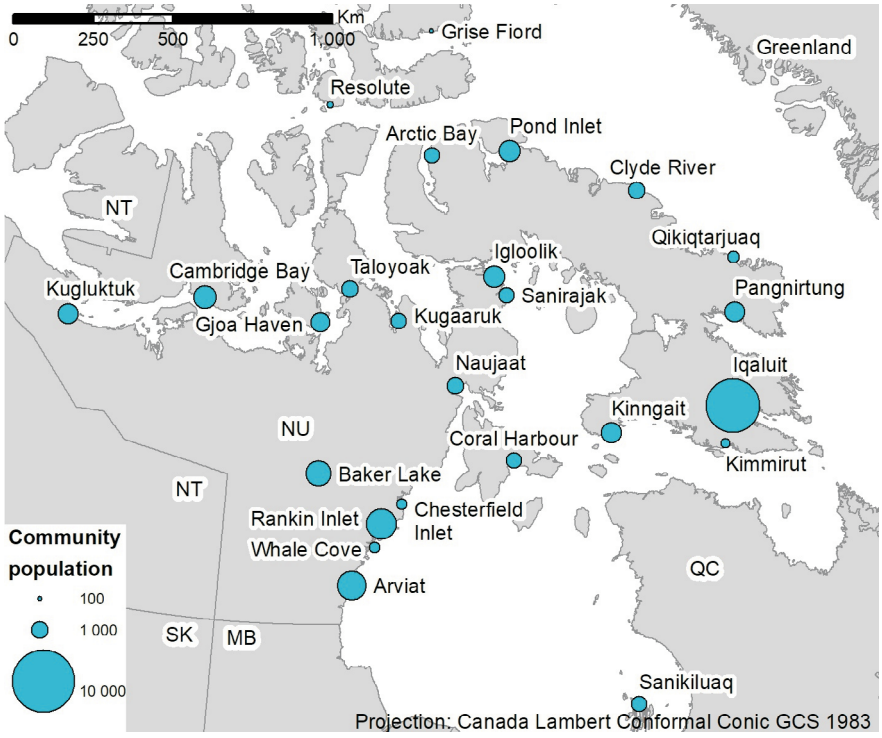

Figure 1: Population of communities in Nunavut (shown with proportional circles). Population data from the 2016 census (Statistics Canada, 2019).

balance of watersheds across the circumpolar Arctic (Whitehead et al., 2009; Holmes et al., 2013; Beel et al., 2021). Nunavut's community water supplies rely on the spring freshet to recharge reservoirs, the annual timing of which is likely occurring earlier in the year given evidence from other circumpolar watersheds (Prowse et al., 2006). Evaporation rates, along with the magnitude and timing of precipitation events, and the relative balance of snow and rain that make up the annual water balance, also determine the degree of recharge and adequacy of the annual supply in community reservoirs (Holmes et al., 2013; Zhang et al., 2021). In continuous permafrost zones, permafrost creates an impermeable layer above which surface water systems are perched and generally isolated from deeper groundwater, except in taliks that extend to the base of the permafrost layer (LeBlanc et al., 2021). In a warming climate, it is uncertain whether lake shorelines will shrink or expand in regions underlain with continuous permafrost. Individual lake response will depend on many factors such as the depth of the lake, the depositional environment (particularly the type of sediment deposited), the ground ice content and local permafrost thaw rates, the lake's hydrology and connectivity, and the lake-ice regimes (LeBlanc et al., 2020). Sudden lake drainage, attributed to permafrost thaw, has been documented in Siberia and the western Arctic of North America (Smith et al., 2005; Swanson, 2018). Some studies suggest this drainage could decrease the number of lakes and their total surface area over the long term (Smith et al., 2005; Ge et al., 2011). At the time of writing, the authors were not aware of any sudden lake or pond drainage in Nunavut that can be attributed to permafrost degradation, however, this may occur under higher greenhouse gas emission scenarios (Nitze et al., 2020). Climate change is also driving direct changes to surface water quality through increased chemical reaction rates in warming waters, as well as indirectly through changes to thermal stratification, lake mixing (Mueller et al., 2009) and many other interconnected biogeochemical processes (Rouse et al., 1997; Williamson et al., 2009; Roberts et al., 2017; Benateau et al., 2019). For example, permafrost thaw and slumping increase the transport of organic matter and associated metals and nutrients into the water column (Louiseize et al., 2014; Fouché et al., 2020; Miner et al., 2021), which can in turn stimulate primary productivity and drive further biogeochemical change (Brubaker et al., 2010; Vincent et al., 2013). There is a scarcity of published data on baseline water quality and biogeochemical conditions in Nunavut (Chiasson-Poirier et al., 2019), making it difficult to know what climate impacts may be occurring now, and how current conditions are likely to change. This information is key to the ability of communities to adapt to climate change, specifically with respect to ensuring long-term water security (Rouse et al., 1997; Mueller et al., 2009).

Availability of monitoring data

Capacity constraints at all levels of government in Nunavut, combined with the territory's large landmass, remote communities and limited infrastructure, make water quality sampling and data collection challenging. Therefore, relatively limited data are available to help understand the current state of water quality and quantity in community drinking source watersheds, and how conditions may be changing with broader environmental and climate changes. The majority of water quality data in Nunavut is collected by researchers involved with independent projects and, as such, there is little spatial and temporal consistency in available datasets (Liang and Aherne, 2020). Some research has been done on the water quality of community drinking water supply (Forte et al., 2017; Hutchinson et al., 2018), however, the majority of water quality data comes from remote sample sites not associated with drinking water supplies. The Government of Canada conducts water quality monitoring at 10 sites in Nunavut through Environment and Climate Change Canada's National Long-Term Water Quality Monitoring Data program. However, the sites are distant from inhabited communities and therefore do not provide direct information about community source water.

Adequate data are required for decision makers to adaptively manage drinking water supplies in the face of climate change. The intent of this paper is to provide a preliminary overview of the availability of water quality data for community drinking water supplies in Nunavut, mostly extracted from Government of Nunavut (GN) archived data. In addition, a case study from the community of Sanikiluaq, in south-central Nunavut, is used to illustrate how climate change appears to have led to relatively sudden changes in water quality.

Water quality data collection in community source water

Communities in Nunavut are remote and are only accessible by plane for most of the year, with the exception of a short period in the summer when they can be reached by boat. Flight schedules can be inconsistent, particularly during the winter, with flights being delayed by several days or longer. These factors affect construction and shipment of equipment, materials and personnel, and delay shipment of drinking water samples to laboratories, which can affect the validity of analytical data obtained from expired water samples.

Water sampling for community drinking water systems in all communities except Iqaluit is done by the operators of individual water treatment plants, and supported by the GN's Department of Community and Government Services (CGS). Operation of the water infrastructure is managed by municipal governments, with support from CGS, with the

exceptions of five communities where this infrastructure is owned and operated by CGS and one community where a contractor operates the water infrastructure. The City of Iqaluit manages its drinking water system independently from CGS and, as such, the data from Iqaluit's drinking water source is not reported in this paper.

Many communities source their drinking water directly from natural lakes or rivers. However, several communities have engineered reservoirs or tanks for raw water storage, which they must refill during the ice-free season with enough water to supply the community for the year. Timing of melt and refreeze can vary year to year, and municipal operators must be prepared to commission and decommission pumping stations based on weather factors. Furthermore, when determining the usable water volume of lakes and reservoirs used as primary water sources, the thickness of the ice cover, which operational staff have observed to persist into the late spring, must be taken into consideration, as that thickness will affect the volume of water available for consumption by the community prior to freshet and/or resupply. Operational staff have observed that the ice cover can be up to 2 m thick (Government of Nunavut, Department of Community and Government Services, unpublished data, 2021).

It is expected that future source water data collection, storage and management within the GN will expand in scope as the GN will eventually hold broad water resource management responsibility after Nunavut's devolution. Currently, the Government of Canada holds broad 'provincial-type' land and water resource management responsibilities in Nunavut (*Department of Indian Affairs and Northern Development Act* [Government of Canada, 2021]; Indigenous and Northern Affairs Canada, 2017). The federal Minister of Northern Affairs is responsible for the enforcement of water-resource legislation and associated regulations, including the terms and conditions of municipal 'Type A' water licenses for all communities in the territory (*Nunavut Waters and Nunavut Surface Rights Tribunal Act* and *Nunavut Waters Regulations*). The CGS is responsible for managing water quality data from community drinking water sources and is in the process of migrating all of the data to a database.

Collection schedules

The frequency of sampling is prescribed by the Nunavut *Public Water Supply Regulations*, part of the *Public Health Act*, and minimum collection schedules are administered by the GN's Department of Health. Raw and treated water at the water treatment plant must be sampled for water quality analyses once every two years. However, this schedule varies among communities as specific events and circumstances may require adjustments to the treatment process. Sampling is recommended to take place more often, specifically at anticipated times of differing water quality, such as early spring, when ice cover is at its thickest, and again in the late summer, nearing the end of the ice-free season; however, the frequency and timing of sampling varies among communities because sampling is managed by numerous municipal governments. Currently, sampling occurs between one and four times a year. The GN is in the process of updating these regulations and anticipates that sampling will be required at least twice per year.

Collection methods

For routine monitoring, samples are collected at the surface of the identified water supply, and near the location from where water is pumped. When formal planning is underway for new infrastructure, additional monitoring of the existing water supply infrastructure is generally undertaken to better understand water characteristics. For communities with a primary and secondary water source, water licence terms and conditions generally require sampling at both sources.

Sample analysis

Some water quality analyses are performed onsite, including measuring the depth of a water supply, water flow rates and turbidity. The Canadian Association for Laboratory Accreditation (CALA) accredit the labs used by the GN. As a requirement for water licensing, a quality assurance and quality control plan is submitted to a laboratory for approval during licence renewal. Water quality analyses generally follow the same accredited methods for each parameter. The data provided by the laboratories or indirectly via the contractor reports are then circulated to CGS and are compared to the Guidelines for Canadian Drinking Water Quality (Health Canada, 2020).

Scope and limitations of this review

This review considers available data from all communities in Nunavut, with the exception of the City of Iqaluit, which independently manages its own drinking water system. Data for Igloolik and Pangnirtung have been collected, however, these data have not yet been uploaded to the CGS water quality database. In addition, only water quality data from raw source water were considered, rather than from any sampling that is done within the treatment train.

Data were accessed through CGS's water quality database (managed in WaterTrax® software), which contains routinely collected water quality data from community source waters from 2014 onward. Available parameters are listed in Table 2. In addition, data from 2013 and earlier are stored in electronic and paper formats that are also being standardized for eventual inclusion in WaterTrax. WaterTrax is primarily used as an operational tool for storing and accessing recent drinking water quality data, including data from raw

source water and the treatment train. This database contains data from drinking water only and does not contain data on broad water quality monitoring. The data are also used by the Nunavut Water Board to ensure annual reporting requirements have been met for municipal water licences under the *Nunavut Waters Regulations*. It is expected that future water data storage and management by the GN will expand in scope, as the GN will eventually hold broad water resource management responsibilities after Nunavut's devolution.

The objectives of this preliminary assessment were to

1) illustrate the range of sample sizes for some common water quality parameters available from the GN's WaterTrax database;
2) provide examples of the distribution of available data for selected communities and parameters; and
3) explore contributing factors to an increase in the concentration of salts in the potable water supply in Sanikiluaq.

For objectives 1 and 2, data were obtained from WaterTrax with the intent of exploring and illustrating what is available in this database. For objective 3, additional data that are not yet incorporated into WaterTrax, along with data from an engineering report conducted as part of the GN's investigation into Sanikiluaq's water quality issues in 2015–2016, were used to look at how parameters related to salinity (chloride, sodium and conductivity) changed in association with ambient air temperatures. As a result, the sources of data for objectives 1 and 2 differed from those of objective 3.

Preliminary data overview and analysis

Data availability and general trends

The available dataset includes bacteria, metals, nutrients and physical properties, however, availability was not consistent between each community (Table 2). Some communities, such as Arviat, Naujaat, Rankin Inlet and Whale Cove (Figure 2), have more data available. Figure 2 illustrates variable levels of conductivity, turbidity, total calcium, chloride, total iron and total phosphorus over the period for which data are available in the four selected communities, where sample sizes were generally higher. Sampling for bacteria is the most common water quality test and water was tested for bacteria more frequently in communities where it is a concern, such as Whale Cove. Research on bacteria in northern drinking water systems is more common than other analytes (Martin et al., 2007; Daley et al., 2018; Gora et al., 2020).

The differences in timing and limited number of sampling events available for different communities introduces biases and prevents robust statistical comparisons and detection of trends. However, variability in the parameters in this dataset were consistent with the gradients presented by Liang and Aherne (2020): conductivity/cation and trace

Table 2: Availability of water sampling data from Nunavut's communities by number of available data points since 2016. The Government of Nunavut, Department of Community and Government Services' water quality database, WaterTrax, contains data from samples collected one or two times a year at each of the communities.

Community	pH	TP	Conductivity	Alkalinity	NH_3^+	NO_3^{2-}	Cl^-	DOC	Turbidity	*E. coli*	SO_4^{2-}	Metals
Arctic Bay	1		1	1	1	10	10	10	7	4	10	7–10
Arviat	16	16	13	16	16	16	16	16	16	70	15	16
Baker Lake	2	5	2	5	5	5	5	5	2	44	5	5
Cambridge Bay	4			4		3	3	4	5	18	4	
Chesterfield Inlet	2	2	2	2	2	2	2	2	2	5	2	2
Clyde River						3	2	3	3		3	3
Coral Harbour	4	4	4	4	4	4	4	4	4	1	4	4
Gjoa Haven	4			4		3	4	4	4		4	
Grise Fiord						5	5	5	5	1	5	5
Kimmirut						1	1				1	1
Kinngait						7	7	7	7	2	7	7
Kugaaruk	5			5		3	5	4	5	14	5	
Kugluktuk	4			4		6	4	3	3	11	4	
Naujaat	7	7	7	7	7	7	7	7	7	36	7	7
Pond Inlet	1		1	1	1	6	6	6	5	3	6	6
Qikiqtarjuaq						2	2	2		2	2	2
Rankin Inlet	12	12	12	12	12	12	12	12	12	25	6	12
Resolute						4	4	4	3	2	4	4
Sanikiluaq	1	2	1	1	1	1	1	1	1	21	1	2
Sanirajak	2		2	2	2	4	4	4	4	4	4	4
Taloyoak	3			3		3	3	3	3	8	3	
Whale Cove	11	11	11	11	11	11	11	11	11	57	11	11

*Selected metals included (total concentrations of) arsenic, barium, cadmium, copper, iron, lead, manganese, selenium, silver and zinc

Abbreviations: DOC, dissolved organic carbon concentration in water; *E. coli, Escherichia coli;* TP, total phosphorus concentration in water

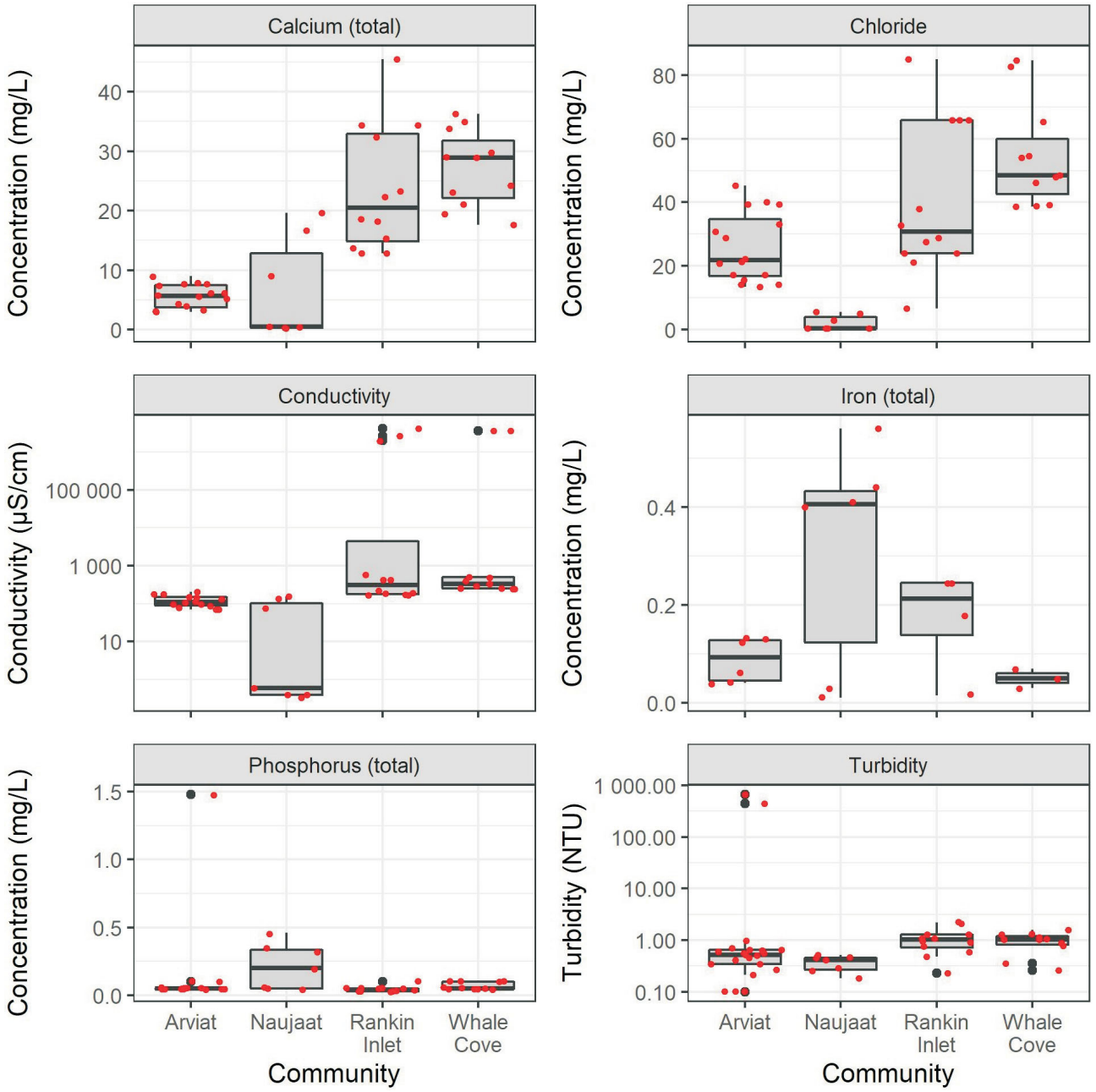

Figure 2: Water quality measurements from drinking water sources in selected Nunavut communities between 2014 and 2020, data from the Government of Nunavut, Department of Community and Government Services' water quality database, WaterTrax. The red dots represent the raw data, with black horizontal lines showing the mean, and vertical 'whisker' lines showing the full range. For Arviat, n = 16 for all parameters except conductivity (n = 13); for Naujaat, n = 7 for all parameters; for Rankin Inlet, n = 12 for all parameters; for Whale Cove, n = 11 for all parameters. In the four communities shown, minimum total phosphorus (TP) concentrations were below detections limits (<0.05 mg/L), and maximum concentrations in Rankin Inlet and Whale Cove were also at or below detection. In Arviat, data were available from February 2017; January and September 2018; October 2019; and May, July and December 2020. In Naujaat, data were available from May and September 2017; May 2018; October 2019; and June, October and December 2020. In Rankin Inlet, data were available from May and September 2017; April and September 2018; July 2019; and September and December 2020. In Whale Cove, data were available from July and August 2016; May, July and August 2019; and May and December 2020. Abbreviations: NTU, nephelometric turbidity units; µS, microsiemens.

metal/nutrient gradients. For example, higher chloride levels and conductivity were observed in Arviat, Rankin Inlet and Whale Cove. This could suggest that salt spray or interstitial water from the thawing of unconsolidated marine sediments contribute to the composition of the water chemistry. Higher total phosphorus was observed in Naujaat. Typically, increased phosphorus is associated with anthropogenic inputs, such as wastewater (Holeton et al., 2011), however, in the Arctic, it may be related to the presence of geese (Côté et al., 2010; Jensen et al., 2019). Data for other nutrient and biological productivity parameters (e.g., total nitrogen, chlorophyll-a) were not available for Naujaat but ammonia concentrations were higher (0.01–0.56 mg/L) in Naujaat when compared to the other three communities (shown in Figure 2) with values of 0.01–0.11 mg/L, 0.01–0.35 mg/L and 0.02–0.05 mg/L in Arviat, Rankin Inlet and Whale Cove, respectively (sample sizes as shown in Table 2). More detailed sampling and watershed characterization are required to assess this possibility. Dissolved organic carbon concentrations in Naujaat (0.20–2.66 mg/L) were not elevated compared to the other three communities (3.18–8.63 mg/L, 2.29–7.96 mg/L and 3.80–5.53 mg/L in Arviat, Rankin Inlet and Whale Cove, respectively), so it is unlikely that runoff and natural organic matter inputs are the source of elevated total phosphorus. Rankin Inlet and Whale Cove waters displayed higher concentrations of calcium, possibly originating from weathering of calcium-bearing bedrock. Higher concentrations of iron in Rankin Inlet and Naujaat may also be related to underlying geology. However, the limited availability of data points to a need for further consistent and frequent sampling in all communities to help understand organic and inorganic influences on metal and nutrient concentrations and other water quality parameters.

Outliers for measurements of turbidity were observed in Arviat; increased turbidity can be associated with increased water runoff events due to climatic or geomorphic factors. Regular sampling would help show the link between water quality and weather patterns; the timing of the spring freshet and other information related to weather events is not recorded in WaterTrax so this information was not available as part of the current assessment. The sampling dates also vary seasonally and differ across years. For example, in Arviat, data were available from February 2017; January and September 2018; October 2019; and May, July and December 2020. The timing of sampling differed each year for other communities as well. Future efforts could be focused on recording the observed timing of the freshet in each community along with 'routine' water chemistry testing so that these factors can be linked and incorporated into a compilation of key local information. Thus, although basic inferences can already be made from a few sites, albeit with substantive uncertainties, an increasing coverage of spatial and temporal water quality data will enhance the understanding of the factors affecting water quality.

As mentioned earlier, data in WaterTrax dates back to 2014; data from 2013 and earlier are currently stored in a variety of formats, which are currently being standardized for eventual inclusion in WaterTrax. As such, these data were not available for inclusion in this overview. As more data are added from current and additional communities, a more comprehensive analysis will be possible.

The composition of geological materials in the watershed can have a large influence on water chemistry (Antoniades et al., 2003; Dranga et al., 2017; Brown et al., 2020; Liang and Aherne, 2020). More specifically, both bedrock and unconsolidated surficial sediments can influence water chemistry, such as in an area north of Iqaluit where water chemistry of the drinking water source is affected by the surficial cover of glacially transported carbonate sediments in the watershed (Tremblay et al., 2016).

In the face of rising temperature and changing precipitation patterns, it is expected that both watershed-scale factors, such as ecoregions, permafrost conditions and geology, and local factors, such as the protection of the immediate vicinity around water sources, will be important in predicting dissolved and suspended material in water sources. Compiling water quality data from community sources, such as those presented in this paper, and from nearby natural sites will help to understand the current trends in water quality, and to predict future potential issues and identify data gaps, which can help direct sampling to underrepresented areas.

Sanikiluaq case study

The case study of Sanikiluaq, a community located on the Belcher Islands in southeastern Hudson Bay, is an example of how climate change may be responsible for changes in water quality. Additionally, it demonstrates how long-term monitoring of water quality and geochemical and geothermal (e.g., permafrost conditions) properties of watersheds can help to anticipate and understand the processes that could lead to variations in water quality. As the WaterTrax database contains very little data on Sanikiluaq, this case study was primarily done using unpublished CGS data, which will be uploaded to WaterTrax, and an unpublished engineering report undertaken in response to Sanikiluaq's water issues in the mid-2010s (EXP, 2016).

In Sanikiluaq, an increase in the concentration of salts (chloride, sodium, conductivity and hardness) in the community water was detected in 2009 (EXP, 2016; Figure 3). In March 2014, it was observed that chloride levels were very high, 654 mg/L, which is above Health Canada's chloride aesthetic objective of ≤250 mg/L (Health Canada, 2020). The aesthetic objective is the level at which water becomes undesirable to consume (e.g., the taste) and can

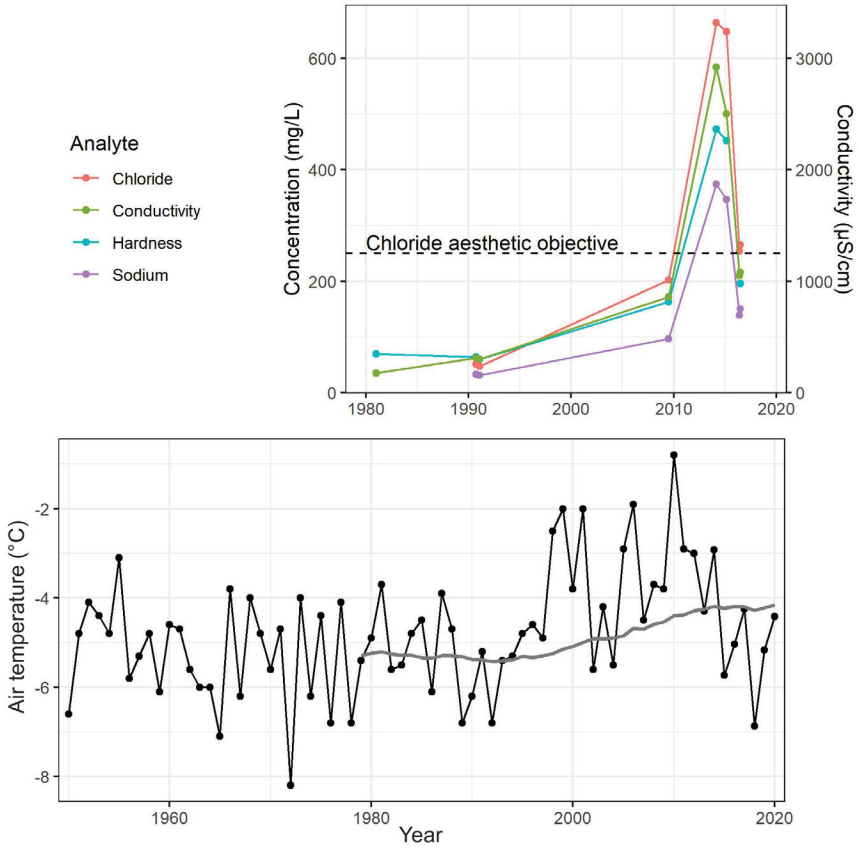

Figure 3: Water quality in Sanikiluaq's drinking water source over time (top) and the average annual air temperature (black line) and 30-year rolling average (grey line) in Sanikiluaq (bottom). The 1981–2016 geochemical data is from EXP (2016) and climate data is from ClimateData.ca (2021). Abbreviation: µS, microsiemens.

corrode the distribution system, but there is no direct impact on human health. When the aesthetic objective is exceeded, people are more likely to reduce their water consumption or seek water from unapproved sources (World Health Organization, 2006).

In July 2016, chloride levels had decreased to 265 mg/L (EXP, 2016) but unpublished CGS data (Figure 4) show that chloride levels remained elevated after the initial spike in 2014. Interviews with community members revealed that there were issues with the taste of the water throughout the year, although it was most noticeable during the spring freshet (EXP, 2016). More recent and regular monitoring confirms that, although there is seasonal variation, chloride is regularly above the aesthetic objective.

The engineering report (EXP, 2016) mentions that no field evidence was found to link the source of salts to intrusions of road salt, saltwater or salt spray or issues with the water treatment, water distribution or truck fill systems, and that the problem was not just due to seasonality or daily variations in conditions. It is suggested that the source of the salts may be from thawing permafrost in fine-grained marine sediments based on a combination of geomorphological observations and recent climate data presented in this section. A preliminary geomorphological examination, using Google Earth satellite images, revealed that about 10–30% of the reservoir watershed is composed of marine sediments. The marine sediments were deposited when the island was submerged under the sea (Dyke et al., 2018) following deglaciation approximately 8.7 ka (Dalton et al., 2020). When the sea retreated from the elevation of the reservoir about 800 years ago (Vacchi et al., 2018), seawater was trapped and frozen in the sediments. The recent climate warming of about 1.2°C observed between 1990 and 2010 (ClimateData.ca, 2021; Figure 3) likely progressively warmed the permafrost and consequently deepened the active layer, as observed in nearby communities (Fortier et al., 2011). The warming may have thawed a thin upper salt-rich layer in the fine-grained marine sediments. The thawing would cause the gradual release of salty water into the overlying watershed and ultimately into the drinking water source (e.g., Lamhonwah et al., 2017). Several of the surrounding ponds, which are underlain by bedrock, had conductivities between 30 and 80 µS/cm in 2016 compared to the reservoir and adjacent lakes that had conductivities of

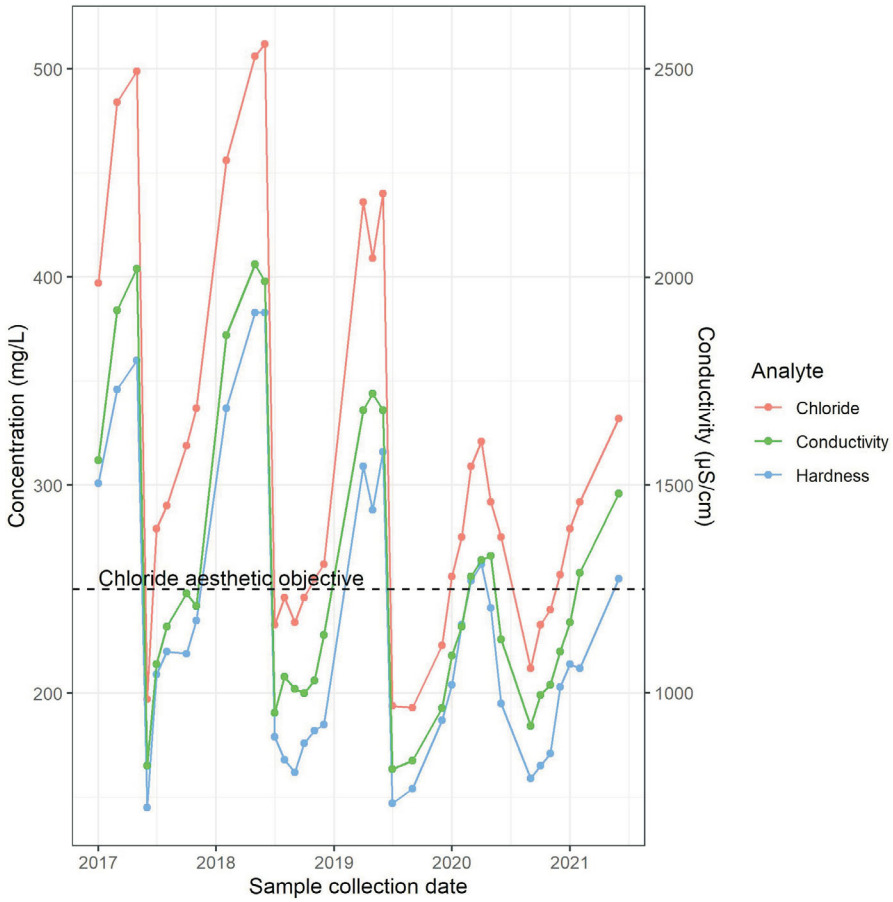

Figure 4: Water quality in Sanikiluaq's drinking water source between 2017 and 2021. The data was collected by Government of Nunavut's Department of Community and Government Services but has not yet been uploaded to their water quality database, WaterTrax. Abbreviation: µS, microsiemens.

approximately 1000 µS/cm (EXP, 2016). The difference in conductivities also suggests that permafrost thaw may be the source of the solute. Similar mobilization of previously frozen solute from thawing permafrost to freshwater lakes has been observed in the High Arctic of Canada (Lamhonwah et al., 2017; Roberts et al., 2017). The Sanikiluaq case study suggests that permafrost thaw, driven by climate change, can affect the quality of community source water, through the release of dissolved elements previously frozen beneath the active layer. Further investigation is needed to better understand the link between thawing permafrost and water quality.

To address the issue of poor water quality, reverse osmosis units were installed in most homes in Sanikiluaq as an interim measure until a new water treatment plant, capable of treating brackish water, can be built. The authors note that cases like Sanikiluaq require costly intervention—the annual cost of maintaining the reverse osmosis system is estimated to be between $80 000 and $100 000. A proper understanding of how water quality is being impacted is needed to properly understand and appropriately manage the new conditions. Different management strategies include adopting alternative technologies, such as in Sanikiluaq, or using an alternate water source. Adequate data on primary and alternate drinking water sources is key to determining how quickly communities are able to adapt and identify safe alternative supplies or implement new technologies. This case also highlights the need for more holistic and routine data collection in primary and alternative source watersheds to anticipate and adapt more quickly to changes in water quality or quantity. In addition to improving the collection of water quality data, a better understanding of local permafrost characteristics (ice richness, total depth, salinity and active layer depth) is needed.

Economic considerations

Accurate data is essential to understanding the relationship between water quality and its local context (geography, geology, hydrology, engineering constraints, proximity to other infrastructure, etc.) so informed decisions can be

made on the current and future drinking water sources of Nunavut's communities. Quality of community source water is essential for the health of Nunavummiut. The cost of water treatment is high and has to be minimized to optimize the allocation of resources within communities. Additionally, when the quality or quantity of water is deemed insufficient for consumption, the cost of quickly finding and replacing the source of water or implementing emergency measures is high.

Implications for future work

Climate change is an external factor that will impact the quantity and quality of community drinking water and it is largely uncertain what the regional and community-specific impacts will be. Changes in the type and quantity of precipitation and the thawing rates of permafrost can alter how elements are stored in or moved through the landscape. Changes of concern include increased organic matter from runoff and the release of contaminants from thawing permafrost (St. Pierre et al., 2018). The impacts of the local environment on drinking water need to be better understood so that the potential impacts of climate change can be incorporated into planning and management.

The data collected by CGS provide a preliminary characterization of community drinking water quality; these data could be further developed into a more robust baseline dataset to detect changes. Compiling historical water quality data on WaterTrax is the first step for a more complete analysis. A second step would be to initiate a more regular schedule of sampling, which would help to better characterize temporal and seasonal trends. Subsequent work could assess linkages between surficial geology and local water quality to assess the vulnerability of drinking water sources to climate change. It is generally understood that vegetation and surficial geology influence local water quality (Dranga et al., 2017; Brown et al., 2020; Liang and Aherne, 2020). Where possible, academic and government data should be combined, and further efforts made to publicize data that have already been collected. This all could be especially beneficial in helping Nunavut communities move toward more comprehensive baseline sampling, which, at this time, they do not have the capacity to do alone.

Acknowledgments

The authors would like to thank the reviewers for providing their feedback. The Government of Nunavut departments of Environment, Community and Government Services and Health, as well as the Canada-Nunavut Geoscience Office, are thanked for supporting this work.

References

Alessa, L., Kliskey, A., Lammers, R., Arp, C., White, D., Hinzman, L. and Busey, R. 2008: The arctic water resource vulnerability index: an integrated assessment tool for community resilience and vulnerability with respect to freshwater; Environmental Management, v. 42, issue 3, p. 523–541.

Antoniades, D., Douglas, M.S.V. and Smol, J.P. 2003: The physical and chemical limnology of 24 ponds and one lake from Isachsen, Ellef Ringnes Island, Canadian High Arctic; International Review of Hydrobiology, v. 88, issue 5, p. 519–538, URL <https://doi.org/10.1002/iroh.200310665>.

Beel, C.R., Heslop, J.K., Orwin, J.F., Pope, M.A., Schevers, A.J., Hung, J.K.Y., Lafrenière, M.J. and Lamoureux, S.F. 2021: Emerging dominance of summer rainfall driving High Arctic terrestrial-aquatic connectivity; Nature Communications, v. 12, art. 1448, URL <https://doi.org/10.1038/s41467-021-21759-3>.

Benateau, S., Gaudard, A., Stamm, C. and Altermatt, F. 2019: Climate change and freshwater ecosystems: impacts on water quality and ecological status; Federal Office for the Environment, Bern, Switzerland, 110 p., URL <https://doi.org/10.5167/uzh-169641>.

Brown, K.A., Williams, W.J., Carmack, E.C., Fiske, G., François, R., McLennan, D. and Peucker-Ehrenbrink, B. 2020: Geochemistry of small Canadian arctic rivers with diverse geological and hydrological settings; Journal of Geophysical Research: Biogeosciences, v. 125, issue 1, art. e2019JG005414, URL <https://doi.org/10.1029/2019JG005414>.

Brubaker, M., Berner, J., Bell, J., Warren, J. and Rolin, A. 2010: Climate change in Point Hope, Alaska, strategies for community health; ANTHC Center for Climate and Health, URL <http://www.anthc.org/chs/ces/climate/climateandhealthreports.cfm> [January 2022].

Chiasson-Poirier, G., Franssen, J., Lafrenière, M.J., Fortier, D. and Lamoureux, S.F. 2019: Seasonal evolution of active layer thaw depth and hillslope-stream connectivity in a permafrost watershed; Water Resources Research, v. 56, art. e2019WR025828, 18 p.

ClimateData.ca 2021: Time-series of the mean temperature data variable in Sanikiluaq, Nunavut; Environment and Climate Change Canada, Computer Research Institute of Montréal, Ouranos, Pacific Climate Impacts Consortium, Prairie Climate Centre and HabitatSeven, URL <https://www.climatedata.ca> [August 2021].

Côté, G., Pienitz, R., Velle, G. and Wang, X. 2010: Impact of geese on the limnology of lakes and ponds from Bylot Island (Nunavut, Canada); International Review of Hydrobiology, v. 95, no. 2, p. 105–129.

Daley, K., Hansen, L.T., Jamieson, R.C., Hayward, J.L., Piorkowski, G.S., Krkosek, W., Gagnon, G.A., Castleden, H., MacNeil, K., Poltarowicz, J., Corriveau, E., Jackson, A., Lywood, J. and Huang, Y. 2018: Chemical and microbial characteristics of municipal drinking water supply systems in the Canadian Arctic; Environmental Science and Pollution Research, v. 25, issue 33, p. 32926–32937.

Dalton, A.S., Margold, M., Stokes, C.R., Tarasov, L., Dyke, A.S., Adams, R.S., Allard, S., Arends, H.E., Atkinson, N., Attig, J.W., Barnett, P.J., Barnett, R.L., Batterson, M., Bernatchez, P., Borns, H.W., Jr., Breckenridge, A., Briner, J.P., Brouard, E., Campbell, J.E., Carlson, A.E. et al. 2020: An updated radiocarbon-based ice margin chronology for the last

deglaciation of the North American Ice Sheet Complex; Quaternary Science Reviews, v. 234, art. 106223, URL <https://doi.org/10.1016/j.quascirev.2020.106223>.

Dranga, S.A., Hayles, S. and Gajewski, K. 2017: Synthesis of limnological data from lakes and ponds across Arctic and Boreal Canada; Arctic Science, v. 4, issue 2, p. 167–185.

Dyke, A.S., Dredge, L.A. and Hodgson, D.A. 2005: North American deglacial marine- and lake-limit surfaces; Géographie physique et Quaternaire, v. 59, no. 2, p. 155–185.

EXP 2016: Sanikiluaq water quality assessment; unpublished report prepared for the Government of Nunavut, report no. OTT-00234315-A0, 34 p.

Forte, S., Lafferty, C., Manzo, L. and Bagley, W. 2017: Challenges with historical water quality data for Inuu'tuti, a collaborative cumulative effects monitoring program in the Baker Lake watershed; Arctic Change 2017, ArcticNet Annual Scientific Meeting, December 11–15, 2017, Québec, Quebec, abstract.

Fortier, R., LeBlanc, A.-M. and Yu, W. 2011: Impacts of permafrost degradation on a road embankment at Umiujaq in Nunavik (Quebec), Canada; Canadian Geotechnical Journal, v. 48, no. 5, p. 720–740.

Fouché, J., Christiansen, C.T., Lafrenière, M.J., Grogan, P. and Lamoureux, S.F. 2020: Canadian permafrost stores large pools of ammonium and optically distinct dissolved organic matter; Nature Communications, v. 11, art. 4500, URL <https://doi.org/10.1038/s41467-020-18331-w>.

Ge, S., McKenzie, J., Voss, C. and Wu, Q. 2011: Exchange of groundwater and surface-water mediated by permafrost response to seasonal and long term air temperature variation; Geophysical Research Letters, v. 38, art. L14402, URL <https://doi.org/10.1029/2011GL047911>.

Gora, S.L., Soucie, T.A., McCormick, N.E., Ontiveros, C.C., L'Hérault, V., Gavin, M., Trueman, B.F., Campbell, J., Stoddart, A.K. and Gagnon, G.A. 2020: Microbiological water quality in a decentralized Arctic drinking water system; Environmental Science: Water Research & Technology, v. 6, no. 7, p. 1855–1868.

Government of Canada 2021: Department of Indian Affairs and Northern Development Act; Revised Statutes of Canada, 1985, chap.1–6, URL <https://laws-lois.justice.gc.ca/eng/acts/I-6/PITIndex.html> [September 2021].

Harper, S.-L., Wright, C., Masina, S. and Coggins, S. 2020: Climate change, water, and human health research in the Arctic; Water Security, v. 10, art. 100062.

Health Canada 2020: Guidelines for Canadian Drinking Water Quality—summary table; Health Canada, Healthy Environments and Consumer Safety Branch, Water and Air Quality Bureau, report, 25 p.

Holeton, C., Chambers, P.A. and Grace, L. 2011: Wastewater release and its impacts on Canadian waters; Canadian Journal of Fisheries and Aquatic Sciences, v. 68, issue 10, p. 1836–1859.

Holmes, R.M., Coe, M.T., Fiske, G.J., Gurtovaya, T., McClelland, J.W., Shiklomanov, A.I., Spencer, R.G.M., Tank, S.E. and Zhulidov, A.V. 2013: Climate change impacts on the hydrology and biogeochemistry of arctic rivers; *in* Climatic Change and Global Warming of Inland Waters: Impacts and Mitigation for Ecosystems and Societies, C.R. Goldman, M. Kumagai and R.D. Robarts (ed.), John Wiley & Sons, Chichester, United Kingdom, p. 1–26.

Hutchinson, N.J., Hadley, K.R., Nesbitt, R.A. and Manzo, L. 2018: Establishing baseline limnological conditions in Baker Lake, Nunavut; *in* Polar Knowledge: Aqhaliat 2018, Polar Knowledge Canada, p. 78–83, URL <https://doi.org/10.35298/pkc.2018.10>.

Indigenous and Northern Affairs Canada 2017: Evaluation of the Land and Water Management Sub-Program, final report; Indigenous and Northern Affairs Canada, Evaluation, Performance Measurement and Review Branch, Audit and Evaluation Sector, URL <https://rcaanc-cirnac.gc.ca/DAM/DAM-CIRNAC-RCAANC/DAM-AEV/STAGING/texte-text/ev_lwms_1524055646519_eng.pdf> [January 2022].

Jensen, T.C., Walseng, B., Hessen, D.O., Dimante-Deimantovica, I., Novichkova, A.A., Chertoprud, E.S., Chertoprud, M.V., Sakharova, E.G., Krylov, A.V., Frisch, D. and Christoffersen, K.S. 2019: Changes in trophic state and aquatic communities in High Arctic ponds in response to increasing goose populations; Freshwater Biology, v. 64, issue 7, p. 1241–1254.

Lamhonwah, D., Lafrenière, M., Lamoureux, S. and Wolfe, B. 2017: Evaluating the hydrological and hydrochemical responses of a High Arctic catchment during an exceptionally warm summer; Hydrological Processes, v. 31, p. 2296–2313, URL <https://doi.org/10.1002/hyp.11191>.

LeBlanc, A.-M., Bellehumeur-Génier, O., Oldenborger, G. and Short, N. 2020: Lake area and shoreline changes due to climate and permafrost-related drivers, Rankin Inlet area, Nunavut; Canada-Nunavut Geoscience Office, Summary of Activities 2019, p. 79–92, URL <https://m.cngo.ca/wp-content/uploads/Summary_of_Activities_2019-Paper_07.en_.pdf> [January 2022].

LeBlanc, A.-M., Chartrand, J. and Smith, S.L. 2021: Estimation of maximum lake depth from the surrounding topography: towards a regional assessment of the occurrence of taliks below Arctic lakes; Geological Survey of Canada, Scientific Presentation 122, 1 sheet, URL <https://doi.org/10.4095/328242>.

Liang, T. and Aherne, J. 2020: Physical and chemical characteristics of 1300 lakes and ponds across the Canadian Arctic; Journal of Limnology, v. 79, no. 3, p. 254–277, URL <https://doi.org/10.4081/jlimnol.2020.1973>.

Louiseize, N.L., Lafrenière, M.J. and Hastings, M.G. 2014: Stable isotopic evidence of enhanced export of microbially derived NO_3^- following active layer slope disturbance in the Canadian High Arctic; Biogeochemistry, v. 121, issue 3, p. 565–580, URL <https://doi.org/10.1007/s10533-014-0023-x>.

Martin, D., Bélanger, D., Gosselin, P., Brazeau, J., Furgal, C. and Déry, S. 2007: Drinking water and potential threats to human health in Nunavik: adaptation strategies under climate change conditions; Arctic, v. 60, no. 2, p. 195–202.

Medeiros, A.S., Wood, P., Wesche, S.D., Bakaic, M. and Peters, J.F. 2017: Water security for northern peoples: review of threats to Arctic freshwater systems in Nunavut, Canada; Regional Environmental Change, v. 17, issue 3, p. 635–647.

Miner, K.R., D'Andrilli, J., Mackelprang, R., Edwards, A., Malaska, M.J., Waldrop, M.P. and Miller, C.E. 2021: Emergent biogeochemical risks from Arctic permafrost degradation; Nature Climate Change, v. 11, p. 809–819, URL <https://doi.org/10.1038/s41558-021-01162-y>.

Mueller, D.R., Van Hove, P., Antoniades, D., Jeffries, M.O. and Vincent, W.F. 2009: High Arctic lakes as sentinel ecosystems: cascading regime shifts in climate, ice cover, and mix-

ing; Limnology and Oceanography, v. 54, issue 6, pt. 2, p. 2371–2385.

Nitze, I., Cooley, S.W., Duguay, C.R., Jones, B.M. and Grosse, G. 2020: The catastrophic thermokarst lake drainage events of 2018 in northwestern Alaska: fast-forward into the future; The Cryosphere, v. 14, issue 12, p. 4279–4297.

Prowse, T.D., Wrona, F.J., Reist, J.D., Gibson, J.J., Hobbie, J.E., Lévesque, L.M. and Vincent, W.F. 2006: Climate change effects on hydroecology of arctic freshwater ecology; AMBIO: A Journal of the Human Environment, v. 35, issue 7, p. 347–358.

Roberts, K.E., Lamoureux, S.F., Kyser, T.K., Muir, D.C.G., Lafrenière, M.J., Iqaluk, D., Pieńkowski, A.J. and Normandeau, A. 2017: Climate and permafrost effects on the chemistry and ecosystems of High Arctic lakes; Scientific Reports, v. 7, art. 13292, URL <https://doi.org/10.1038/s41598-017-13658-9>.

Rouse, W.R., Douglas, M.S., Hecky, R.E., Hershey, A.E., Kling, G.W., Lesack, L., Marsh, P., McDonald, M., Nicholson, B.J., Roulet, N.T. and Smol, J.P. 1997: Effects of climate change on the freshwaters of arctic and subarctic North America; Hydrological Processes, v. 11, issue 8, p. 873–902.

Smith, L.C., Sheng, Y., Macdonald, G.M. and Hinzman, L.D. 2005: Disappearing arctic lakes; Science, v. 308, issue 5727, p. 1429, URL <https://doi.org/10.1126/science.1108142>.

Statistics Canada 2019: Census profile, 2016 census, Nunavut; Statistics Canada, URL <https://www12.statcan.gc.ca/census-recensement/2016/dp-pd/prof/search-recherche/lst/results-resultats.cfm?Lang=E&TABID=1&G=1&Geo1=&Code1=&Geo2=&Code2=&GEOCODE=62&type=0> [August 2021].

St. Pierre, K.A., Zolkos, S., Shakil, S., Tank, S.E., St. Louis, V.L. and Kokelj, S.V. 2018: Unprecedented increases in total and methyl mercury concentrations downstream of retrogressive thaw slumps in the western Canadian Arctic; Environmental Science & Technology, v. 52, issue 24, p. 14099–14109.

Swanson, D.K. 2018: Thermokarst and precipitation drive changes in the area of lakes and ponds in the National Parks of northwestern Alaska, 1984–2018; Arctic, Antarctic and Alpine Research, v. 51, issue 51, p. 265–279, URL <https://doi.org/10.1080/15230430.2019.1629222>.

Tremblay, T., Day, S., Shirley, J., Smith, K.A. and McNeil, R. 2016: Geochemical, mineralogical and sedimentological results from till, stream and lake sediment and water samples in the Sylvia Grinnell Lake area, Baffin Island, Nunavut; *in* Summary of Activities 2016, Canada-Nunavut Geoscience Office, p. 13–26, URL <https://m.cngo.ca/wp-content/uploads/Summary_of_Activities_2016-P03-Tremblay.pdf> [January 2022].

Vacchi, M., Engelhart, S.E., Nikitina, D., Ashe, E.L., Peltier, W.R., Roy, K., Kopp, R.E. and Horton, B.P. 2018: Postglacial relative sea-level histories along the eastern Canadian coastline; Quaternary Science Reviews, v. 201, p. 124–146, URL <https://doi.org/10.1016/j.quascirev.2018.09.043>.

Vincent, W.F., Laurion, I., Pienitz, R. and Walter Anthony, K.M. 2013: Climate impacts on arctic lake ecosystems; *in* Climatic Change and Global Warming of Inland Waters: Impacts and Mitigation for Ecosystems and Societies, C.R. Goldman, M. Kumagai and R.D. Robarts (ed.), John Wiley & Sons, Chichester, United Kingdom, p. 27–42.

Whitehead, P.G., Wilby, R.L., Battarbee, R.W., Kernan, M. and Wade, A.J. 2009: A review of the potential impacts of climate change on surface water quality; Hydrological Sciences Journal, v. 54, issue 1, p. 101–123.

Williamson, C.E., Saros, J.E., Vincent, W.F. and Smol, J.P. 2009: Lakes and reservoirs as sentinels, integrators, and regulators of climate change; Limnology and Oceanography, v. 54, issue 6, pt. 2, p. 2273–2282.

World Health Organization 2006: Guidelines for drinking-water quality, first addendum to third edition, volume 1, recommendations; World Health Organization, Geneva, Switzerland, 68 p.

Zhang, Y., Ma, N., Park, H., Walsh, J.E. and Zhang, K. 2021: Evaporation processes and changes over the northern regions; *in* Arctic Hydrology, Permafrost and Ecosystems, D. Yang and D.L. Kane (ed.), Springer, Cham, Switzerland, p. 101–131, URL <https://doi.org/10.1007/978-3-030-50930-9>.

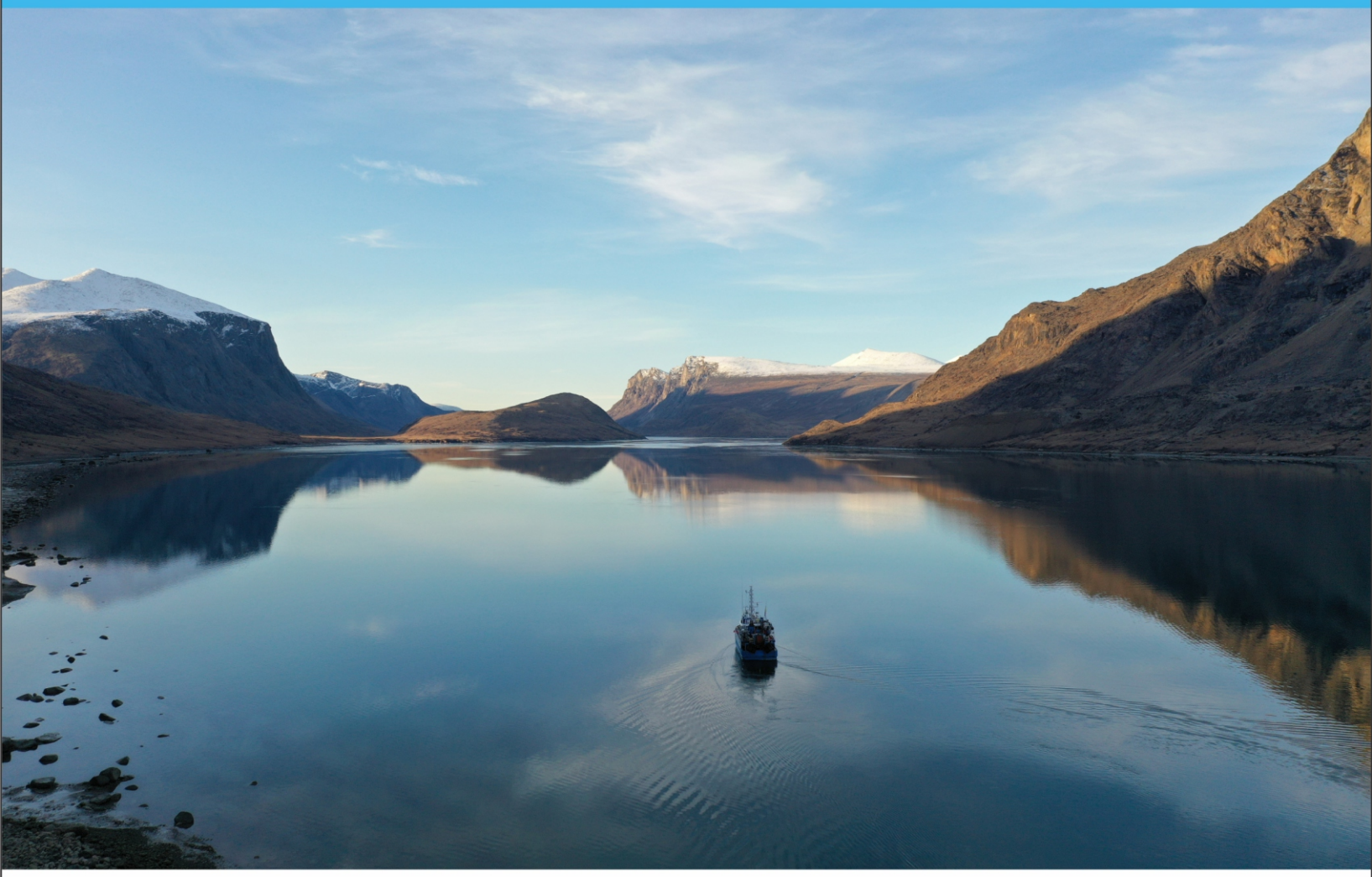

The **Canada-Nunavut Geoscience Office** conducts new geoscience mapping and research, supports geoscience-capacity building, disseminates geoscience information and develops collaborative geoscience partnerships for Nunavut.

cngo.ca